CHEMISTRY AND CATALYSIS OF COAL LIQUEFACTION CATALYTIC AND THERMAL UPGRADING OF COAL LIQUID AND HYDROGENATION OF CO TO PRODUCE FUELS. QUARTERLY PROGRESS REPORT, JANUARY-MARCH 1982

UTAH UNIV., SALT LAKE CITY. DEPT. OF MINING AND FUELS ENGINEERING

JUN 1982

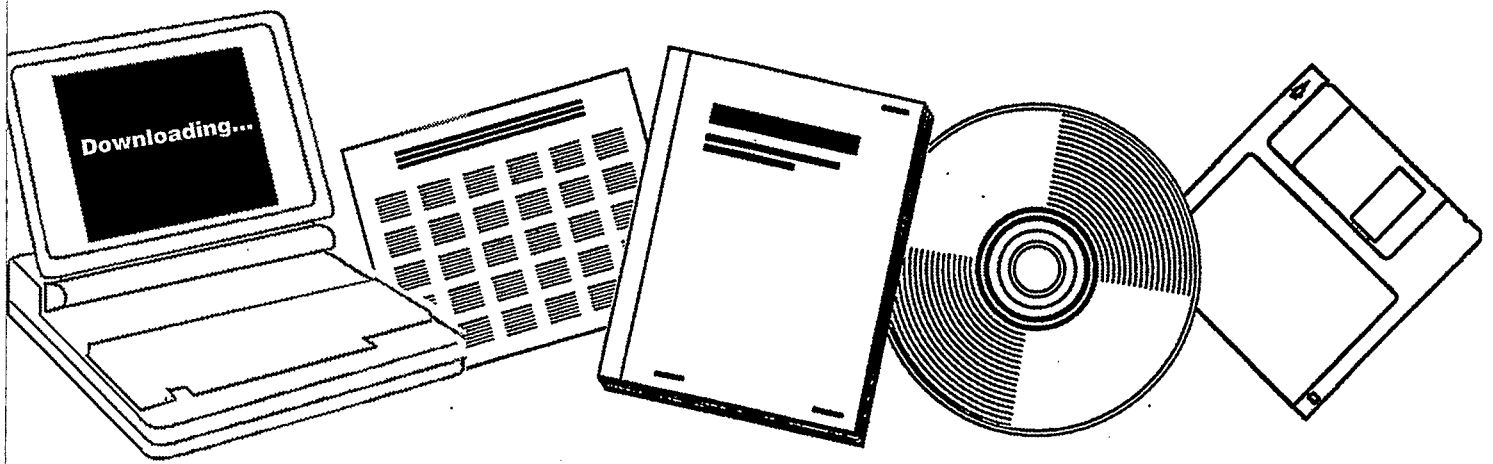

DE82020554

DOE/ET/14700-10
(DE82020554)
Distribution Category UC-90d

Chemistry and Catalysis of Coal Liquefaction Catalytic and Thermal Upgrading of Coal Liquid and Hydrogenation of CO to Produce Fuels

Quarterly Progress Report
for the Period Jan - Mar 1982

Dr. Wendell H. Wiser

University of Utah - Department of
Mining and Fuels Engineering
Salt Lake City, Utah 84112

Date Published - June 1982

Prepared for the United States Department
of Energy
Under Contract No. DE-AC01-79ET14700

CONTENTS

OBJECTIVE AND SCOPE OF WORK

I. The chemistry and Catalysis of Coal Liquefaction

Task 1 Chemical-Catalytic Studies

Coal will be reacted at subsoftening temperatures with selective reagents to break bridging linkages between clusters with minimal effect on residual organic clusters. The coal will be pretreated to increase surface area and then reacted at 25 to 350°C. Reagents and catalysts will be used which are selective so that the coal clusters are solubilized with as little further reaction as possible.

Task 2 Carbon-13 NMR Investigation of CDL and Coal

Carbon-13 NMR spectroscopy will be used to examine coal, coal derived liquids (CDL) and residues which have undergone subsoftening reactions in Task 1 and extraction. Improvements in NMR techniques, such as crosspolarization and magic angle spinning, will be applied. Model compounds will be included which are representative of structural units thought to be present in coal. Comparisons of spectra from native coals, CDL and residues will provide evidence for bondings which are broken by mild conditions.

Task 3 Catalysis and Mechanism of Coal Liquefaction

This fundamental study will gain an understanding of metal salt chemistry and catalysis in coal liquefaction through study of reactions known in organic chemistry. Zinc chloride and other catalytic materials will be tested as Friedel-Crafts catalysts and as redox catalysts using coals and selected model compounds. Zinc chloride, a weak Friedel-Crafts catalyst, will be used at conditions common to coal liquefaction to participate in well defined hydrogen transfer reactions. These experiments will be augmented by mechanistic studies of coal hydrogenation using high pressure thermogravimetric analysis and structural analysis. The results of these studies will be used to develop concepts of catalysis involved in coal liquefaction.

Task 4 Momentum Heat and Mass Transfer in CoCurrent Flow of Particle-Gas Systems for Coal Hydrogenation

A continuation of ongoing studies of heat and transport phenomena in cocurrent, co-gravity flow is planned for a one-year period. As time and development of existing work permits, the extension of this study to include a coiled reactor model will be undertaken. Mathematical models of coal hydrogenation systems will utilize correlations from these straight and coiled reactor configurations.

Task 5 The Fundamental Chemistry and Mechanism of Pyrolysis of Bituminous Coal

Previous work at the University of Utah indicates that coal pyrolysis, dissolution (in H-donor) and catalytic hydrogenation all have similar rates and activation energies. A few model compounds will be pyrolyzed in the range of 375 to 475°C. Activation energies, entropies and pro-

duct distributions will be determined. The reactions will assist in formulating the thermal reaction routes which also can occur during hydro-liquefaction.

II. Catalytic and Thermal Upgrading of Coal Liquids

Task 6 Catalytic Hydrogenation of CD Liquids and Related Polycyclic Aromatic Hydrocarbons

A variety of coal derived (CD) liquids will be hydrogenated with sulfided catalysts prepared in Task 10 from large pore, commercially available supports. The hydrogenation of these liquids will be systematically investigated as a function of catalyst structure and operating conditions. The effect of extent of hydrogenation will be the subject of study in subsequent tasks in which crackability and hydropyrolysis of the hydrogenated product will be determined. To provide an understanding of the chemistry involved, model polycyclic arenes will be utilized in hydrogenation studies. These studies and related model studies in Task 7 will be utilized to elucidate relationships between organic reactants and the structural-topographic characteristics of hydrogenation catalysts used in this work.

Task 7 Denitrogenation and Deoxygenation of CD Liquids and Related Nitrogen- and Oxygen-Containing Compounds

Removal of nitrogen and oxygen heteroatoms from CD liquids is an important upgrading step which must be accomplished to obtain fuels corresponding to those from petroleum sources. Using CD liquids as described in Task 6, exhaustive HDN and HDO will be sought through study of catalyst systems and operating conditions. As in Task 6, catalysts will be prepared in Task 10 and specificity for N- and O-removal will be optimized for the catalyst systems investigated. Model compounds will also be systematically hydrogenated using effective HDN/HDO catalysts. Kinetics and reaction pathways will be determined. A nonreductive denitrogenation system will be investigated using materials which undergo reversible nitridation. Conditions will be sought to cause minimal hydrogen consumption and little reaction of other reducible groups.

Task 8 Catalytic Cracking of Hydrogenated CD Liquids and Related Polycyclic Naphthenes and Naphthenoaromatics

Catalytic cracking of hydrogenated CD liquid feedstocks will be studied to evaluate this scheme as a means of upgrading CD liquids. Cracking kinetics and product distribution as a function of preceding hydrogenation will be evaluated to define upgrading combinations which require the minimal level of CD liquid aromatic saturation to achieve substantial heteroatom removal and high yields of cracked liquid products. Cracking catalysts to be considered for use in this task shall include conventional zeolite-containing catalysts and large-pore molecular sieve, CLS (cross-linked smectites) types under study at the University of Utah. Model compounds will be subjected to tests to develop a mechanistic understanding of the reactions of hydro CD liquids under catalytic cracking conditions.

Task 9 Hydropyrolysis (Thermal Hydrocracking) of CD Liquids

Heavy petroleum fractions can be thermally hydrocracked over a specific range of conditions to produce light liquid products without excessive hydrogenation occurring. This noncatalytic method will be applied to a variety of CD liquids and model compounds, as mentioned in Task 6, to determine the conditions necessary and the reactibility of these CD feedstocks with and without prior hydrogenation and to derive mechanism and reaction pathway information needed to gain an understanding of the hydropyrolysis reactions. Kinetics, coking tendencies and product compositions will be studied as a function of operating conditions.

Task 10 Systematic Structural-Activity Study of Supported Sulfide Catalysts for Coal Liquids Upgrading

This task will undertake catalyst preparation, characterization and measurement of activity and selectivity. The work proposed is a fundamental study of the relationship between the surface-structural properties of supported sulfide catalysts and their catalytic activities for various reactions desired. Catalysts will be prepared from commercially available. Supports composed of alumina, silica-alumina, silica-magnesia and silica-titania, modification of these supports to change acidity and to promote interaction with active catalytic components is planned. The active constituents will be selected from those which are effective in a sulfided state, including but not restricted to Mo, W, Ni and Co. The catalysts will be presulfided before testing. Catalyst characterization will consist of physico-chemical property measurements and surface property measurements. Activity and selectivity tests will also be conducted using model compounds singly and in combination.

Task 11 Basic Study of the Effects of Coke and Poisons on the Activity of Upgrading Catalysts

This task will begin in the second year of the contract after suitable catalysts have been identified from Tasks 6, 7 and/or 10. Two commercial catalysts or one commercial catalyst and one catalyst prepared in Task 10 will be selected for a two-part study, (1) simulated laboratory poisoning/coking and (2) testing of realistically aged catalysts. Kinetics of hydrogenation, hydrodesulfurization, hydrodenitrogenation and hydrocracking will be determined before and after one or more stages of simulated coking. Selected model compounds will be used to measure detailed kinetics of the above reactions and to determine quantitatively how kinetic parameters change with the extent and type of poisoning/coking simulated. Realistically aged catalysts will be obtained from coal liquids upgrading experiments from other tasks in this program or from other laboratories conducting long-term upgrading studies. Deactivation will be assessed based on specific kinetics determined and selective poisoning studies will be made to determine characteristics of active sites remaining.

Task 12 Diffusion of Polyaromatic Compounds in Amorphous Catalyst Supports

If diffusion of a reactant species to the active sites of the catalyst is slow in comparison to the intrinsic rate of the surface reaction, then only sites near the exterior of the catalyst particles will be utilized effectively. A systematic study of the effect of molecular size on the sorptive diffusion kinetics relative to pore geometry will

be made using specific, large diameter aromatic molecules. Diffusion studies with narrow boiling range fractions of representative coal liquid will also be included. Experimental parameters for diffusion kinetic runs shall include aromatic diffusion model compounds, solvent effects, catalyst sorption properties, temperature and pressure.

III. Hydrogenation of CO to Produce Fuels

Task 13 Catalyst Research and Development

Studies with iron catalysts will concentrate on promoters, the use of supports and the effects of carbiding and nitriding. Promising promoters fall into two classes: (1) nonreducible metal oxides, such as CaO, K_2O, Al_2O_3 and MgO, and (2) partially reducible metal oxides which can be classified as co-catalysts, such as oxides of Mn, Mo, Ce, La, V, Re and rare earths. Possible catalyst supports include zeolites, alumina, silica, magnesia and high area carbons. Methods of producing active supported iron catalysts for CO hydrogenation will be investigated, such as development of shape selective catalysts which can provide control of product distribution. In view of the importance of temperature, alternative reactor systems (to fixed bed) will be investigated to attain better temperature control. Conditions will be used which give predominately lower molecular weight liquids and gaseous products.

Task 14 Characterization of Catalysts and Mechanistic Studies

Catalysts which show large differences in selectivity in Task 13 will be characterized as to surface and bulk properties. Differences in properties may provide the key to understanding why one catalyst is superior to another and identify critical properties, essential in selective catalysts. Factors relating to the surface mechanism of CO hydrogenation will also be investigated. Experiments are proposed to determine which catalysts form "surface" (reactive) carbon and the ability of these catalysts to exchange C and O of isotopically labelled CO. Reactions of CO and H_2 at temperatures below that required for CO dissociation are of particular interest.

Task 15 Completion of Previously Funded Studies and Exploratory Investigations

This task is included to provide for the orderly completion of coal liquefaction research underway in the expiring University of Utah contract, EX-76-C-01-2006.

III Highlights to Date

ESCA studies on Mo-supported catalysts have shown that a high degree of dispersion of the Mo phase is associated with a specific interaction with alumina. Changes in catalytic activity for HDS and hydrogenation with different supports are explained by differences in the monolayer cluster size. When alumina is absent from the support, three-dimensional MoS_2 crystallites are formed, which exhibit lower catalytic activity.

Task 1

Chemical-Catalytic Studies of Coal Liquefaction

Faculty Advisor: J. Shabtai
Graduate Student: R. Jensen

Introduction

This project is concerned with the development of suitable processing conditions and catalyst-solvent systems for coal liquefaction under mild temperature (<350°C) and pressure (<2000 psi).

Project Status

One of the main conditions for effective use of catalyst-solvent systems in liquefaction below the coal softening point is the necessity of increasing the micropore volume of the solid coal. Previous studies in this department show that pretreatment of coal with metal halides, e.g., $ZnCl_2$, at relatively mild temperatures (200-350°C) causes considerable increase in surface area and microporosity. Elucidation of the nature of chemical reactions between metal halides and coal has attracted recently considerable interest. In the framework of this work on homogeneously catalyzed liquefaction, it was considered of importance to develop a better understanding of such reactions. Therefore, systematic studies of metal halide-catalyzed reactions were undertaken, using the following types of model compounds:

(a) Alkylbenzenes with branched alkyl groups;

(b) Alkylbenzenes with n-alkyl groups; and

(c) Diarylalkanes.

These studies were intended to provide information on (1) the mode of catalytic activity of metal halides in a wide range of experimental conditions; and (2) the direction and rate of metal halide-catalyzed dealkylation and hydrodealkylation processes, as related to cleavage reactions of intercluster linkages in the coal structure.

In previous reports (DE/ET/14700-6, 14700-7 and 14700-8) we described the results obtained in a systematic study of hydrodealkylation reactions of representative monoalkylbenzenes of type (a), i.e., isopropylbenzene (2), sec-butylbenzene (3) and tert-butylbenzene (1), and of type (b), i.e., n-propylbenzene, n-butylbenzene, and n-hexylbenzene. Further, in the preceding report (DE/ET/14700-9) we provided data on the hydrodealkylation of a compound of type (c), i.e., diphenylmethane (7). All of these studies were performed using a silica-gel supported $ZnCl_2$ catalyst.[1,2]

The present report describes the results obtained in a hydrodealkylation study of two additional compounds of type (c), i.e., 1,4-diphenylbutane (8) and 1-benzylnaphthalene (9). Reactions were carried out at 350° and 450°C, under a hydrogen pressure of 850 psig, using the previously described micro-autocalve reactor.[1,2] The total reaction time in each run was kept

constant at 90 sec. Products obtained were identified and quantitatively analyzed by a combination of gas chromatography and mass spectrometry.

Table 1 shows the change in product composition from $ZnCl_2$-catalyzed hydrodealkylation of 1,4-diphenylbutane (8) as a function of reaction temperature (reaction time, 90 sec; hydrogen pressure, 850 psig). As seen from Table 1, the conversion of 8 increases markedly with increase in temperature (from 9.9% at 350°C to 50.2% at 450°C). The main component of the liquid product at both temperatures is benzene. Significantly, this compound is accompanied by small amounts of cyclohexane, which is indicative of the occurrence of some ring hydrogenation. Another important liquid product is tetralin, which could be formed by cyclization of an intermediate butylbenzene carbonium ion (see below) and could serve as a hydrogen donor responsible for the partial hydrogenation of benzene into cyclohexane. In acting as a hydrogen donor, tetralin is converted into naphthalene, which is also found in the products (Table 1). The liquid products at both temperatures contain also significant amounts of (a) n-butylbenzene and sec-butylbenzene, which are anticipated intermediate products from hydrodealkylation of 8; and (b) toluene and xylenes, which are probably formed by secondary transalkylation reactions. The gaseous product contains important amounts of C_4 hydrocarbons, in particular isobutane and n-butane, which are anticipated from hydrodealkylation of 8. There is also significant formation of C_1-C_3 gases which are probably derived by secondary cleavage reactions of intermediate C_4 carbonium ions (see below, mechanistic discussion).

Table 2 summarizes the change in product composition from $ZnCl_2$-catalyzed hydrodealkylation of 1-benzylnaphthalene (9) as a function of reaction temperature (350-450°C), keeping a constant reaction time of 90 sec and a hydrogen pressure of 850 psig. As seen from Table 2 the conversion of 9 is very high in this temperature range (79.3-82.7%). The main liquid products derived from 9 at 350°C are naphthalene (ca 47.2%), toluene (ca 13.6%) and benzene (ca 25.7%). As temperature is increased there is only a minor change in the relative concentrations of benzene and toluene. The concentration of naphthalene increases slightly (from 47.2% at 350°C to ca 52.1% at 450°C), while that of methylnaphthalenes correspondingly decreases (from 12.7% at 350°C to 7.2% at 450°C). The main gaseous product observed from hydrodealkylation of 9 is methane. The concentration of this compound increases as temperature is increased (from 68.9 to 74.8%). Small amounts of C_2-C_4 hydrocarbons are also formed.

The product compositions from compounds 8 and 9, and their change with temperature, can be rationalized by the following mechanistic schemes.

(a) 1,4-diphenylbutane (8)

The formation of benzene as main product from 1,4-diphenylbutane (8) indicates that both rings in this compound can undergo hydrodealkylation with elimination of the bridging C_4 alkylene group. Further, the presence of n-butylbenzene and its isomers in the product (Table 1) indicates that the hydrodealkylation process is stepwise:

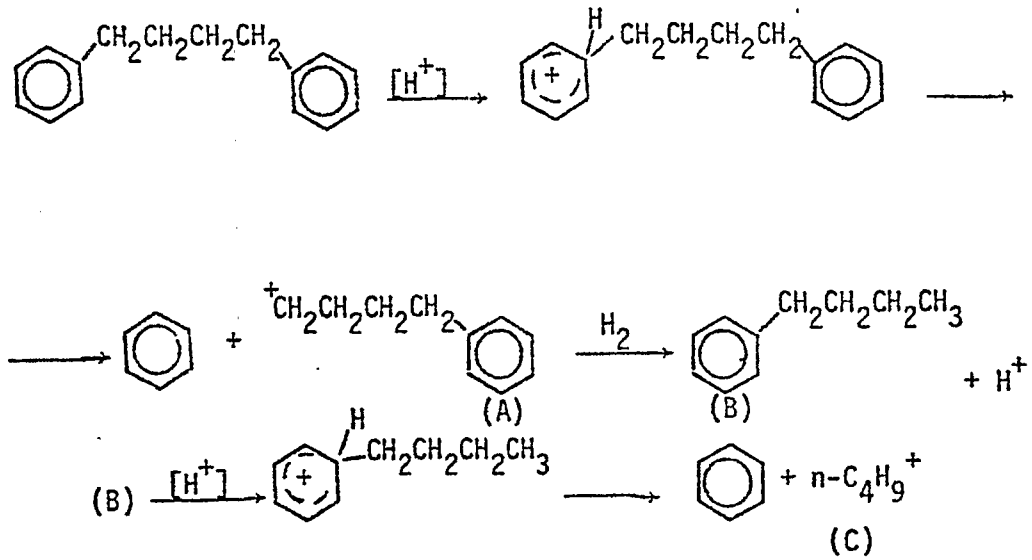

The carbonium ion (C) can then undergo the previously described (DE/ET/14700-8) skeletal isomerization and cleavage reactions to give isobutane and C_1-C_3 β-cleavage gaseous products.

The formation of tetralin (D) as an important liquid product (Table1) can be ascribed to intromolecular Friedel-Crafts cyclialkylation of the intermediate carbonium ion (A):

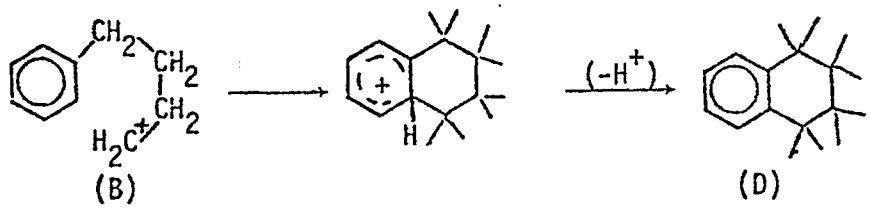

An interesting consequence of the formation of (D) is that the benzene product undergoes to a minor extent ring hydrogenation to yield cyclohexane (Table 1). The reactiom probably involved noncatalytic hydrogen transfer from (D), as evidenced by the formation of some naphthalene:

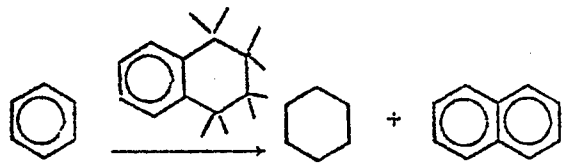

The limited extent of this reaction is due to the limited extent of cyclization of (B) to yield (D), as well as to the lack of catalytic regeneration of (D) by direct ring hydrogenation of the naphthalene

formed by hydrogen transfer. It should be noted that in the absence of a hydrogen-donor compound, $ZnCl_2$ shows no catalytic ring hydrogenation activity, as demonstrated in these model studies.

(b) 1-Benzylnaphthalene (9)

Hydrodealkylation of compound (9) proceeds in a manner analogous to that of diphenylmethane (DE/ET/14700-9). The first hydrodealkylation step can proceed either by protonation of the naphthalene moiety to give naphthalene and toluene (reaction III), or by protonation of the benzene moiety to give benzene and 1-methylnaphthalene (reaction IV). The toluene and 1-methylnaphthalene could undergo subsequent hydrodealkylation to yield correspondingly additional benzene and naphthalene as products:

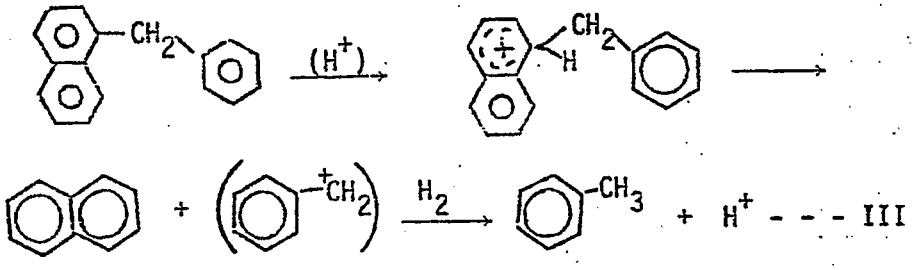

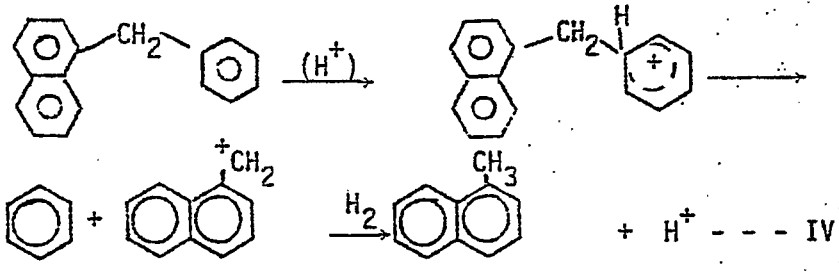

The higher concentration of naphthalene as compared to benzene in the product indicates qualitatively that protonation of the naphthalene moiety (reaction III) is somewhat faster than protonation of the benzene ring (reaction IV), and/or that 1-methylnaphthalene is hydrodealkylated faster to naphthalene than toluene to benzene.

The study of hydrodealkylation of diarylalkanes presented in this report clearly indicates the manner by which zinc chloride can catalyze the cleavage of alkylene bridging groups between aromatic clusters in coal liquefaction processes, resulting in formation of lower molecular weight products.

Future Work

Low temperature (150-250°C) coal liquefaction studies, using soluble catalyst systems, have been initiated by Mr. Peter Rose, a new Ph.D. student assigned to Task 1. Approaches being presently applied and initial results obtained will be provided in the next report.

References

1. R.E. Jensen, M.S. Thesis, University of Utah, Salt Lake City, Utah, 1981.

2. J.S. Shabtai and R.E. Jensen, Proc. 7th Symposium Rocky Mountain Fuel Soc., Salt Lake City, Utah, 1982, Paper 9.

TABLE 1

Product Composition from $ZnCl_2$-Catalyzed Hydrodealkylation of 1,4-Diphenylbutane (8)

Experiment No.	181	221
Reaction temperature, °C	350	450
Conversion of 8, mole %	9.9	50.2
Catalyst	$ZnCl_2$	$ZnCl_2$
Catalyst wt. %	7.2	7.4
Gaseous Product Component, mole %		
CH_4	27.9	18.6
C_2H_6	10.6	12.1
C_2H_4	13.2	6.2
C_3H_8	15.1	25.7
C_3H_6	4.8	3.7
i-C_4H_{10}	24.3	27.0
n-C_4H_{10}	3.1	3.8
i-Butene	1.1	2.2
1-Butene	----	0.2
Liquid Product Component, mole %		
Cyclohexane	2.3	4.5
Benzene	64.0	65.0
Toluene	5.1	3.1
o-, p-Xylenes	13.1	2.6
sec-Butylbenzene & t-Butylbenzene	4.0	2.3
n-Butylbenzene	5.1	7.5
Tetralin	5.1	9.3
Naphthalene	1.3	5.5

[a]In each run were used 0.15g (.001 mole) of 8 and 0.05g of 5% $ZnCl_2/SiO_2$ catalyst. [b]Hydrogen pressure, 850 psig.

TABLE 2

Change in Product Composition from Hydrodealkylation of 1-Benzylnaphthalene (9) as a Function of Reaction Temperature

Experiment No.	191	222
Reaction temperature, °C	350	450
Conversion of 9, mole %	79.3	82.7
Catalyst	$ZnCl_2$	$ZnCl_2$
Catalyst wt. %	6.9	7.5
Gaseous Product Component, mole %		
CH_4	68.9	74.8
C_2H_6	11.3	10.4
C_2H_4	1.2	1.7
C_3H_8	11.0	1.2
C_3H_6	0.6	0.6
i-C_4H_{10}	5.0	8.4
n-C_4H_{10}	1.3	1.6
i-Butene	0.7	1.3
1-Butene	trace	trace
Liquid Product Component, mole %		
Benzene	25.7	26.8
Toluene	13.6	13.3
Ethylbenzene	0.5	0.4
Styrene	0.2	----
Naphthalene	47.2	52.1
Tetrahydronaphthalene	0.1	0.2
Methylnaphthalenes	12.7	7.2

[a]In each run were used 0.15g (.001 mole) of 9 and 0.05g of 5% $ZnCl_2/SiO_2$ catalyst. [b]Hydrogen pressure, 850 psig.

Task 2

Carbon-13 NMR Investigation of CDL and Coal

Faculty Advisor: R.J. Pugmire
Postdoctorals: D.K. Dalling
K.W. Zilm

Introduction

Since the inception of this study, one of the goals has been to advance NMR techniques for the study of solid coal and coal derived liquids. In the previous report high resolution data was presented on an SRC-II distillate using INEPT and J-resolved 2-dimensional techniques to determine if additional definition could be obtained in complex liquids. The results presented were indicative that such advanced NMR techniques have high promise. The other aspect of this work is the development of techniques that will enhance the quality and type of data NMR obtainable on solid coals.

Project Status

Major advances have been made in instrumentation and data collection for fossil fuel samples in this laboratory. A Varian XL-100 spectrometer was used during the early stages. At that time, 10,000 to 25,000 scans taken every 3 seconds were required to obtain reasonable signal to noise. Approximately one year ago a Bruker CXP-100 spectrometer became operational and the use of this instrument has eliminated many of the earlier difficulties associated with data collection. With support from other sources, several projects were started on various rotor and probe designs which have had important impacts on improved sensitivity. With the new Bruker spectrometer, these alternatives were evaluated and an optimal design was established. This was the barrel rotor system. The barrel rotor work was an integral part of another contract (the Industrial Associates Program at UURI which provided partial salary support for Dr. Zilm). The final form of the barrel rotor probe is still evolving, but the current prototype model has operated quite successfully routinely at a spin rate of 4 KHz. The increased filling factor and sample size allow useable coal spectra to be acquired in as little as 200 scans. An example of this sensitivity is presented in Figure 1. The top trace represents the spectra acquired in one minute on Kemmerer coal. The probe/rotor system is this laboratory's own design and represents a significant improvement in S/N over commercially available spectrometers that operate at 100 MHz field strength. The bottom trace was obtained in one minute also using the prototype barrel rotor/probe system. An improvement of 2.6 in S/N represents a 6.8 savings in instrument time. This probe will be phased into use on this contract in the future as the probe moves from the prototype to the routine stage. At present, an attempt is being made to increase the sensitivity by another factor of two.

A relaxation study have also been carried out on a set of coals. This has proved to be very useful since the coals covered a wide range of rank (lignite through anthracite), and aided in determing the range of relaxation parameters. One of the major conclusions gleaned from this work is that

the ^1H $T_{1\rho}$ in coals are short enough to repeat the experiment every 0.3 seconds instead of the formerly employed 3 seconds. This tenfold increase in data acquisition rate along with the increased sensitivity of the barrel rotor/probe has the potential to cut data acquisition in some cases down to minutes instead of the five to twelve hours previously required on the XL-100. About 30 minutes is spent on this barrel rotor to acquire data sinces it takes this long to plot the last spectrum and prepare the next sample. The resulting spectra are of a much higher quality than those obtained on the XL-100.

The previously mentioned relaxation studies on the set of coals has provided a clear understanding of the relaxation processes involved in coals and their implications for quantitation of the results. A number of significant findings were uncovered in this work. The $T_{1\rho}$ for coal protons are very short and, hence, decrease the data acquisition time by approximately an order of magnitude. Other conclusions arrived at are:

1) Oxygen plays a significant role in coal relaxation. Enough O_2 is absorbed on coals to decrease the proton $T_{1\rho}$ by a factor of two compared to a degassed sample.

2) The most rapidly relaxing component of proton spectra (T_1 and $T_{1\rho}$) of the coals is the absorbed H_2O. This has not been recognized in the past. Since quantitation is impeded by rapidly relaxing protons ($T_{1\rho}$), this is an important observation as the H_2O protons make no significant contribution to the cross polarization process in CP/MAS spectroscopy. Thus, the quantitation problem is not as severe as was previously expected.

3) The relaxation process most important with respect to quantitation is the proton $T_{1\rho}$. The multiple exponential relaxation is due to the effects of naturally occurring free radicals in the coal. The $T_{1\rho}$ data also provides a measure of the free electron concentration and the relaxation time for the free radical.

4) T_{CH} data, which was reported earlier, are consistent with those measured for model compounds. (A manuscript on model compounds by Alemany, Grant, Pugmire, Alger, and Zilm has been submitted for publication as part of a project supported by the Office of Energy Research.)

5) One of the most serious problems in quantifying CP/MAS data arises if the proton $T_{1\rho}$'s vary across the sample leading to nonquantitative response. Except in the case of the highest rank coals, it has been demonstrated that the distribution of $T_{1\rho}$'s is similar for aromatic and aliphatic carbons. This finding suggests that quantitative results for the coals in question are as accurate as those in typical hydrocarbon model systems.

These conclusions were reached over approximately a nine-month period of time in which a number of new theories were applied to coal relaxation, the most significant of which was the spin-diffusion restricted relaxation by paramagnetic centers (3, above) described in more detail in a manuscript being prepared for publication.

Further work needs to be completed in relating the T_{CH}'s measured and the $T_{1\rho}$ behavior observed to quantitative results. As a function of contact time, the magnetization develops as:

$$1)\quad M_{^{13}C}(\tau) = M\alpha/(1-\frac{T_{CH}}{T_{1\rho}})\ (e^{-\tau/T_{1\rho}}-e^{-\tau/T_{CH}})$$

assuming a single $T_{1\rho}$ and T_{CH}.

For any one functional type of carbon (i.e., one T_{CH}) a distribution of $T_{1\rho}$'s is observed giving the proton magnetization as a function of spin lock time

$$2)\quad M_{^{1}H}(\tau) = M_0 e^{-\sqrt{\tau}/T_\rho}$$

Thus, a solution needs to be developed similar to Eq (1) in which the $T_{1\rho}$ distribution giving Eq (2) is incorporated. One program has now been written which will numerically simulate such a system for comparison to the coal data. However, it is felt that an analytical solution can still be found which will facilitate incorporation into this curve-fitting program.

The current set of samples were chosen to encompass a wide range of rank so as to present a better overall picture of coal relaxation processes. These coals were also those for which a good deal of liquefaction data had been acquired at the University of Utah.

In the early days of CP/MAS spectroscopy on coals, one observed the separation of two peaks attributed to aromatic and aliphatic carbons.[1,2] The work of Zilm et al.[3-5] demonstrated that additional structural detail could be observed.

Further structural information can be obtained by means of the dipolar dephasing (DD) technique reported by Opella[6,7] which discriminates protonated from nonprotonated carbons in a CP/MAS spectrum on the basis of the ^{1}H-^{13}C dipolar interaction. Brief reports have recently appeared on the application of DD techniques to coals.[8-11] In model compounds, Alemany[12] has observed that a 40-μs interruption in the proton decoupling will cause all of the CH and CH_2 resonances to vanish, while the intensity of the nonprotonated carbons experience only minor attenuation (ca. 10-20%).

Carbon resonances arising from both nonprotonated and protonated aromatic carbons possess very different relaxation behavior and in a solid evolve very differently due to local proton dipolar fields which attenuate with the carbon proton distances as $1/r_{CH}^3$. When the spin locking for proton and carbon nuclei is terminated, carbons with directly bound protons such as methines and methylenes rapidly dephase in the local proton fields and their spectral response is rapidly diminished. The rapid internal motion of CH_3 groups greatly decreases the effectiveness of methyl protons. Nonprotonated carbons are only dephased by remote and therefore much weaker magnetic fields. This type of response is given in Figures 2 and 3 using the pulse sequences first proposed by Rybaczewski et al.[13] and popularized by Opella[6,7] for powders. These two figures illustrate the spectral responses of the aromatic and aliphatic regions, respectively, as a function of dephasing time. The intensity decay curves demonstrate a complex multiple relaxation behavior which is a combination of several factors: 1) dipolar interaction between ^{1}H and ^{13}C nuclei; 2) rotational modulation; and 3) dipolar modulation. These

effects have been previously reported for simple organic molecules.[12-15] The spectral response on a San Juan, New Mexico coal for dipolar dephasing time of 0-120 μsec is illustrated in Figure 4. By comparing the 0 and 40 μsec spectra, one observes that the strong upper field portion of the aromatic peak due to protonated carbons and essentially all of the aliphatic region are attenuated with a 40 μsec dipolar dephasing time leaving primarily the nonprotonated aromatic carbons and methyl carbons with a small vestigial remnant (marked "a") of either the once very strong methylene peak or possibly methyl carbons in gem-methyl or tert-butyl structures. Thus, the 40 μsec spectral response is limited to a subportion of the total spectrum contained in the upper trace. From the 0 μsec trace the spectral parameter f_a can be obtained while f_a^H, f_a^N and f_s^* (= f_s^{CH3} + f_s^N) (vida infra) are directly obtainable from the lower trace.

The dephasing of a methyl group is more complex but approximately 50% of the methyl carbon signal is still observed after 40 μsec.[12] Hence, by appropriately varying the interruption of the proton decoupler one can differentiate between methine, methylene, methyl and nonprotonated carbons. The fraction of the carbon in the sample which is aromatic and nonprotonated, f_a^N, if obtained by comparing the relative intensities of the aromatic region of the spectra with decoupler pulse delays of 0 and 40 μsec before data acquisition. The fraction of protonated aromatic carbon is f_a^H; thus $f_a^H + f_a^N = f_a$. Using a solvent refined coal tar for which high resolution ^1H and ^{13}C NMR data were taken, Wilson[16] has obtained values of f_a and f_a^H in the solid material, and these agree nicely with corresponding values obtained for the dissolved material. (f_a = 0.62, 0.62; f_a^H = 0.24, 0.23 for the solid and dissolved solvent refined coal, respectively.)

The preceding discussion describes a new experiment and summarizes the type of information that one can obtain. A note of caution however. The structural parameters obtained are semi-quantitative only and one cannot carry out a mass balance calculation with the current data. As more information is gained on experimental parameters on coal, it may be possible to do so. At the present time such considerations are not appropriate. However, the data can be used to examine trends in structural changes and these changes can be quite useful.

The CP/MAS spectra of three of the coals studied (Wyodak, New Mexico and Hiawatha are compared with two other higher rank coals not associated with this study) are given in Figure 5. It is noted that the structural features of the three low rank coals (Wyodak, New Mexico and Hiawatha) are different from the higher rank coals presented for comparison. The major difference in the aliphatic region is the relatively large intensity of the 30 ppm peak (presumably due to CH_2 groups) in the lower rank coals. However, the line width at half height of the aromatic band decreases in the higher rank coals. Furthermore, the carbonyl content (peak at approximately 175 ppm) decreases in the higher rank coals and, in fact, is essentially absent in the two high rank coals. The intensity of the peak due to phenolic aromatic carbons (150-155 ppm) also decreases relative to the intensity of the resonance band (125-130 ppm) attributed to unsubstituted aromatic carbons. In these coals the f_a values fall in the range 0.55-0.69 ± 0.03.

Dipolar dephasing data has been obtained on these coals. Figure 2 illustrates the spectral intensity (integrated intensity) of the aromatic

band of the Braztah coal as a function of the dipolar dephasing time. It is evident that more than one time constant is responsible for the spectral response. The rapidly decreasing intensity at τ values less than 40 μsec is due to CH carbons while larger values for τ (> 40 μsec) are due to nonprotonated aromatic carbons. The spectral response of the aliphatic region displays what appears to be a single time constant.

Figure 4 shows the spectral changes associated with dipolar dephasing times ranging from 0-120 μsec. As previously discussed, spectral lines arising from CH and CH_2 carbons will be absent in spectra obtained with dipolar dephasing times of 40 μsec or more. The peak at 30 ppm (marked as "a") in the 40-120 μsec spectra does not decay with the same time constant as CH or CH_2 carbons studied in crystalline solids. Two explanations for this behavior are possible: 1) the presence of t-butyl and/or gem-methyl groups or 2) CH_2 groups with unusually high degrees of motional freedom as might be expected from non-crystalline components of the coal.

The structural parameters obtained from the DD experiment are given in Table I. Within experimental error there is an increase in the fraction of total carbon that is protonated and aromatic with increasing rank. Conversely, the experimental value for the fraction of total carbon that is aliphatic (CH + CH_2) decreases with rank. In addition, the amount of methyl carbon appears to decrease with increasing rank although that variation may be insignificant.

A different basis for the calculation of structural parameters is presented in Table II. The parameters given are based on a fraction of aromatic or aliphatic carbons present in the coal. This presentation of the data emphasizes changes that occur in the aromatic or aliphatic carbons as opposed to the total carbon in the coal. Hence the distribution of three types of aromatic structural units Ar-H, Ar-R and Ar-Ar, (protonated aromatic substituted aromatic and aromatic bridgehead carbons) are obtained. It is noted that the Ar-H and Ar-R parameters for Wyodak coal are significantly different from the other two coals studied.

References

1. V.J. Bartuska, G.E. Maciel, J. Schaefer and E.O. Stejskal, Fuel, 56, 354 (1977).

2. V.J. Bartuska, G.E. Maciel and F.P. Miknis, "C-13 NMR Studies of Coals and Oil Shales," American Chemical Society, Div. of Fuel Chemistry, Preprints, 23 (1978).

3. K.W. Zilm, R.J. Pugmire, D.M. Grant, W.H. Wiser and R.E. Wood, Fuel, 58, 11 (1979).

4. K.W. Zilm, R.J. Pugmire, S.R. Larter, J. Allen and D.M. Grant, Fuel, 60, 717 (1981).

5. R.J. Pugmire, K.W. Zilm, D.M. Grant, S.R. Larter, J. Allen, A. Davis, W. Spackman and J. Sentfle, New Approaches in Coal Chemistry, ACS Symposium Series No. 169, 23 (1981).

6. S.J. Opella and M.H. Fry, J. Amer. Chem. Soc., 101, 5854 (1979).

7. S.J. Opella, M.H. Fry and T.A. Cross, J. Amer. Chem. Soc., 101, 5856 (1979).

8. E.W. Hagaman and M.C. Woody, Proceedings of the International Conference on Coal Science, Dusseldorf, September, 1981, pp 34-38.

9. F.P. Miknis, N. Sullivan, V.J. Bartuska, G.E. Maciel, Org. Geochem., 3, 19 (1981).

10. V.L. Winberg, T.F. Yen, B.C. Gerstein, D.D. Murphy, Fuel Div., Preprints, Amer. Chem. Soc., 26, 816 (1981).

11. D.W. Kuehn, A. Davis, R.W. Snyder, M. Starsunic, P.C. Painter, J. Haven and J.L. Koenig, Fuel Div., Preprints, Amer. Chem. Soc., 27 (2), 55 (1982).

12. L.B. Alemany, R.J. Pugmire, D.M. Grant and T.D. Alger, Cross Polarization and Magic Angle Spinning NMR Spectra of Model Organic Compounds III. The Effect of the Dipolar Interaction on Cross Polarization and Carbon-Proton Dephasing, manuscript in preparation, submitted to J. Amer. Chem. Soc.

13. E.F. Rybaczewski, B.L. Neff, J.S. Waugh and J.S. Sherfinski, J. Chem. Phys., 67, 1231 (1977)

14. B. Bodenhausen, R.E. Stark, D.J. Ruben and R.G. Griffin, Lett., 67, 424 (1979).

15. M.G. Munowitz, R.G. Griffin, G. Bodenhausen and T.H. Huang, J. Amer. Chem. Soc., 103, 2529 (1981).

16. M.A. Wilson, R.J. Pugmire, N.J. Russel and D.M. Grant, Structure of Australian Oil Shales and Solvent Refined Coal as Revealed by ^{13}C CP/MAS Studies, manuscript in preparation.

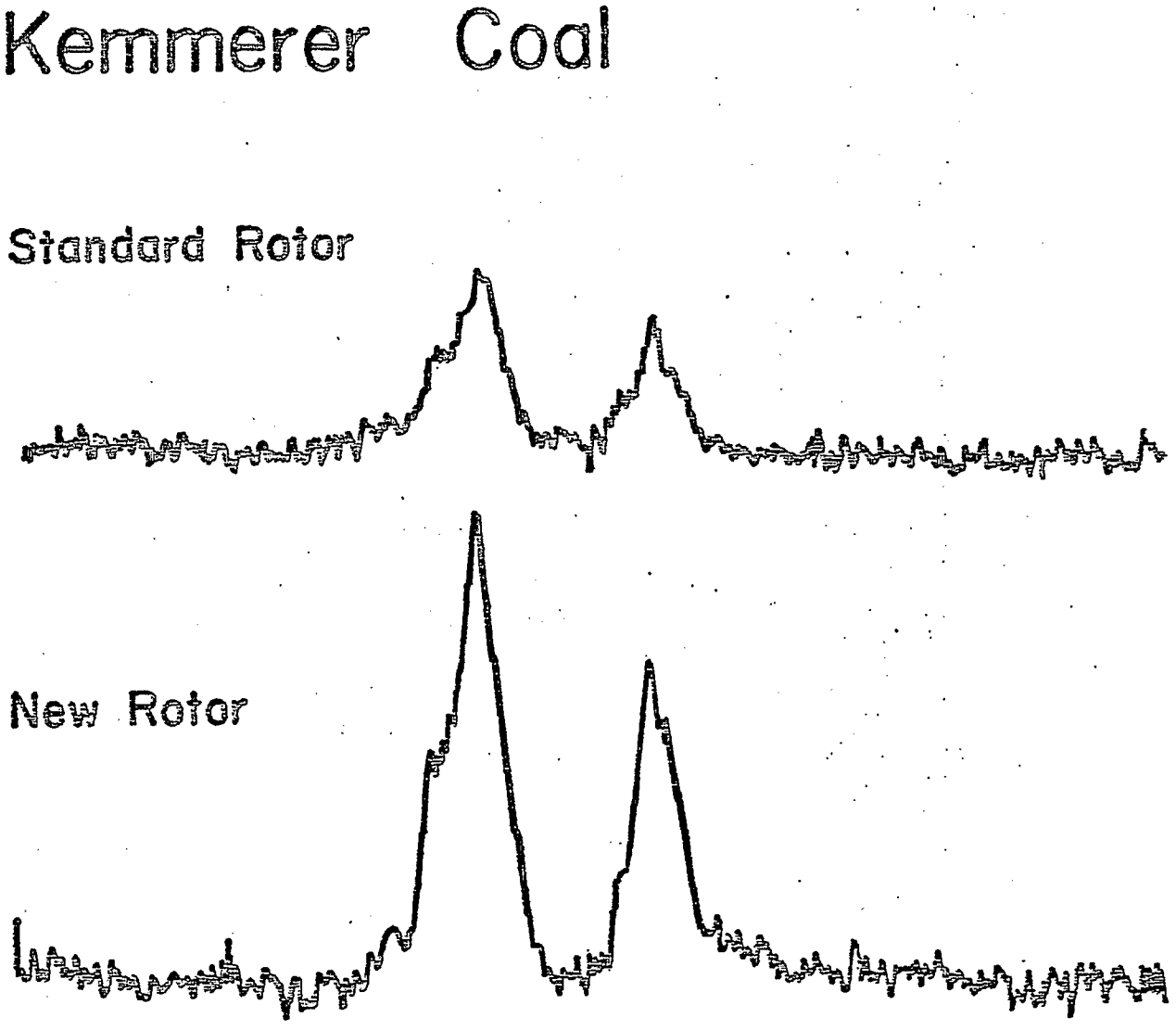

Figure 1. Comparison of spectra obtained in one minute on Kemmerer coal using our standard rotor and the new prototype rotor. The S/N is 2.6 fold greater in the lower trace representing a 6.8 fold savings in time to acquire a comparable spectrum.

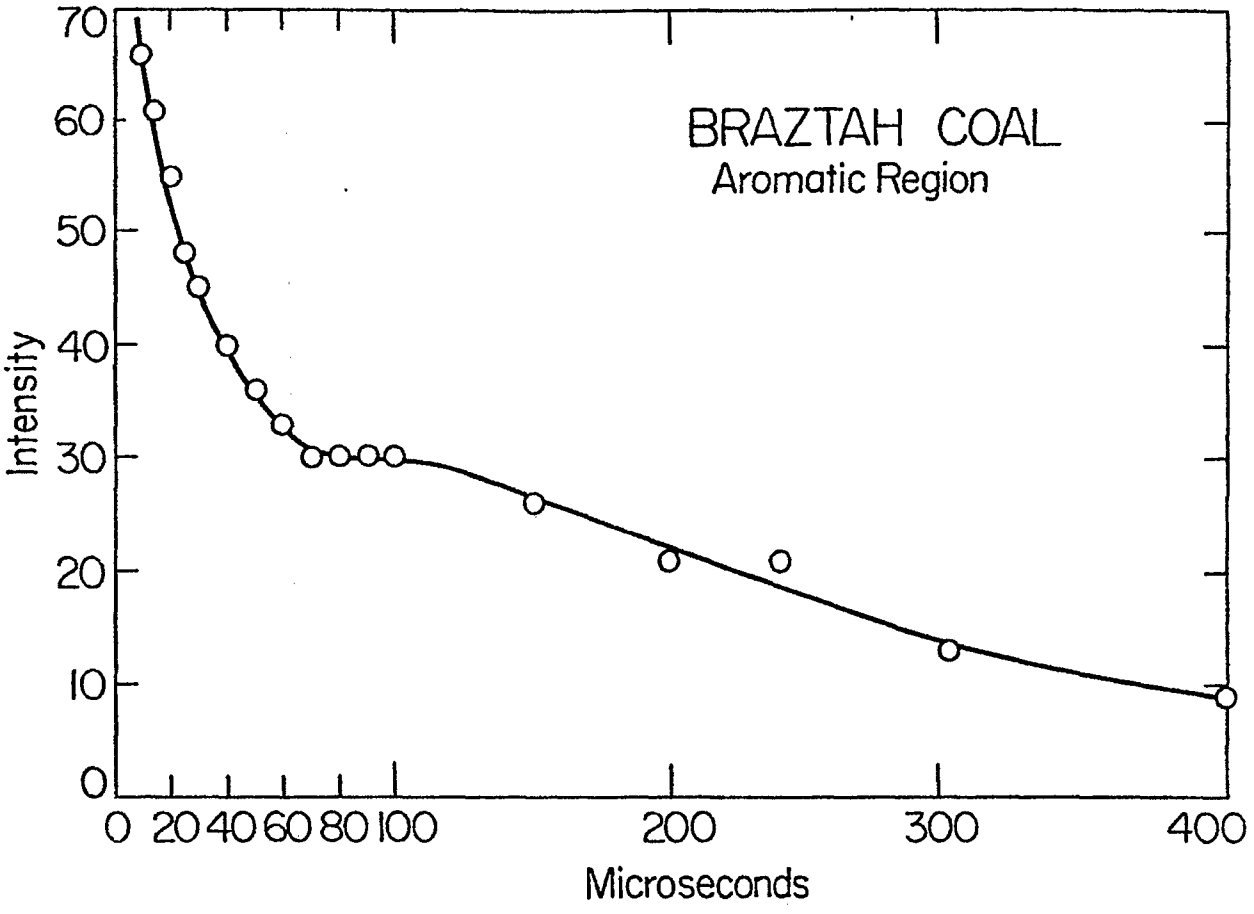

Figure 2. Spectral response as a function time of dipolar interaction of the aromatic carbon region.

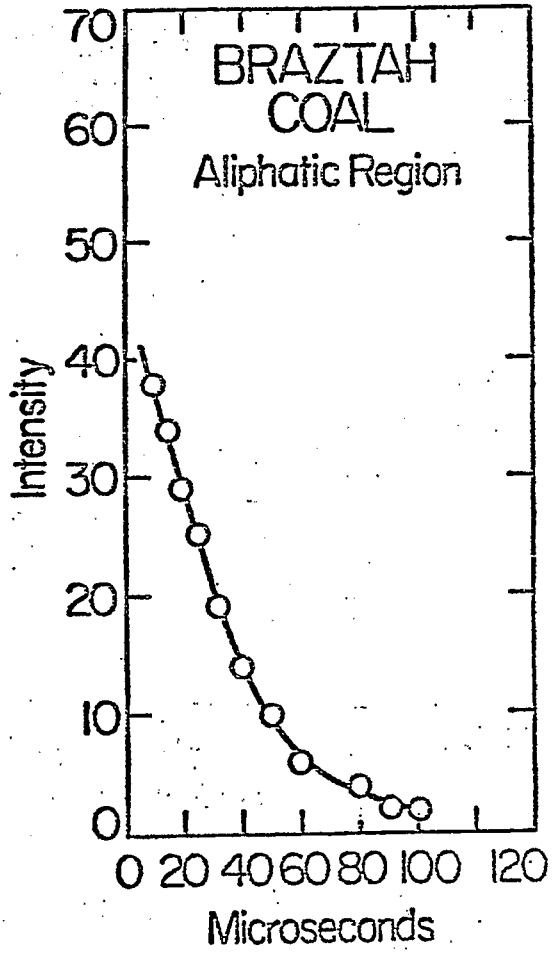

Figure 3. Spectral response of aliphatic carbons with variation of dephasing time.

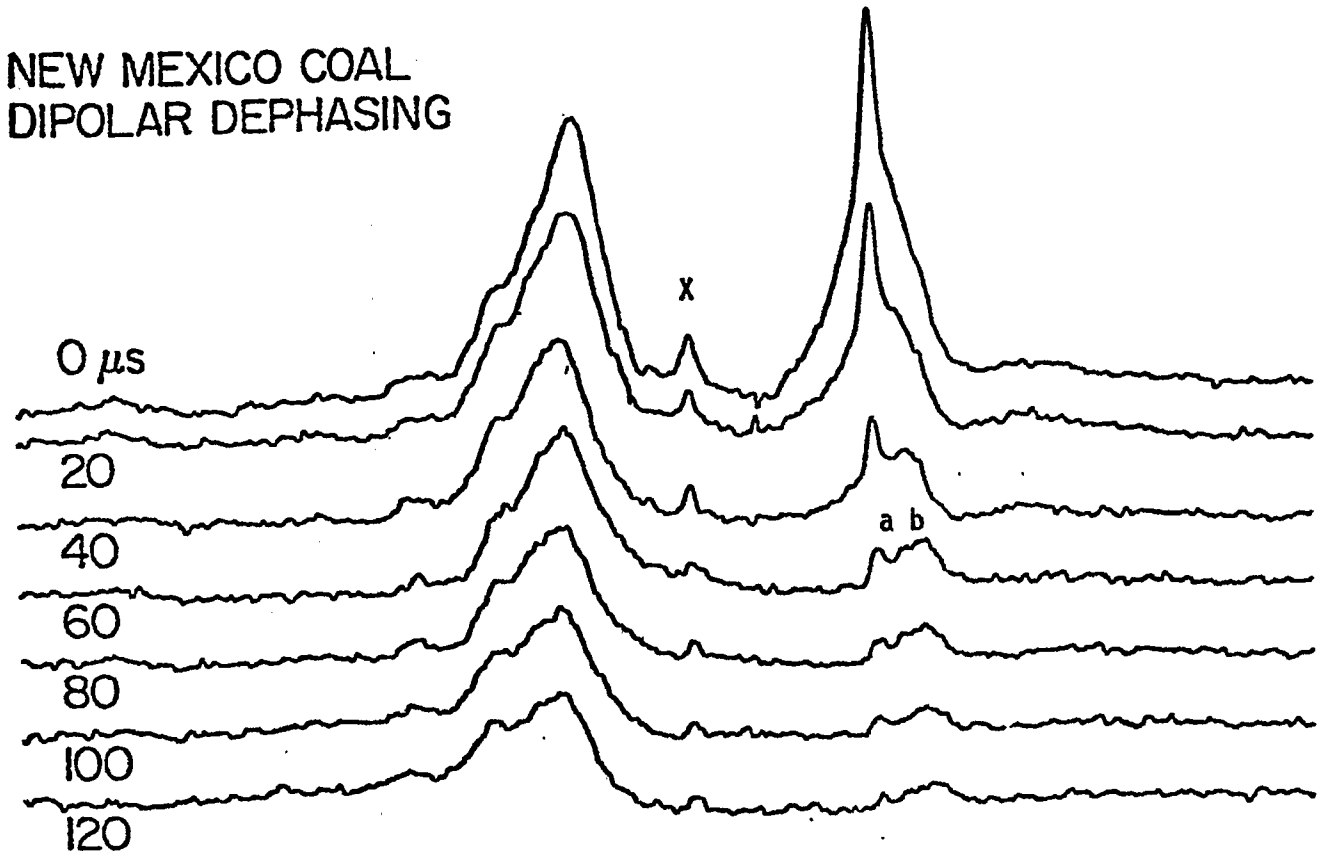

Figure 4. Dipolar dephasing spectra of New Mexico coal. The peak at 30 ppm, and marked a "a", decays with a time constant similar to that of the band ("b") due to methyl carbons. "X" arises from the delrin base of the composite rotor used for this experiment.

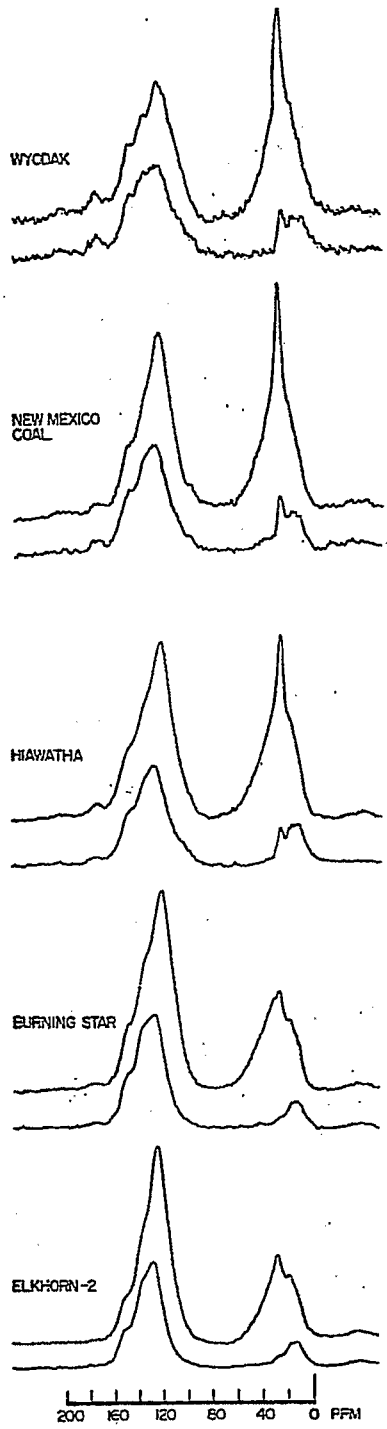

Figure 5. Dipolar dephasing data for coals studied. Upper trace is CP/MAS spectrum, 10,000 transients, 1 msec mixing time, and 300 msec recycle time, 1 K data points zero filled to 2 K. Bottom trace taken under the same conditions except a 40 μsec interruption in the proton decoupling pulse is inserted prior to FID acquisition.

TABLE I. STRUCTURAL PARAMETERS BASED ON TOTAL CARBON IN COAL

Sample	f_a	f_a^H	f_a^N	f_a^S	f_a^B	f_s^H	f_s^*
Wyodak	0.55	0.16	0.39	0.23	0.16	0.33	0.12
New Mexico	0.56	0.22	0.34	0.19	0.15	0.36	0.08
Hiawatha	0.60	0.25	0.35	0.18	0.17	0.30	0.10

$f_a + f_s = 1$

$f_a = f_a^H + f_a^N = f_a^H + f_a^S + f_a^B$

$f_s = f_s^H + f_s^N$

f_s^* = non-protonated aliphatic carbons plus methyl carbons.

TABLE II. STRUCTURAL PARAMETERS

Sample	Ar-H[a]	Ar-R[a]	Ar-Ar[a]	R-H[b]	$R-CH_3$[b]
Wyodak	0.28	0.42	0.29	0.74	0.26
New Mexico	0.40	0.34	0.27	0.81	0.19
Hiawatha	0.41	0.31	0.28	0.74	0.26

a = fraction of aromatic structure

b - fraction of aliphatic structure

Task 3

Catalysis and Mechanism of Coal Liquefaction

Faculty Advisor: D.M. Bodily
Graduate Student: Tsejung Ray

Introduction

Metal halides such as $ZnCl_2$ are well-known to be active catalysts for coal hydrogenation. Zinc chloride has been shown to be a very effective catalyst for coal hydrogenation in the entrained-flow reactor developed at the University of Utah.[1,2] Bell and co-workers[3-5] have studied the reactions of model compounds with $ZnCl_2$ under conditions similar to those employed in coal hydrogenation. They observed cleavage of C-O and C-C bonds in the model compound and proposed that the active catalytic species is a Bronsted acid formed $ZnCl_2$.

Shibaoka, Russell and Bodily[6] proposed a model to explain the liquefaction of coal, based on microscopic examination of the solid products from metal halide catalyzed coal hydrogenation. The model involves a competition between hydrogenation and carbonization reactions. The hydrogenation process starts at the surface of vitrinite particles and progresses toward the center. The vitrinite is converted to a plastic material of lower reflectance, which is the source of oils, asphaltenes and preasphaltenes. Concurrently, carbonization occurs in the center of the particles, resulting in vesiculation and a higher reflectance material. The partially carbonized material can be hydrogenated at later stages, but at a lower rate than the original coal.

Thermal and/or catalytic bond rupture occurs during the liquefaction process. The initial products of the bond cleavage reactions may be stabilized by hydrogen addition, resulting in cleavage of bridges between aromatic ring systems and in dealkylation of aromatic rings. If the initial products of the reaction are not stabilized, they may polymerize to form semicoke-like material. This primary semicoke may be isotropic or exhibit a fine-grained anisotropic mosiac texture, depending on the rank of the coal. The plastic material formed by stabilization of the initial products may be further hydrogenated or, under hydrogen deficient conditions, may form secondary semicoke. The secondary semicoke is of medium to course-grained anisotropic mosiac texture. Bodily and Shibaoka[7] used this model to explain the nature of the residues from hydrogenation in the short-residence, entrained-flow hydrogenation reactor. The role of the $ZnCl_2$ catalyst is examined in this study.

Project Status

The short reaction time reactor was tested for heat-up times and temperature control. Coal samples were analyzed by scanning electron microscopy and electron microprobe analysis. Mapping of the zinc and chlorine distributions with the electron microprobe were unsuccessful. The $ZnCl_2$ was removed during the polishing of grain mounts.

Future Work

The polishing of grain mounts using a minimum of water contact will be attempted. The studies of the effect of $ZnCl_2$ on the softening of coal and the reactivity to hydrogenolysis will begin.

References

1. R.E. Wood and W.H. Wiser, Ind. Eng. Chem., Proc. Design Devel., 15, 144 (1976).
2. J.M. Lytle, R.E. Wood and W.H. Wiser, Fuel, 59, 471 (1980).
3. D.P. Mobley and A.T. Bell, Fuel, 58, 661 (1979).
4. N.D. Taylor and A.T. Bell, Fuel, 59, 499 (1980).
5. D.P. Mobley and A.T. Bell, Fuel, 59, 507 (1980).
6. M. Shibaoka, N.J. Russell and D.M. Bodily, Fuel, 61, 201 (1982).
7. D.M. Bodily and M. Shibaoka, Fuel, submitted.
8. R. Yoshida and D.M. Bodily, Preprints, Fuel Chem. Div., Am. Chem. Soc., 24 (2), 371 (1979).

Task 3

Catalysis and Mechanism of Coal Liquefaction

Faculty Advisor: D.M. Bodily
Graduate Student: Jason Miller

Introduction

The hydroliquefaction of coal may be characterized by a mechanism which involves the initial rupture of covalent bonds to form reactive intermediates. These intermediates may be stabilized by hydrogen transfer to form lower molecular weight products or they may polymerize to form insoluble char or coke. Metal halides such as zinc chloride have been shown to be active in the bond scission stage of the reaction where as many catalysts are active only in stabilizing the intermediates, often by regenerating a hydrogen donor. The combination of thermal and catalytic reactions occurring simultaneously results in a complicated reaction mechanism. The chemistry of $ZnCl_2$ will be studied with model compounds and coal by such reactions as hydrogen transfers, cleavage of specific bonds and interaction with π electron systems.

A high performance liquid chromatograph, HPLC, will be used to analyze liquid products of the reactions under study. Further characterization of the products will be by nuclear magnetic resonance, NMR, structural analysis and vapor pressure osmometry.

Project Status

All experimental measurements have been completed with the exception of gas chromatography-mass spectrometry measurements. A literature survey has been completed.

Future Work

The gas chromatography-mass spectrometry studies will be completed and the results of all experiments interpreted. A thesis will be completed and also issued as a report.

Task 5

The Mechanims of Pyrolysis of Bituminous Coal

Faculty Advisor: W.H. Wiser
Graduate Studnet: J.K. Shigley

Introduction

In the present state of knowledge concerning the fundamental chemistry of coal liquefaction in the temperature range 375-550°C, the liquefaction reactions are initiated by thermal rupture of bonds in the bridges joining configurations in the coal, yielding free radicals. The different approaches to liquefaction, except for Fischer-Tropsch variations, represent ways of stabilizing the free radicals to produce molecules. The stabilization involving abstraction by the free radicals of hydrogen from the hydro-aromatic structures of the coal is believed to be the predominant means of yielding liquid size molecules in the early stages of all coal liquefaction processes, except Fischer-Tropsch variations. The objective of this research is to understand the chemistry of this pyrolytic operation using model compounds which contain structures believed to be prominant in bituminous coals.

Project Status

The problems encountered with the apparent limitations of the gas chromatograph's oven when using 1/4" stainless steel columns have been solved. It was discovered after considerable consultation with Perkin-Elmer engineers and experimentation that the oven is not capable of heating ten-foot by 1/4" stainless steel columns at 40°C/min. The highest heating rate the oven is capable of heating the 1/4" column is 20°C/min.

The calibration of the outlet splitter has been completed with some very surprising results. After numerous repetitions to insure that the results were accurate, it appears that the split ratio is dependent on the sample size injected. This is true for all seven prospective reaction products of 9-benzyl-1,2,3,4-tetrahydrocarbazole: benzene, toluene, bibenzyl, diphenylmethane, 1,2,3,4-tetrahydrocarbazole, carbazole and the starting material.

Future Work

Future spot checks will be made on the outlet splitter to insure its consistency and to check previous results. Pyrolysis experiments will be conducted with stable compounds to determine if consistent material balances can be made on the system. Problems from these tests will be addressed as they arise.

Task 6

Catalytic Hydrogenation of CD Liquids and Related Polycyclic Aromatic Hydrocarbons

Faculty Advisor: J. Shabtai
Research Associate: C. Russell

Introduction

The main objective of this research project is to develop a versatile process for controllable hydrotreating of highly aromatic coal liquids, viz., a process permitting production of naphthenic-aromatic feedstocks containing variable relative concentrations of hydroaromatic vs. aromatic ring structures. Such feedstocks, including the extreme case of a fully hydrogenated coal liquid, are suitable starting materials for catalytic cracking, as applied for preferential production of light liquid fuels. The overall objective of this project and of a parallel catalytic cracking study is, therefore, to develop and optimize a hydrotreating-catalytic cracking process sequence for conversion of coal liquids into conventional fuels.

The present project includes also a study of metal sulfide-catalyzed hydrogenation of model polycyclic arenes present in coal liquids, e.g., phenanthrene, pyrene, anthracene and triphenylene, as a function of catalyst type and experimental variables.[1] This part of the study provides basic information on the rate, mechanism and stereochemistry of hydrogenation of structurally distinct aromatic systems in the presence of sulfided catalysts.

Project Status

The systematic study of the stepwise hydrogenation of chrysene (1) in the presence of sulfided Ni-Mo, Ni-W, and Co-Mo catalysts (see DE/ET/14700-6, Task 8) has been resumed. Partially hydrogenated reaction intermediates, e.g., 1,2,3,4-tetrahydrochrysene, two isomeric octahydrochrysenes, and 1,2,3,4,5,6,7,8,9,10,17,18-dodecahydrochrysene, were identified by a combination of gas chromatography and mass spectrometry. The kinetics of the stepwise hydrogenation reaction is presently being investigated in the temperature range of 225-375°C.

In a parallel study the kinetics of hydrogenation of an SRC-II distillate (b.p. range 230-455°C) is being determined. This study is simultaneously providing data on the kinetics of hydrodenitrogenation and hydrodeoxygenation (Task 7) of a typical coal liquid in the range of 200-375°C. The dependence of chrysene hydrogenation kinetics upon sulfided catalyst type, including newly prepared catalysts (Task 10) is also being determined.

Future Work

The study of hydrogenation kinetics of a typical coal liquid (SRC-II middle-heavy distillate) and of tetracyclic model compound, i.e., chrysene, will be continued and completed.

Reference

1. J. Shabtai, C. Russell, L. Veluswami and A.G. Oblad, to be published.

Task 7

Denitrogenation and Deoxygenation of CD Liquids and Related N- and O- Compounds

Catalytic Hydrodeoxygenation of Coal-Derived Liquids and Related Oxygen-Containing Compounds

Faculty Advisors: J. Shabtai
A.G. Oblad
Graduate Student: G. Haider

Introduction

Coal-derived liquids are characterized by the presence of a considerable concentration of oxygen-containing components. Therefore, a systematic catalytic hydrodoxygenation (HDO) study of coal-derived liquids and related model compounds is being carried out. The study provides information not only on the mechanism of HDO as related to catalytic upgrading of coal liquids, but also on the role of oxygen-containing compounds in primary coal liquefaction processes.

Project Status

In a previous report (DE/ET14700-8) data were provided on the change in elemental composition and H/C atomic ratio of HDO products obtained from an SRC-II distillate (Bp 230-455°C) as a function of hydrotreatment temperature and sulfided catalyst type.

The present report provides data on the change of infrared absorption maxima of hydrotreatment products from the same SRC-II distillate as a function of temperature and catalyst type. The SRC-II distillate and hydrotreated products obtained from it were analyzed by infrared (IR) spectroscopy. The infrared spectrum of the SRC-II distillate used as feed in the hydrotreatment experiments is given in Figure 33, with proper indication of absorption bands in the O-H stretching, C-O stretching, C-H stretching and aromatic C-H out-of-plane bending regions (3200-3700 cm^{-1}, 1000-1300 cm^{-1}, 2800-3100 cm^{-1} and 600-900 sm^{-1}, respectively). The positions of absorption maxima and corresponding structural assignments are summarized in Table 25. The strong O-H stretching band near 3590 cm^{-1} is attributed to nonassociated phenols, e.g.

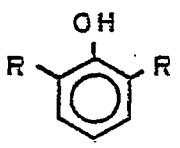

(2,6-dialkylphenol)

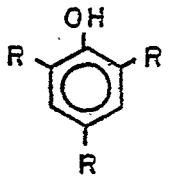

(2,3,6-trialkylphenol)

The weaker band at 3550 cm^{-1} is assigned to single-bridge intramolecular complexes, e.g.,

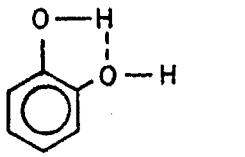

(1,2-dihydroxygenzene)

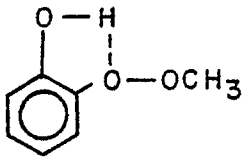

(o-methoxyphenol)

The medium O-H stretching band at 3465 cm^{-1} is most likely due to single or double-bridge intermolecular association of partly hindered phenols, e.g., 2-alkylsubstituted phenols,

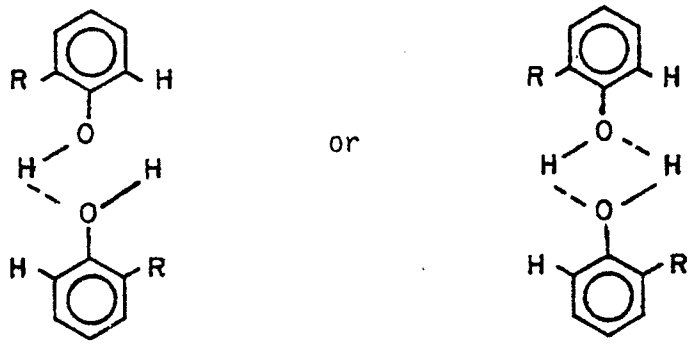

The broad O-H stretching bands in the 3200-3400 cm^{-1} range indicate the presence of polymeric association of sterically unhindered phenols. The degree of association may depend to some extent upon the dilution of the SRC-II sample in the solvent (CS_2), but it is probably due mainly to the inherent steric-structural characteristics of different coal-liquid phenolic components capable of forming polymeric associations by H-bonding. It should be noted that N-H stretching absorptions could also appear in the 3300-3500 cm^{-1} range. In particular, heterocyclic N-H stretching bands may overlap and contribute to the observed absorption band near 3450 cm^{-1}. However, for the purpose of the present study, N-H stretching absorption bands were neglected in view of the lower intensities of such bands (relative to those of O-H stretching bands) as well as due to the much lower nitrogen content (as compared to oxygen content) of the examined products. The medium-strong stretching bands at 1267 and 1237 cm^{-1} are assigned to aryl ethers. The presence of aryl ethers is also confirmed by the C^{13} NMR spectral data (vide infra). The medium C-O stretching band at 1148 cm^{-1} is tentatively assigned to benzofuran structures.

No absorption bands due to carbonyl functional groups were observed in the SRC-II distillate used as feed in this study. Although stretching bands between 1700-1740 cm^{-1}, due to carbonyl groups, were previously detected in IR spectra of coal extracts obtained under very mild conditions (100-200°C), it is probable that such groups undergo fast chemical transformations under the severe liquefaction conditions of the SRC-II process.

Table 25 contains also assignments of absorption bands due to CH stretching and (aromatic) C-H out-of-plane bending vibrations in the 2800-3100 cm^{-1} and 650-900 cm^{-1} range, respectively. While the C-H stretching bands near 2960, 2920 and 2860 provide information on the concentration of CH_3, CH_2 and CH groups in the samples, the C-H out-of-plane bending bands in the 650-900 cm^{-1} range allow for evaluation of different aromatic substitution types in the product components. Thus, the strong band at 805 cm^{-1} indicates the presence of aromatic rings with two and/or three adjacent hydrogens as the preferred ring substitution type, e.g.,

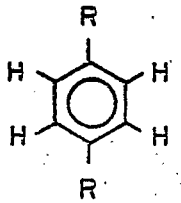

1,4-disubstituted monocyclic aromatics

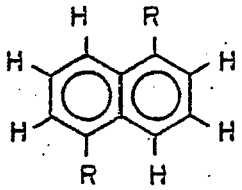

1,2,3-trisubstituted rings in bicyclic aromatics

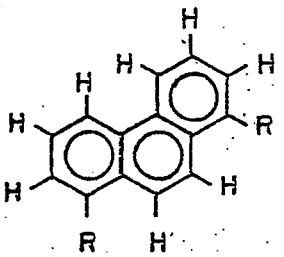

1,2,3-trisubstituted and 1,2,3,4-tetrasubstituted rings in polycyclic aromatics, e.g. 1,8-disubstituted phenanthrenes, etc.

The minor absorption bands in the 860-900 cm^{-1} range indicate that alternative possible substitution types, in which (in addition to the two or three adjacent hydrogens) there is also a single (lone) hydrogen in the aromatic ring, are apparently of lesser importance. Such less favored structural types include 1,3-disubstituted benzenes, 2,6-disubstituted naphthalenes, 2,7-disubstituted phenanthrenes, etc. The strong band at 740 cm^{-1} is attributed to C-H out-of-plane bending in mono- and o-disubstituted aromatic rings, and the strong band at 690 cm^{-1} is assigned to C-H out-of-plane bending of monosubstituted rings.

Figure 34 summarizes the change in relative intensities of OH stretching bands as a function of reaction temperature between 200-370°C, using sulfided Co-Mo/Al_2O_3 as catalyst. As seen, at 200°C there is a slight increase in the intensity of the 3590 cm^{-1} band. This may be a result of very limited extent of hydrogenolysis of highly substituted phenolic ethers to yield nonassociated phenols. Between 200-260°C, there is a minor decrease in the intensity of the 3590, 3550 and 3465 cm^{-1} bands, while the bands in the range of 3200-3400 cm^{-1}, due to polymerically associated phenols, decrease to a significant extent. At 290°C there is noticeable decrease in the intensity of the 3590 and 3550 cm^{-1} bands, and the decrease becomes marked at 320°C. The only presisting band at 350°C is that at 3465 cm^{-1}

(intermolecular single- or double-bridged phenolic complexes; vide supra). This band persists even at 370°C, and is illustrative of phenolic components showing resistance to HDO even under severe experimental conditions.

Figure 35 shows the change in intensity of O-H stretching bands as a function of reaction temperature (230-370°C), using sulfided Ni-W/Al_2O_3 as catalyst. As seen, at 230°C there is slight increase in the intensity of the3590 cm^{-1} band, as in the case with the sulfided Co-Mo catalyst. Between 200-260°C there is only a minor decrease in the intensity of the 3590, 3550 and 3465 cm^{-1} bands while the band in the region 3200-3400 cm^{-1} decreases to a significant extent and is completely removed at 290°C. Above 260°C, there is also a gradual decrease in the intensity of the 3590, 3550 and 3465 cm^{-1} bands, and these bands disappear completely at 350°C.

Comparison of Figures 34 and 35 shows that the changes in the intensities of O-H stretching bands follow a similar pattern with both catalysts, e.g., sulfided Co-Mo/Al_2O_3 and sulfided Ni-W/Al_2O_3. However, there are some significant differences: (a) HDO of all types of phenols is somewhat faster with the Ni-W as compared with the Co-Mo catalyst. This is reflected in the essentially complete removal of phenolic components from the SRC-II distillate already at 350°C, while some phenolic types persist in the reaction with Co-Mo at 350°C and even 370°C; (b) the concentration of free phenols (3590 cm^{-1}) remains higher than that of single- or double-bridged bimolecular complexes (3465 cm^{-1}) with Ni-W as catalyst, whereas the opposite is observed with sulfided Co-Mo catalyst (with the latter catalyst the bimolecular phenolic complexes remain as the only HDO-resistant phenolic type at 350-370°C). The higher efficiency of the sulfided Ni-W catalyst for HDO of this type of phenols may be related to its higher ring hydrogenation activity. Thus, the HDO reaction with Ni-W may proceed via ring hydrogenation to the corresponding cyclohexanol, followed by fast (aliphatic) C-OH hydrogenolysis (See Ref. 1). This assumption is consistent with previous above results indicating that HDO with Ni-W as catalyst is associated with higher hydrogen consumption per gram atom of oxygen removed, in comparison with that in the presence of Co-Mo as catalyst.

Figure 36 summarizes the change in relative intensities of C-O stretching bands as a function of reaction temperature in the range 200-370°C, using sulfided Co-Mo/Al_2O_3 as catalyst. As seen, there are negligible changes up to 260°C in the intensity of C-O stretching (see bands at 1267, 1237 and 1148 cm^{-1}). Between 290-370°C, there is gradual decrease in the intensity of these C-O stretching bands and they essentially disappear at 370°C. Among the C-O stretching bands, the band at 1267 cm^{-1}, apparently due to activated (e.g., m-substituted) aryl ethers, disappears fastest, whereas the bands at 1237 cm^{-1} (deactivated aryl ethers) and at 1148 cm^{-1} (benzofurans) are somewhat more persistant.

Figure 37 shows the change in relative intensities of C-O stretching bands as a function of reaction temperature in the range 230-370°C, using sulfided Ni-W/Al_2O_3 as catalyst. As seen, there are minor changes up to 290°C in the intensity of the C-O stretching bands at 1237 and 1148 cm^{-1}, whereas the band at 1267 cm^{-1} quickly disappears. The latter band may be due to m-substituted aromatic ethers which should be more susceptible to hydrodeoxygenation. Between 320-350°C, there is a sharp decrease in the intensity of the 1237 and 1148 cm^{-1} bands. At 370°C, the aryl ethers (1237 cm^{-1}) disappear, but alkyl ethers (bands near 1050 cm^{-1}) still persist.

Comparison of Figures 36 and 37 show similar trends in the changes of C-O stretching bands, but some differences are also observed. The sulfided Ni-W catalyst is more active for HDO of some of the aryl ethers (compare changes in the band intensity at 1267 cm^{-1}). On the other hand, sulfided Co-Mo catalyst seems to be much more effective for HDO of aliphatic ethers (bands near 1050 cm^{-1}).

The assignments of the bands in other regions, i.e., 2800-3100 cm^{-1} and 600-900 cm^{-1} are given in Table 25.

Figure 38 shows the change in intensity of C-H stretching bands as a function of reaction temperature in the range 200-370°C, using sulfided Co-Mo/Al_2O_3 as catalyst. As seen, between 200-290°C there is gradual decrease in the intensity of the 3050 cm^{-1} band with corresponding relative increase in the intensity of the 2920 cm^{-1} band. At 320°C, this change becomes quite significant. It is most likely due to saturation of aromatic rings in the feed. Above 320°C, the extent of ring hydrogenation apparently does not increase, due to the general displacement of hydrogenation-dehydrogenation equilibria in the direction of dehydrogenation. It is also noted that the intensities of the band near 2960 cm^{-1} (CH_3 groups) remain essentially unaffected up to 320°C. This indicates that at mild temperatures (up to 320°C) with Co-Mo/Al_2O_3 as catalyst methyl substituents do not undergo considerable reaction, e.g., ring dealkylation.

Figure 39 summarizes the change in intensity of C-H stretching bands as a function of reaction temperature in the range of 230-370°C, using Ni-W/Al_2O_3 as catalyst. Figure 39 shows that between 230-290°C, there is gradual increase in the intensity of the 2920 cm^{-1} band. As with the Co-Mo catalyst, this is probably a consequence of partial saturation of the aromatic rings. The band near 2960 cm^{-1} (CH_3 groups) remains unchanged up to 260°C, but then seems to decrease at higher temperatures (370°C) apparently due to ring hydrodemethylation (methyl group removal) reactions. These results are in agreement with the C^{13}NMR analysis of reaction products (vide infra).

Comparison of Figures 38 and 39 shows that the intensity of the C-H stretching (aromatic rings) bands near 3050 cm^{-1} decreases faster between 290-350°C and C-H stretching (CH_2 group) bands near 2920 cm^{-1} increases faster with the sulfided Ni-W catalyst as compared to the sulfided Co-Mo catalyst. This is obviously due to the difference in the ring hydrogenation-dehydrogenation activity of these catalysts.

Figure 40 shows the change in intensity of C-H out-of-plane deformation bands as a function of reaction temperature between 200-370°C, using sulfided Co-Mo/Al_2O_3 as catalyst. As seen, between 200-260°C there is essentially no change in the relative intensities of the bands between 650-900 cm^{-1}. However between 290-370°C there is a gradual decrease in the intensities of the bands at 805 cm^{-1} and at 830-860 cm^{-1} (polysubstituted aromatic rings) while the intensities of the bands at 740 cm^{-1} and 705 cm^{-1} (mono- and o-disubstituted aromatic rings) increase. The observation clearly indicates some extent of dealkylation reactions leading to lower ring substitution, as temperature is increased. This is in conformity with the C^{13}NMR data (next report). It is also noted that the overall intensity of the aromatic bands in the 650-900 cm^{-1} range decreases between 260-350°C due to ring saturation reactions. At 370°C the overall intensity of the 650-900 cm^{-1} bands starts to increase again due to displacement of the hydrogenation-dehydrogenation equilibria.

Figure 41 summarizes the changes in bands in the range 650-900 cm^{-1}, associated with C-H out-of-plane bending in the aromatic rings, as a function of reaction temperature (230-370°C), using sulfided Ni-W/Al_2O_3 as catalyst. As seen, the changes in relative band intensities follow the same patterns as in the hydrogenation experiments with sulfided Co-Mo, although the extent of hydrodealkylation seems to be slightly higher with the Co-Mo catalyst, while ring hydrogenation is somewhat more pronounced with the Ni-W catalyst. The results are again in agreement with C^{13}NMR data (next report) indicating that aromatics are partially saturated at lower temperatures, followed by partial dealkylation at still higher temperatures.

Future Work

A semi-batch autoclave for kinetic studies was constructed and put in operation. Kinetic HDO studies of coal-derived liquids and representative ethers, e.g., dibenzyl ether (1), diphenyl ether (6) and anisole (25) will be carried out.

Reference

1. G. Haider, Ph.D. Thesis, University of Utah, Salt Lake City, Utah 1981.

TABLE 25

ASSIGNMENTS OF INFRARED ABSORPTION MAXIMA[a] FOUND IN SPECTRA OF SRC-II MIDDLE-HEAVY DISTILLATE AND HYDROGENATION-HDO PRODUCTS

Absorption Maxima, cm^{-1}	Assignments
3590 (s)	-OH stretching (nonassociated phenols)
3550 (w)	-OH stretching (single-bridged intramolecular complexes)
3465 (m)	-OH stretching (single- or double-bridged intermolecular associations
3400-3200 (w)	-OH stretching (polymeric association, sterically unhindered phenols)
3050 (m)	CH stretching (aromatic rings)
3020 (m)	CH stretching (aromatic rings)
2960 (s)	CH stretching (CH_3 groups)
2920 (s)	CH stretching (CH_2 groups)
2860 (s)	CH stretching (CH_3, CH_2 and CH groups)
1267 (m)	C-O stretching (aryl ethers)
1237 (s)	C-O stretching (aryl ethers)
1148 (s)	C-O stretching (benzofurans)
860 (w)	CH out-of-plane bending (1,4-disubstituted; and/or 1,2,3,4-tetra-substituted aromatic rings)
830 (w)	CH out-of-plane bending (1,4-disubstituted; and/or 1,2,3,4-tetra-substituted aromatic rings)
805 (s)	CH out-of-plane bending (1,4-disubstituted; and/or 1,2,3,4-tetra-substituted aromatic rings)
740 (s)	CH out-of-plane bending (mono- and o-disubstituted aromatic rings)
705 (w)	CH out-of-plane bending (mono-substituted aromatic rings
690 (s)	CH out-of-plane bending (mono-substituted aromatic rings)

(a) (s)-strong; (m)-medium; (w)-weak band intensity.

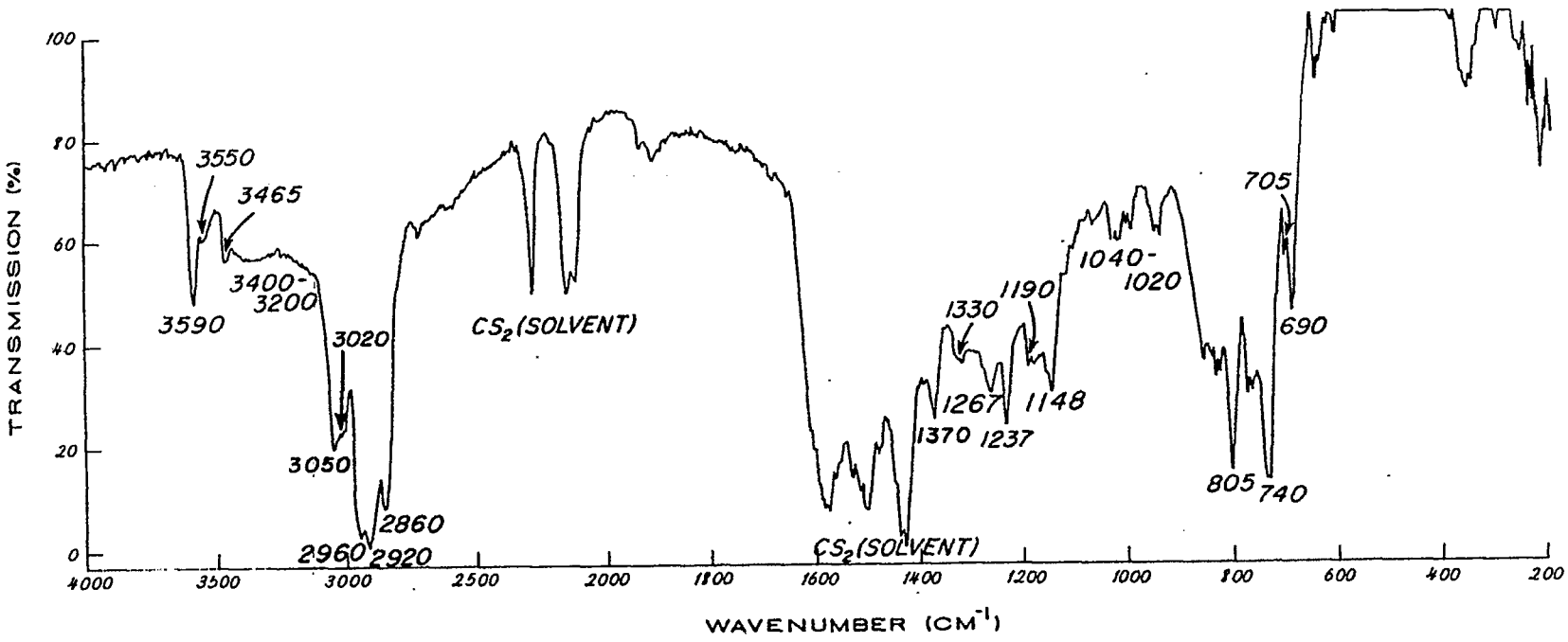

Figure 33. Infrared Absorption Maxima (cm^{-1}) of SRC-II Distillate (b.p. 230 - 455°C); Solvent CS_2.

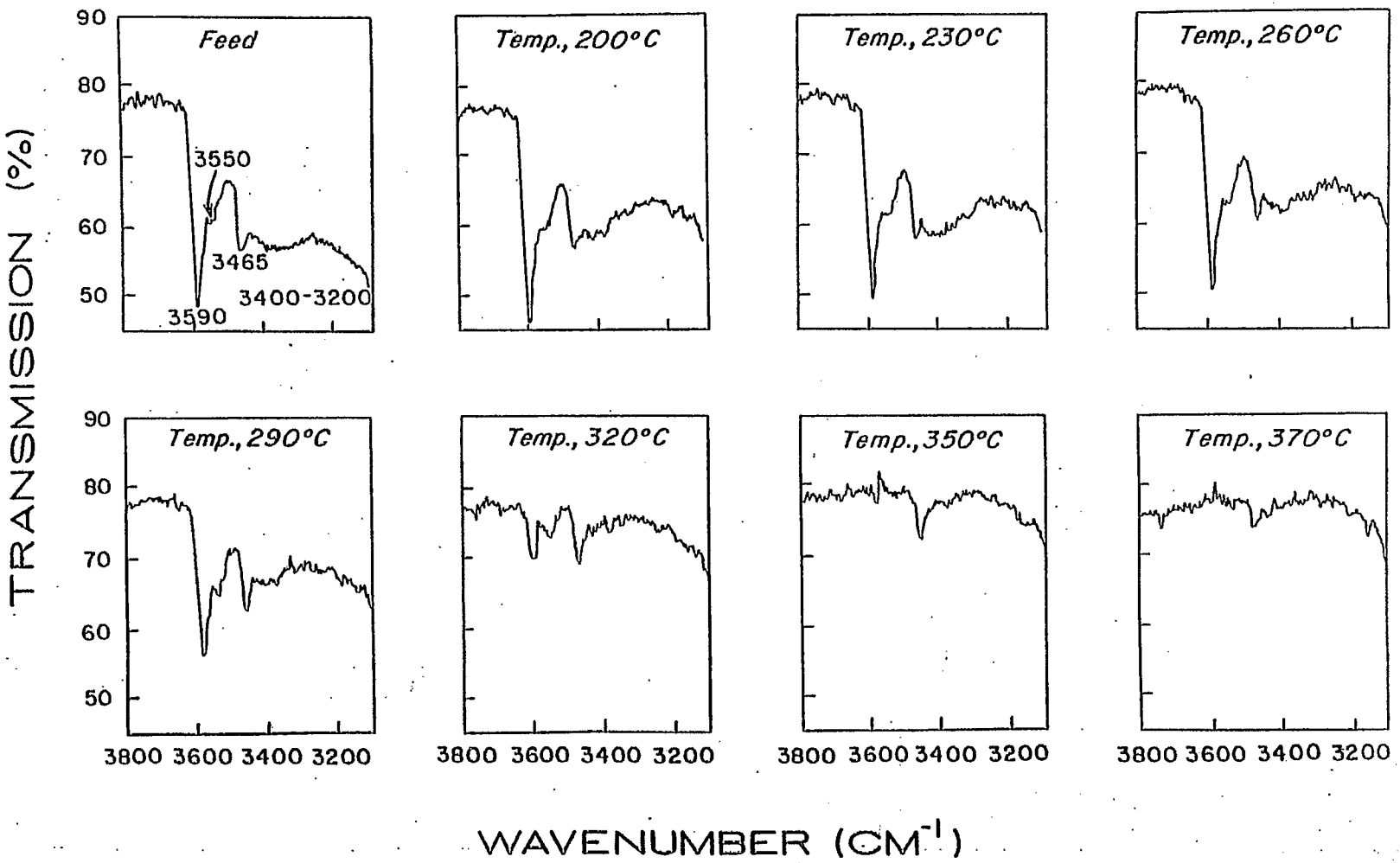

Figure 34. Change in Relative Intensities of O-H Stretching Bands of Product from Hydrodeoxygenation of SRC-II Distillate (b.p. 230 - 455°C) as a Function of Reaction Temperature (Hydrogen Pressure: 1750 psig; Reaction Time: 1 hr.; Catalyst: Sulfided Co-Mo/Al_2O_3).

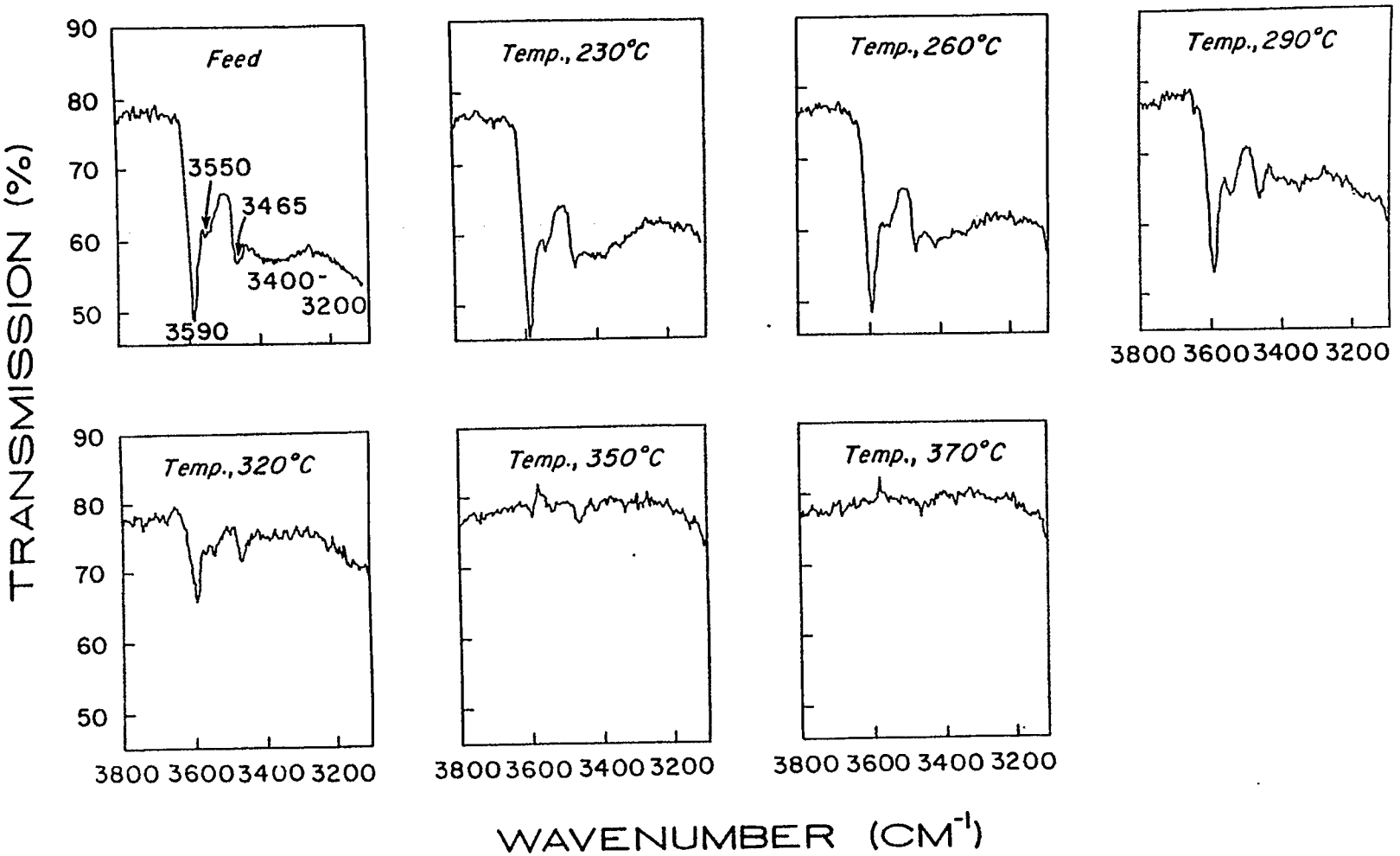

Figure 35. Change in Relative Intensities of O-H Stretching Bands of Product from Hydrodeoxygenation of SRC-II Distillate (b.p. 230 - 455°C) as a Function of Reaction Temperature (Hydrogen Pressure: 1750 psig; Reaction Time: 1 hr.; Catalyst: Sulfided Ni-W/Al_2O_3).

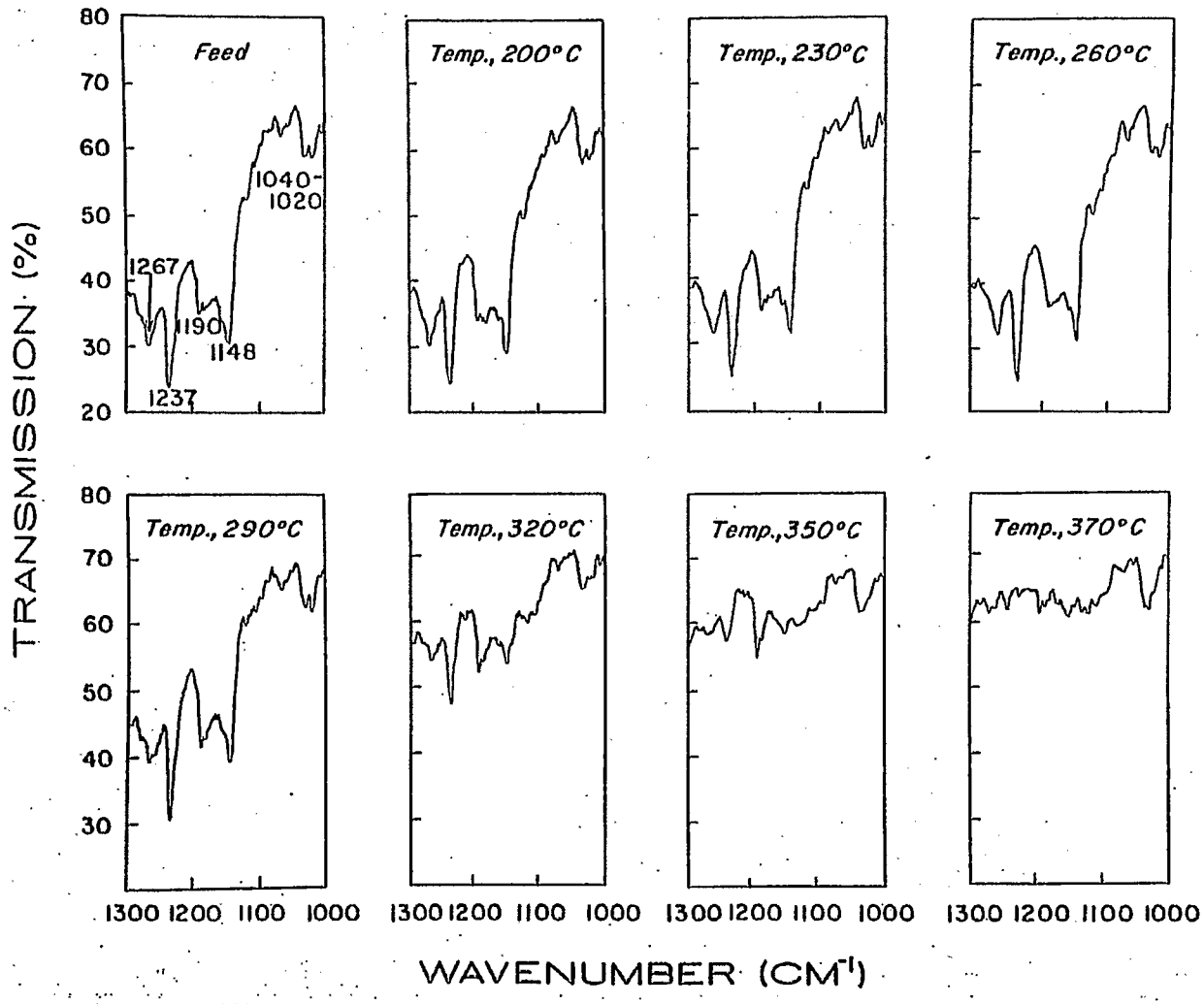

Figure 36. Change in Relative Intensities of C-O- Stretching Bands of Product from Hydrodeoxygenation of SRC-II Distillate (b.p. 230 - 455°C) as a Function of Reaction Temperature (Hydrogen Pressure: 1750 psig; Reaction Time: 1 hr.; Catalyst: Sulfided Co-Mo/Al_2O_3).

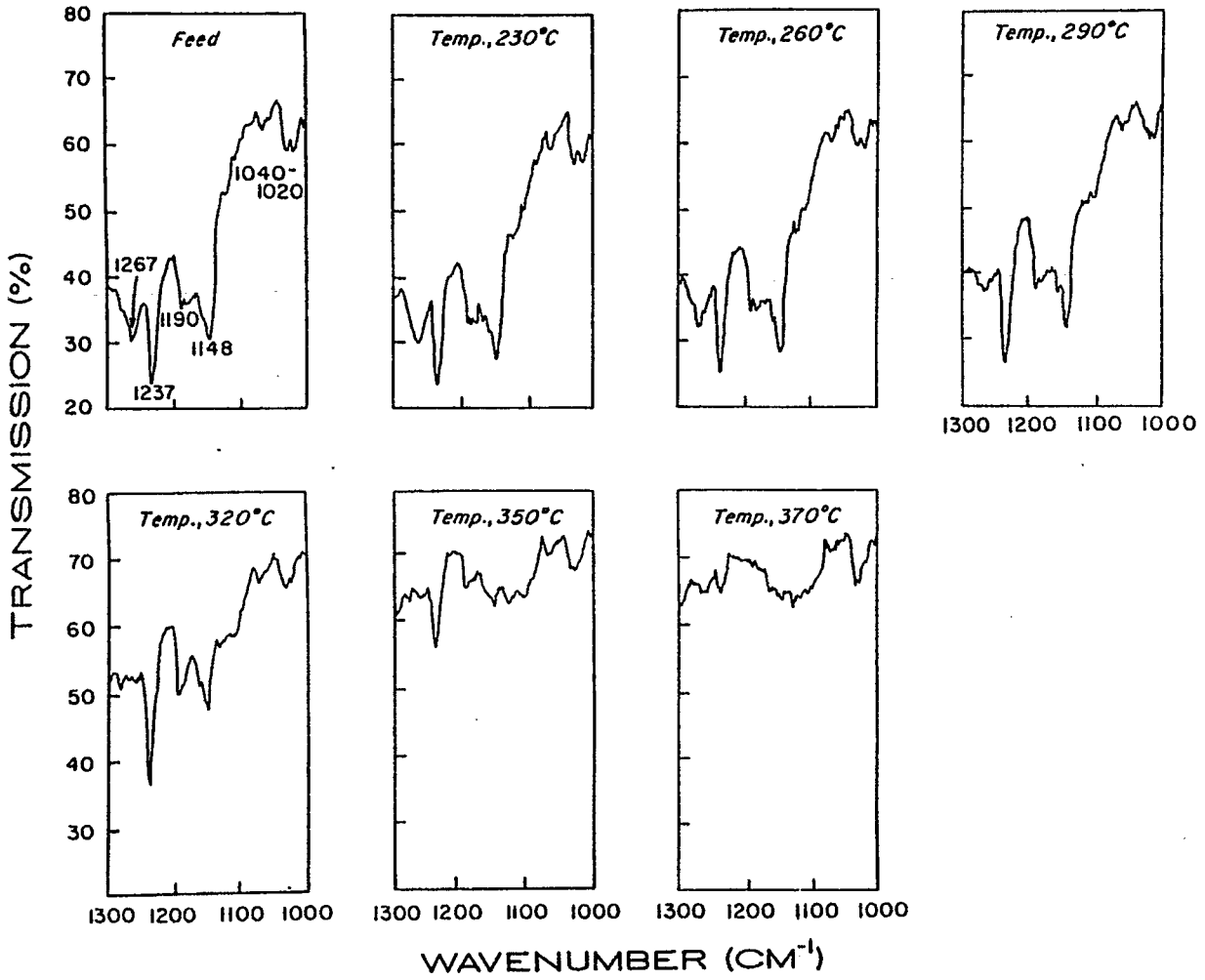

Figure 37. Change in Relative Intensities of C-O- Stretching Bands of Product from Hydrodeoxygenation of SRC-II Distillate (b.p. 230 - 455°C) as a Function of Reaction Temperature (Hydrogen Pressure: 1750 psig; Reaction Time: 1 hr.; Catalyst: Sulfided Ni-W/Al_2O_3).

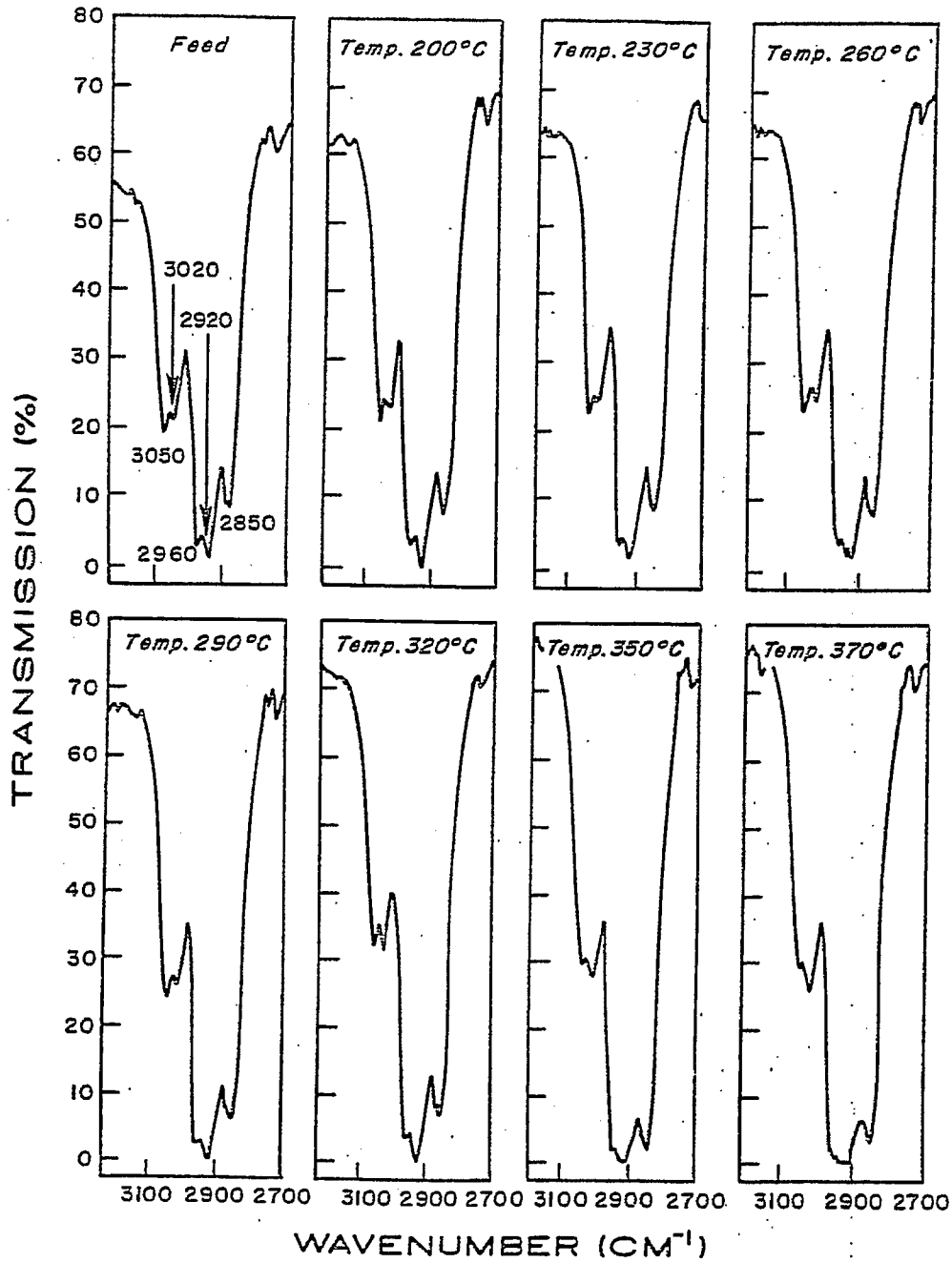

Figure 38. Change in Relative Intensities of C-H Stretching Bands (2800 - 3100 cm^{-1}) of Product from Hydrodeoxygenation of SRC-II Distillate (b.p. 230 - 455°C) as a Function of Reaction Temperature (Hydrogen Pressure: 1750 psig; Reaction Time: 1 hr.; Catalyst: Sulfided Co-Mo/Al_2O_3).

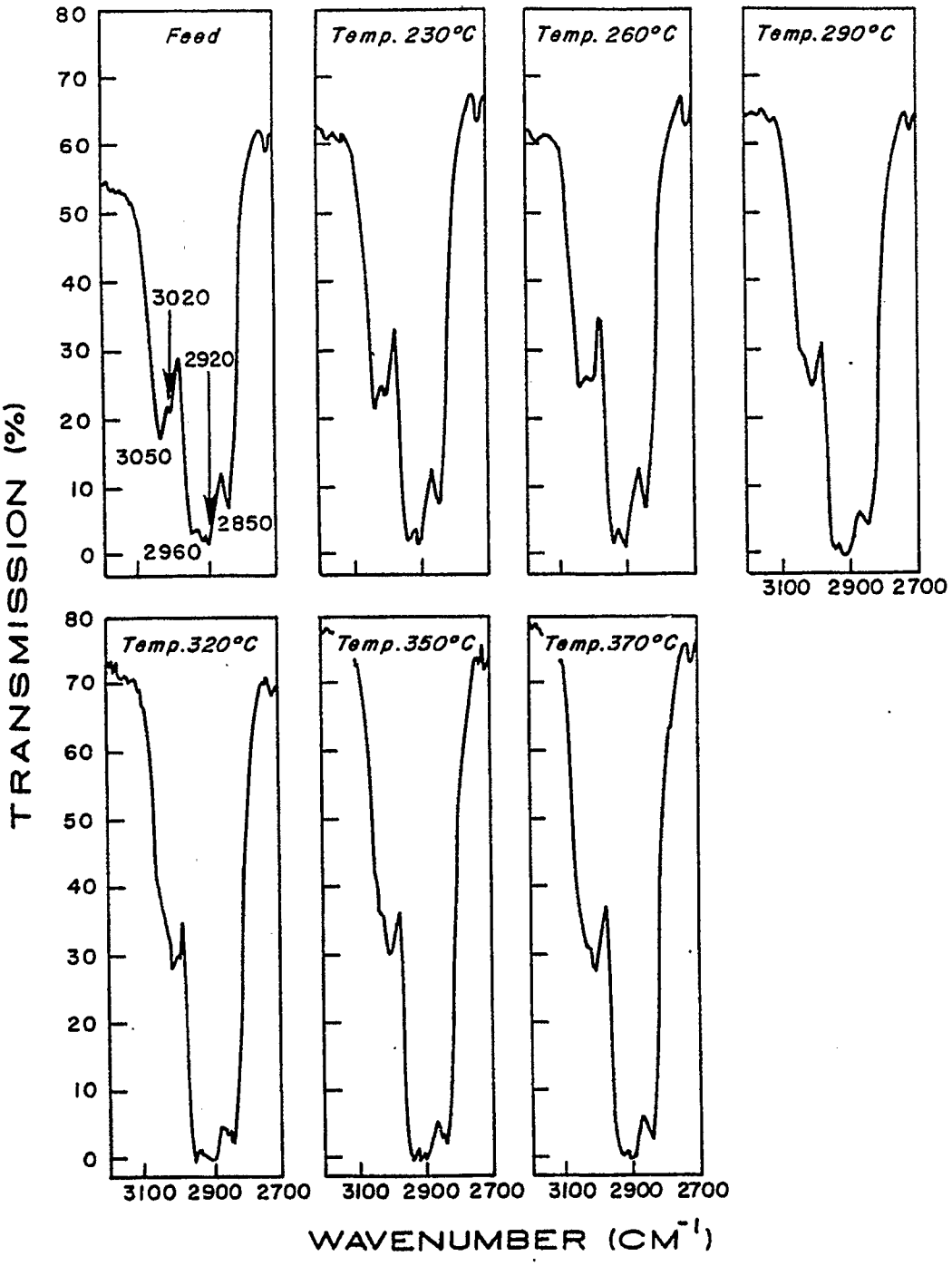

Figure 39. Change in Relative Intensities of C-H Stretching Bands (2800 - 3100 cm^{-1}) of Product from Hydrodeoxygenation of SRC-II Distillate (b.p. 230 - 455°C) as a Function of Reaction Temperature (Hydrogen Pressure: 1750 psig; Reaction Time: 1 hr.; Catalyst: Sulfided Ni-W/Al_2O_3).

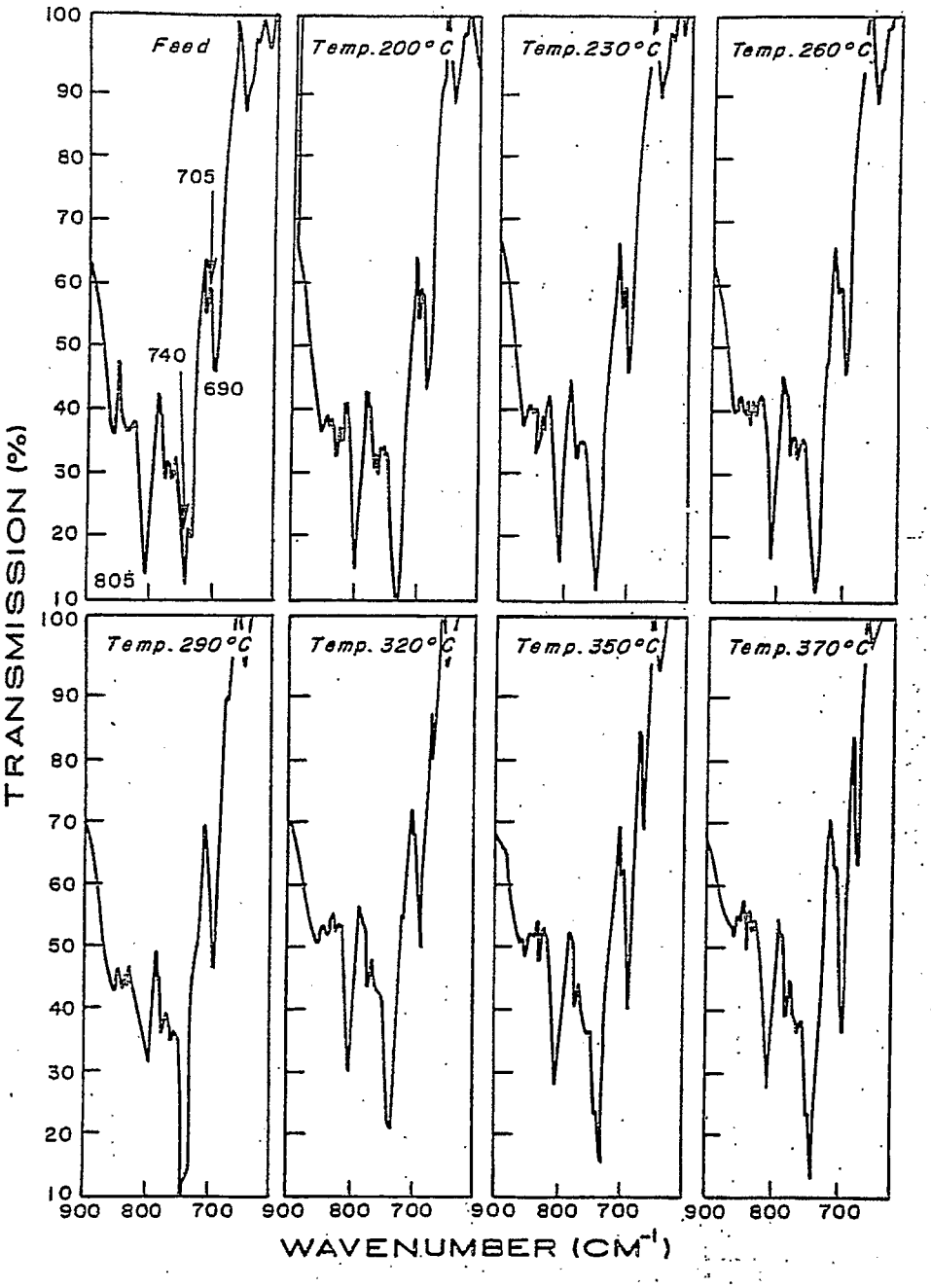

Figure 40. Change in Relative Intensities of C-H Out-of-Plane Stretching Bands (600 - 900 cm^{-1}) of Product from Hydrodeoxygenation of SRC-II Distillate (b.p. 230 - 455°C) as a Function of Reaction Temperature (Hydrogen Pressure: 1750 psig; Reaction Time: 1 hr.; Catalyst: Sulfided Co-Mo/Al_2O_3).

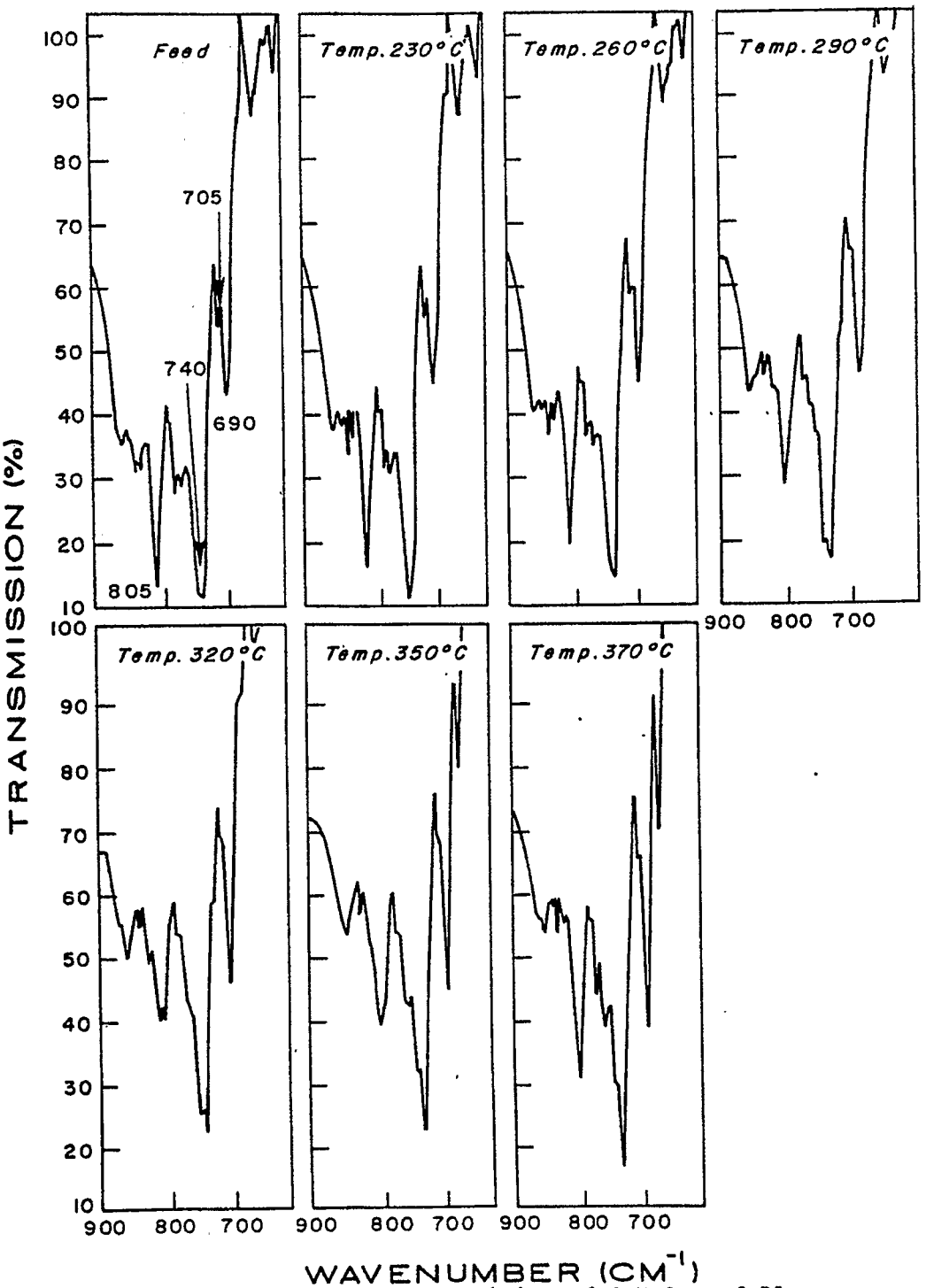

Figure 41. Change in Relative Intensities of C-H Out-of-Plane Stretching Bands (600 - 900 cm^{-1}) of Product from Hydrodeoxygenation of SRC-II Distillate (b. p. 230 - 455°C) as a Function of Reaction Temperature (Hydrogen Pressure: 1750 psig; Reaction Time: 1 hr.; Catalyst: Sulfided Ni-W/Al_2O_3).

Task 8

Catalytic Cracking of Hydrogenated Coal-Derived Liquids and Related Compounds

Faculty Advisors: J. Shabtai
A.G. Oblad
Graduate Student: John McCauley

Introduction

Hydrogenation followed by catalytic cracking provides a feasible process sequence for conversion of coal liquids into conventional fuels. Such a sequence has certain advantages in comparison with a hydrocracking-catalytic reforming scheme.

The present project is concerned with the following interrelated subjects: (1) systematic catalytic cracking studies of polycyclic naphthenes and naphthenoaromatics found in hydrogenated coal liquids and (2) systematic catalytic cracking studies of hydrotreated coal-derived liquids.

Project Status

Systematic catalytic cracking studies, using newly synthesized cross-linked smectite (CLS) molecular sieves,[1,2] are in progress. The CLS type of catalysts are characterized by enlarged critical pore sizes (approximate range, 10-40 Å) suitable for intrasorption and cracking of bulky hydrocarbon molecules present in coal liquids. Studies are presently being carried out to determine the effective pore sizes and activities of RE^{3+}-exchanged CLS catalysts, using model feeds of gradually increasing kinetic diameters, i.e., cumene, t-butylbenzene, 1,3-diisopropylbenzene, 1,3,5-triisopropylbenzene, 1,3,5-tri-t-butylbenzene, polliisopropyl-substituted naphthalenes, and polycyclic (3- to 5-ring) naphthenoaromatic hydrocarbons (obtained in Task 6). With completion of the characterization of CLS catalysts, the latter will be applied in systematic cracking studies of partially hydrogenated coal liquids (SRC-II distillates and SRC-I product fractions). Feeds for this part of the study are being presently prepared.

The catalytic cracking experiments are performed in a previously described flow system.[3]

Future Work

The above indicated studies will be continued.

References

1. J. Shabtai, U.S. Patent 4,238,364 (1980).

2. J. Shabtai, R. Lazar and A.G. Oblad, Proc. 7th International Congress on Catalysis, Tokyo, Japan, 1980, pp 828-840.

3. S. Sunder, Ph.D. Thesis, University of Utah, Salt Lake City, Utah, 1980.

Task 9

Hydropyrolysis (Thermal Hydrocracking) of CD Liquids

Faculty Advisors: J. Shabtai
A.G. Oblad
Graduate Student: Y. Wen

Introduction

This project is concerned with a systematic investigation of hydropyrolysis (thermal hydrocracking) as an alternative processing concept for upgrading of heavy coal-derived liquids into light liquid products. The high efficiency and versatility of hydropyrolysis has been indicated in previous studies with heavy CDL feedstocks and with model compounds.[1-3] The present project is an extension of this previous work for the purpose of (a) further developing and enlarging the scope of the hydropyrolytic reaction, and (b) optimizing the operating conditions for different types of feedstocks, e.g., coal liquids from different liquefaction processes, partially hydrotreated coal liquids, and relevant model compounds. The project includes systematic studies of reaction kinetics, product composition, and coking tendencies, as a function of operating variables. The work with model compounds provides necessary data for further elucidation of mechanistic aspects of the hydropyrolysis process.

Project Status

Systematic hydropyrolysis studies of representative polycyclic naphthenoaromatic hydrocarbons are in progress. The hydropyrolysis of tetralin (1) was first investigated in the temperature range of 500-600°C and in the hydrogen pressure range of 500-2500 psig. It is found that compound 1 undergoes two competing reactions, i.e., (A) dehydrogenation to naphthalene (2); and (B) hydropyrolysis (thermal hydrocracking) of the hydroaromatic ring moiety. Under mild temperature and pressure conditions the desirable reaction B yields predominantly C_{10} aklybenzenes, i.e., 1-methyl-2-propylbenzene (3), 1,2-diethylbenzene (4), and n-butylbenzene (5). The latter are produced by cleavage reactions of the hydroaromatic ring in 1. With increase in temperature and/or hydrogen pressure compounds 3-5 undergoes secondary hydrodealkylation reactions to yield benzene, toluene and ethylbenzene, as well as C_1-C_4 gaseous products. The undesirable aromatization reaction A is important at low hydrogen pressure (500-1000 psig). On the other hand, the desirable hydropyrolysis reaction B increases in relative importance at higher pressure, e.g., 1500-1800 psig, and becomes predominant at pressures above 2000 psig. More detailed data will be provided in subsequent reports.

Future Work

Hydropyrolysis studies with (a) partially hydrogenated coal liquids, and (b) polycyclic naphthenoaromatics as feeds will be continued.

References

1. J. Shabtai, R. Ramakrishnan and A.G. Oblad, Advances in Chemistry, No. 183, Thermal Hydrocarbon Chemistry, Amer. Chem. Soc., 1979, pp 297-328.

2. R. Ramakrishnan, Ph.D. Thesis, University of Utah, Salt Lake City, Utah, 1978.

3. A.G. Oblad, J. Shabtai and R. Ramakrishnan, U.S. Patent 4,298,457 (1981).

Task 10

Systematic Structural Activity Study of Supported Sulfide Catalysts for Coal Liquids Upgrading

Faculty Advisors: F.E. Massoth
J. Shabtai
Post-Doctoral Fellows: G. Muralidhar
Y. Liu

Introduction

The objective of this research is to develop an insight into the basic properties of supported sulfide catalysts and to determine how these relate to coal liquids upgrading. The proposed program involves a fundamental study of the relationship between the surface-structural properties of various supported sulfide catalysts and their catalytic activities for various types of reactions. Thus, there are two clearly defined and closely related areas of investigation, viz., (1) catalyst characterization, especially of the sulfided and reaction states and (2) elucidation of the mode of interaction between catalyst surfaces and organic substrates of different types. The study of subject (1) will provide basic data on sulfided catalyst structure and functionality, and would allow the development of catalyst surface models. Subject (2), on the other hand, involves systematic studies of model reactions on sulfide catalysts, and the utilization of data obtained for development of molecular level surface reaction models correlating the geometry (and topography) of catalyst surfaces with the steric-conformational structure of adsorbed organic reactants. The overall objective of the project is to provide fundamental data needed for design of specific and more effective catalysts for upgrading of coal liquids.

Atmospheric activity tests using model compounds representative of hydrodesulfurization (thiophene), hydrogenation (hexene) and cracking (isooctene) have been developed. These were employed to assay changes in the catalytic functions of various supported CoMo catalysts. It was found that hydrodesulfurization (HDS) and hydrogenation activities were generally unaffected by the type of alumina used or by the cobalt salt used in the preparation; whereas, cracking activity varied considerably, being highest for γ-Al_2O_3 and cobalt sulfate addition. Addition of acidic, basic or neutral ions to the standard γ-alumina catalyst at 0.5 wt % level showed interesting changes in catalytic activities for various functions. In a series of catalysts employing silica-alumina as the support, the HDS and hydrogenation functions decreased with increasing silica content, while cracking went through a maximum in activity. Catalysts prepared by supporting CoMo on TiO_2, SiO_2·MgO and carbon showed low activities, except for high cracking activity for the two former catalysts.

Oxide precursors of CoMo and Mo catalysts supported on various silica-aluminas evaluated by ESCA showed that support active component interaction decreased with increase of silica in the support. It was also found that cobalt did not influence the Mo dispersion.

Project Status

During this quarter, ESCA measurements were made on $CoMo/Al_2O_3$ catalysts containing 5% Zn and Mo dispersions on all the catalysts were reevaluated. Testing of catalysts at high pressure has begun.

Previous calculations of Mo "surface dispersions" for Mo and CoMo catalysts on various supports[1] fail to account for variations in surface area of the catalyst. Actually, the measurements reported as surface dispersion more accurately relate to "surface coverage." To assess the actual dispersion of Mo in these catalysts, a more theoretical approach was adopted. The basis of these calculations follows the method of Kerhof and Moulijn.[2] Their method involved calculation of theoretical intensity ratios of a promoter (here Mo) to the support element for a monolayer dispersion of the promoter. Experimental ratios are then compared to the theoretical monolayer ratios to determine the degree of dispersion of the promoter.

Theoretical intensity ratios of Mo to support components were calculated according to the method outlined by Kerhof and Moulijn.[2] The theoretical relationship for a monolayer of a component on the support is

$$\left[\frac{I_p}{I_s}\right]_{mono} = \left[\frac{X_p}{X_s}\right]\frac{\sigma_p}{\sigma_s} z \qquad (1)$$

where subscript p stands for promoter (Mo) and s for support component (Al, Si or Mg) and I is peak intensity (area), X is atomic fraction, σ is photoelectron cross section and z is a correction factor. The correction term is given by

$$z = \frac{\beta(1+e^{-\beta})}{2(1-e^{-\beta})} \qquad (2)$$

$$\beta = t/\lambda_s \qquad (3)$$

$$t = 2/\rho_s S \qquad (4)$$

where β is a dimensionless support thickness, t is the sheet thickness of the support, λ is the escape depth, ρ_s is the average density and S is the surface area of the catalyst (assumed identical to the support). Values used for these calculations are given in Table 1.

Theoretical values of Mo to support component ESCA intensities for monolayer dispersion are compared to experimental values in Table 2. Good agreement, showing essentially monolayer coverage, is obtained for Al_2O_3 and 10% SiO_2-Al_2O_3 catalysts, and fair agreement for 25% SiO_2-Al_2O_3. The 75% SiO_2-Al_2O_3 also seems to exhibit high Mo dispersion. However, lower dispersions are evident for the 73% SiO_2-MgO and SiO_2 catalysts, in line with MoO_3 crystallites observed by XRD for these catalysts.

The ESCA results for the CoMo catalysts are similar to those for Mo. A reasonably high dispersion of the Mo for Al_2O_3-rich catalysts is indicated. The somewhat lower I_{Mo}/I_s ratios compared with the Mo catalysts may be due to a Co overlayer on the dispersed Mo phase, as Co was added after Mo in

the preparation of the catalysts. Gajardo et al.[3] and Okamoto et al.[4] have reported similar results. The lower (I_{Mo}/I_{Al}) experimental versus monolayer ratio for the 75% SiO_2-Al_2O_3 catalyst indicates poor Mo dispersion for this catalyst, in accordance with $CoMoO_4$ found by XRD.

Previous studies on these catalysts have shown appreciably lower catalytic activities for thiophene HDS and hexene hydrogenation (HYD) when compared to the Al_2O_3 catalyst. Also, O_2 chemisorption was lower for the same catalysts. In particular, for the SiO_2-Al_2O_3 series, the HDS activity dropped sharply and the HYD activity more slowly with increase in SiO_2 content, indicating a decrease in active sites. Nevertheless, the present results show essentially monolayer dispersion on the Mo for the lower SiO_2 content catalysts of this series.

It is will known that Mo interacts strongly with Al_2O_3.[5] Recent studies have shown that Mo on Al_2O_3 exists as small clusters of monolayer dimension.[6] It has been proposed that the amount of Mo strongly adsorbed depends on the OH content replaceable by F ions on the support.[7] We may imagine that the Mo cluster size will depend on the surface concentration of the OH groups, which in turn is related to the Al_2O_3 content. As SiO_2 is added to Al_2O_3, the OH concentration decreases (See Task 11 of current progress report), resulting in less bonding to the surface. The clusters thus will grow laterally forming larger clusters in contrast to Al_2O_3, where the clusters are strongly bonded and remain small. As the SiO_2 content continues to increase, insufficient bonding sites remain and three-dimensional growth of MoO_3 or $CoMoO_4$ occurs. Only at this state would the Mo dispersion as determined by ESCA decrease, since ESCA cannot distinguish between cluster sizes in a monolayer.

During sufiding, the Mo oxide phase is converted to a sulfide phase. Other studies have shown that the Mo dispersion in the oxide form does not essentially change during sulfiding.[8] Furthermore, the cluster size is maintained in forming a monolayer of MoS_2.[6] Thus, the change in cluster size deduced from the ESCA results on the oxide catalysts should also pertain to the sulfide state. (We intend to confirm this by ESCA measurements on the sulfided catalysts.) Further analysis is in progress to attempt to expalin differences in the HDS and HYD activities as a function of the Mo dispersion.

Testing of catalysts under high pressure conditions with model compounds has been carried out in the system previously described.[9] Because of leak problems with the stirred tank reactor, the preheater has been adapted to a fixed bed reactor. Model compounds employed are dibenzothiophene for HDS, naphthalene for HYD and indole for HDN. An OV-17 column, used with a temperature program sequence and FID detector, is employed for separation of products. After sulfiding the catalyst (about 1/2 g) in 10% H_2S/H_2 at 400°C for 2 hours at atmospheric pressure, the system pressure is raised to 500 psig, the temperature lowered to 277°C and a mixture of dibenzothiophene/heptane plus CS_2 and H_2 is passed over the catalyst for two days to achieve line out. Following, the conversion is measured at several feed flow rates. Next, the feed is changed to naphthalene/heptane plus CS_2, and conversion obtained as before. Finally, a mixture of indole/heptane plus CS_2 is run at 350°C.

Observed products of these reactions were: (1) from dibenzothiophene-biphenyl and cyclohexylbenzene; (2) from naphthalene-tetralin; and (3) from

indole-indoline, ethylaniline and ethylcyclohexane. In HDN, indoline was taken to be a reactant and ethylaniline and ethylcyclohexane as products in calculating conversion. This represents breaking of the first C-N bond in the heterocyclic ring.

Figure 1 displays conversions at several liquid feed rates. The total flow was essentially constant during these runs, the partial pressure of reactant (and added CS_2) increasing with increase in liquid feed rate. The declining conversions with increasing liquid feed indicate that none of the reactions are first order, but rather are inhibited by reactant. The sharper fall in HDS activity is attributed to the retardation in reaction due to increasing H_2S partial pressure.

Preliminary kinetic treatment of the HYD and HDN reaction data showed good agreement with the general rate form,

$$r_i = \frac{k_i p_i}{1+K_i p_i} \tag{5}$$

where r is the reaction rate, k the rate constant, p the partial pressure and k the adsorption constant, subscript i standing for naphthalene or indole + indoline. For a fixed-bed reactor, equation (5) integrates to

$$k_i \frac{W}{F} = -\ln(1-x_i) + k_i p_i^o x_i \tag{6}$$

where W is catalyst weight, F is total flow, x_i is conversion and p_i^o is initial reactant in the feed. For the HDS reaction, the best correlation was obtained from,

$$r_T = \frac{k_T p_T}{(1+k_S p_S)^2} \tag{7}$$

where subscript T stands for benzothiophene and s for H_2S. The H_2S comes from conversion of the CS_2 in the feed, which is in considerable excess over that generated from the reaction. Equation (7) integrates to

$$k_T \frac{W}{F} = -(1+k_S p_S)^2 \ln(1-x_T) \tag{8}$$

In equations (6) and (8), p_i^o and p_S are directly proportional to the liquid feed rate, F_L. Linearized forms of equations (6) and (8) were used to test the fit of the data, the results of which are shown in Figure 2. Although the correlations are reasonable, a greater range in the parameters would be required to obtain accurate values of the appropriate constants, especially at lower liquid feed rates. Unfortunately, lower feed rates are not possible due to limitations in the liquid pump speed.

One of the important objectives of these tests is to compare reactivities of different catalysts to relate these to catalyst characterization studies. Another objective is to compare the high pressure runs to the atmospheric

pressure runs on the same catalysts. Accordingly, the $CoMo/SiO_2$-Al_2O_3 series of catalysts was run in the high pressure reactor. It was found that 10% SiO_2 and 25% SiO_2-content catalysts followed similar trends as for the Al_2O_3 catalyst (although conversions were different), giving reasonable agreement to equations (6) and (8). However, for the 75% SiO_2 and the SiO_2 catalyst, fits to these equations were poor. This interesting finding, in conjunction with the physical properties of these catalysts discussed above, would seem to indicate that the reaction kinetics are different for monolayer dispersion of the Mo and crystallites of MoS_2.

As for the order of reactivity of the various catalysts, due to the complexity of the kinetics of the reactions, catalysts were ranked by conversion at a given feed rate of 7 cm^3/hr. The following relative ranking was obtained:

$$HDS: Al_2O_3 \approx 25\%\ SiO_2 > 10\%\ SiO_2 > 75\%\ SiO_2 > SiO_2$$

$$HYD: Al_2O_3 > 25\%\ SiO_2 > 10\%\ SiO_2 \approx 75\%\ SiO_2 > SiO_2$$

$$HDN: Al_2O_3 \approx 10\%\ SiO_2 > 25\%\ SiO_2 > 75\%\ SiO_2 > SiO_2$$

Thus, there is a general decline in activity with increase in SiO_2 content, except for a reversal in the 10% and 25% SiO_2 catalysts for HDS and HDN. The comparable low pressure ranking was:

$$HDS: Al_2O_3 > 10\%\ SiO_2 > 25\%\ SiO_2 \approx 75\%\ SiO_2 > SiO_2$$

$$HYD: Al_2O_3 \approx 10\%\ SiO_2 > 25\%\ SiO_2 > 75\%\ SiO_2 > SiO_2$$

Although the general ranking for HDS and HYD for the high and low pressure runs are similar (except for the 10% and 25% catalysts), greater differences are evident when the actual conversions are compared. This may indicate that different sites are involved for the different model compounds used. However, a more likely explanation is that benzothiophene has formed coke on the lined-out catalyst which has decreased the active site concentrations differently for the different catalysts. Some support for this view comes from the fact that considerable coke was generated with benzothiophene,[10] whereas very little was formed in the low pressure thiophene tests. Further tests are needed to resolve this point.

Future Work

ESCA measurements will be made on several sulfided catalysts to compare results with the oxide catalysts. Catalyst testing of new formulations will continue. High pressure runs will be made on additional catalysts that have already been run at low pressure to compare results.

References

1. W.H. Wiser, F.E. Massoth, J. Shabtai, G. Muralidhar and Y. Liu, DOE Contract No. DE-AC01-79ET14700, Quarterly Progress Report, Salt Lake City, Utah, July-Sept, 1981.

2. F.P.J.M. Kerhof and J. Moulijn, J. Phys. Chem. 83, 1612 (1979).

3. P. Gajardo, P. Grange and B. Delmon, J. Catal., 63, 201 (1980)

4. Y. Okamoto, T. Imanaka and S. Teraneshi, J. Catal., 65, 448 (1980).

5. F.E. Massoth, Adv. Catal., 27, 665 (1978).

6. B.S. Clausen, H. Topsoe, R. Candia, J. Villadsen, B. Lengeler, J. Als-Nielsen and F. Christensen, J. Phys. Chem., 85, 3868 (1981).

7. N. Yamagata, Y. Owada, S. Okazaki and K. Tanabe, J. Catal., 47, 358 (1977).

8. J. Grimblot, P. Hyfresne, L. Gengemgre and J. Bonnelle, Bull. Soc. Chim. Belgium, 90, 1261 (1981).

9. W.H. Wiser et al., DOE Contract No. DE-AC01-79ET14700, Quarterly Progress Report, Salt Lake City, Utah, Apr-June, 1981.

10. R. Ramachandran, Ph.D. Thesis, University of Utah, Salt Lake City, Utah, 1980.

11. J.H. Scofield, J. Electron Spectrosc. Relat. Phenom., 8, 129 (1976).

12. D.R. Penn, ibid., 9, 29 (1976).

13. C. Defosse, ibid., 23, 157 (1981).

Table 1. Parameter values used ESCA calculations.

Component	τ(11)	λ,nm
Al-2s	0.75	1.8 (12)
Si-2s	0.99	2.0 (2)
Mo-3d	9.50	2.3 (13)
Co-2p	12.62	
Mg-2s	0.57	
Ti-2p	5.22	

Numbers in () are references.

Table 2. ESCA intensity ratios for Mo and CoMo catalysts.

Support	$(I_{Mo}/I_{Al})_{mono}$	$(I_{Mo}/I_{Al})_{expt}$	$(I_{Mo}/I_{Si})_{mono}$	$(I_{Mo}/I_{Si})_{expt}$	$(I_{Mo}/I_{Mg})_{mono}$	$(I_{Mo}/I_{Mg})_{expt}$
	Mo Catalysts					
Al_2O_3	0.79	0.77				
10%SiO_2-Al_2O_3	0.76	0.76	5.8	5.1		
25%SiO_2-Al_2O_3	0.89	0.74	2.3	2.2		
75%SiO_2-Al_2O_3	2.8	3.1	0.77	0.94		
SiO_2			0.64	0.23		
73%SiO_2-MgO			0.84	0.67	2.5	1.4
	CoMo Catalysts					
Al_2O_3	0.83	0.70				
10%SiO_2-Al_2O_3	0.80	0.61	6.0	4.6		
25%SiO_2-Al_2O_3	0.93	0.76	2.4	2.4		
75%SiO_2-Al_2O_3	2.9	1.9	0.81	0.95		
SiO_2			0.66	0.22		
73%SiO_2-MgO			0.87	0.96	2.7	1.9
5%Zn-Al_2O_3	0.88	0.70				

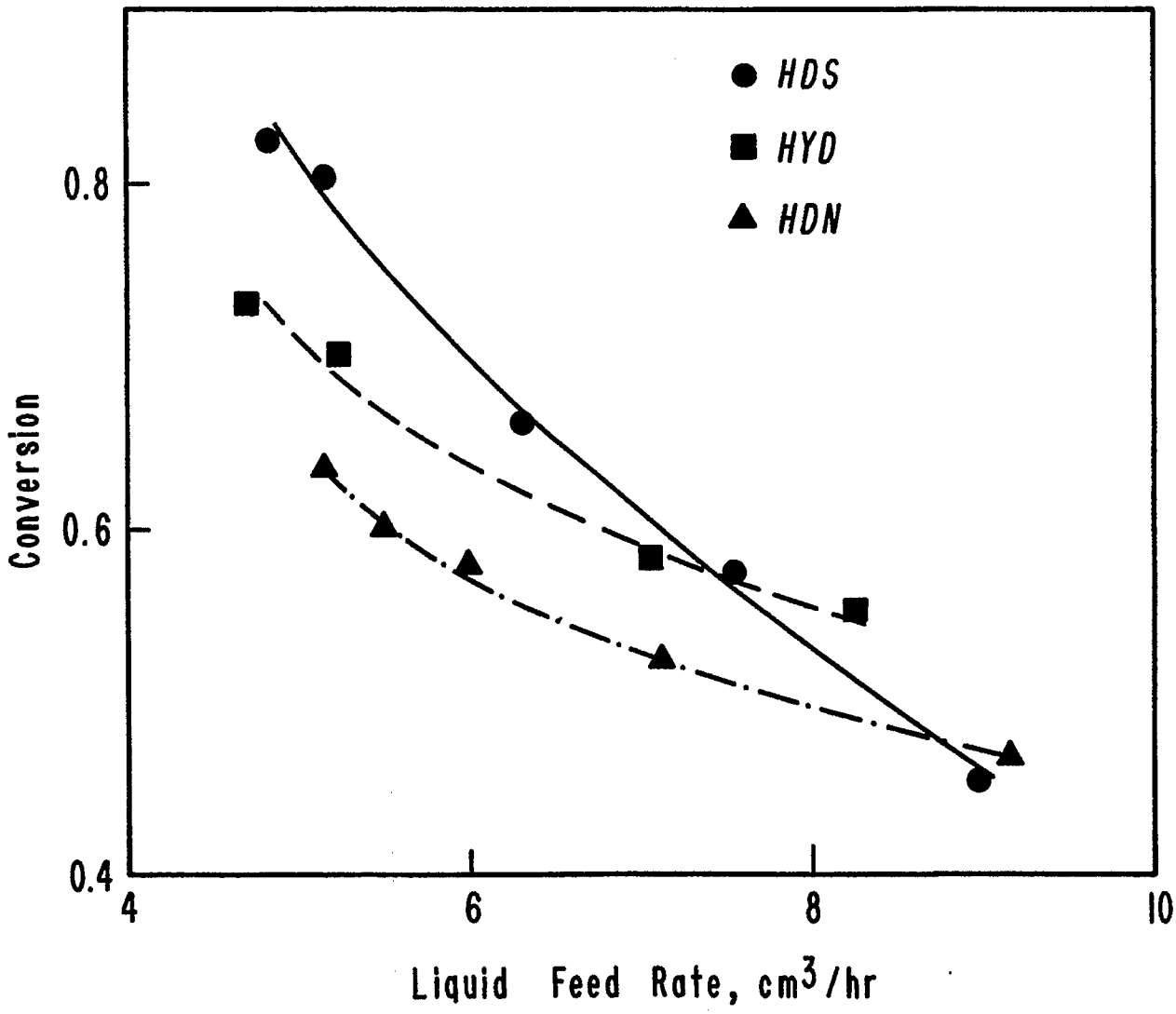

Figure 1. Variation in conversion with liquid feed rate for high pressure tests for HDS, HYD and HDN with $CoMo/Al_2O_3$ catalyst.

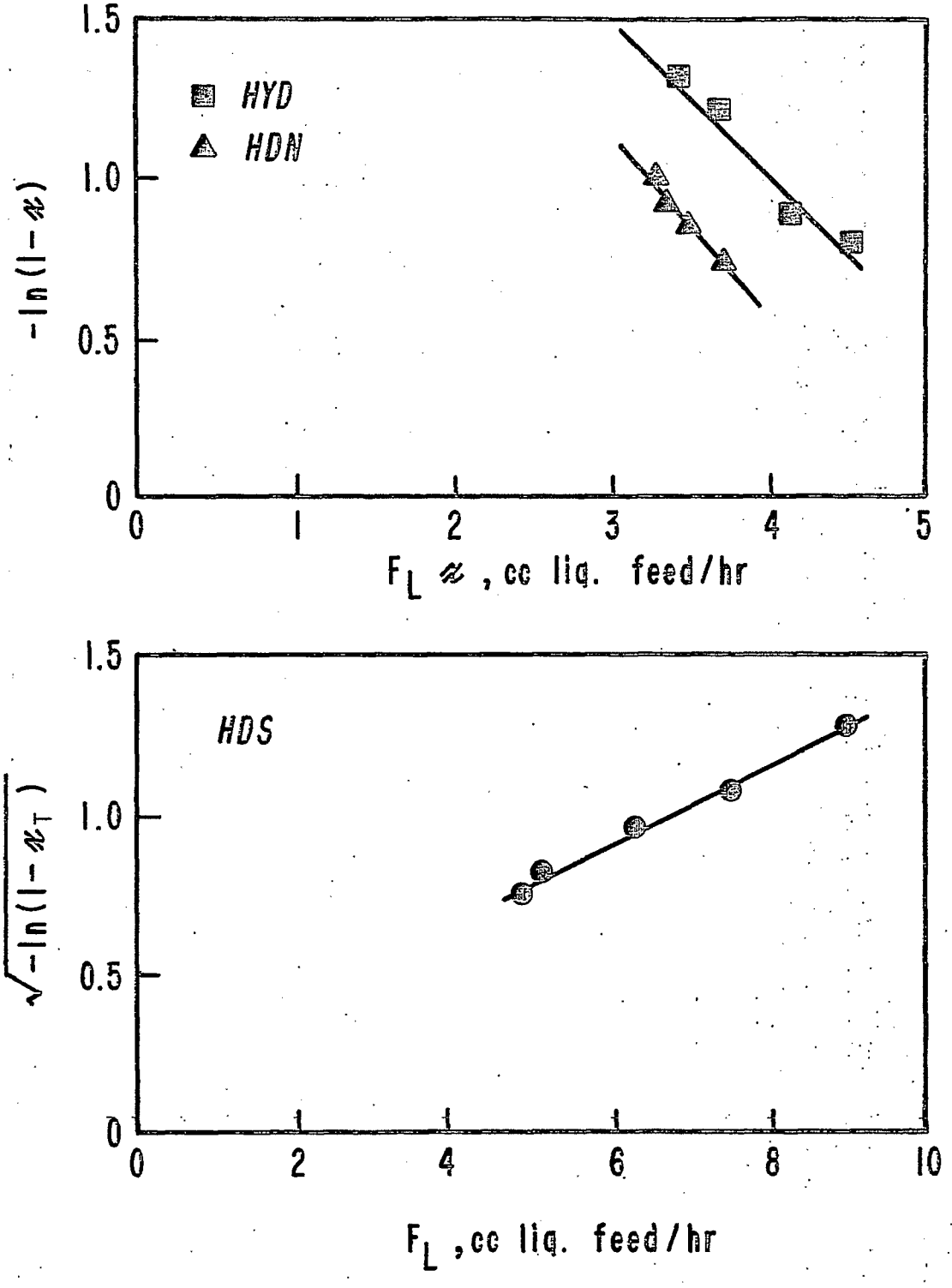

Figure 2. Linearized plots for data conformance to equations (2) and (4) for $CoMo/Al_2O_3$ catalyst.

Task 11

Basic Study of the Effects of Poisons on the Activity of Upgrading Catalysts

Faculty Advisor: F.E. Massoth
Post-Doctoral Fellow: W. Zmierczak

Introduction

The importance of cobalt-molybdena catalysts for hydrotreating and hydrodesulfurization of petroleum feedstocks is well-known. These catalysts are also being studied for hydrodesulfurization and liquefaction of coal slurries and coal-derived liquids. However, such complex feedstocks result in rapid deactivation of the catalysts. To gain an insight into the deactivation mechanism, the detailed kinetics of reactions of model compounds representative of heteroatom hydrogenolysis and hydrogenation are compared before and after addition of various poisons and coke precursors. The studies are carried out using a constant stirred microbalance reactor, which enables simultaneous measurement of catalyst weight change and activity. Supplementary studies are made to gain additional insight into the effect of poisons on the active catalyst sites. Finally, catalysts aged in an actual coal pilot plant run are studied to compare with laboratory studies.

Previous work on this project has shown that catalyst poisoning by pyridine or coke results in loss of active HDS sites, but that the remaining unpoisoned sites retain their original activity. Pyridine appeared to be site selective in poisoning effect whereas coke was non-specific. Furthermore, a distribution of HDS site strengths was observed with pyridine poisoning.

Investigation of the use of oxygen chemisorption for quantitatively assessing the number of active sites on sulfided HDS catalysts showed that oxygen uptake at -78°C best represented true chemisorption. For oxygen chemisorption performed on a limited number of catalysts at -78°C: (1) Mo/Al_2O_3 and $CoMo/Al_2O_3$ catalysts showed essentially the same values; (2) oxygen chemisorption on CoMo catalysts showed a rough correlation with HDS and hydrogenation activity; (3) preadsorbed pyridine reduced the oxygen adsorption of the catalyst in an almost linear manner; (4) on coked catalysts, oxygen uptake was higher than on freshly sulfided catalysts. HDS and HYD catalytic activity for either supported Mo or CoMo catalysts did not correlate well with O_2 chemisorption, indicating that this technique is not specific for either HDS or HYD sites. Possibly, O_2 chemisorbs on both sites.

Project Status

During this period, active OH concentration on various supports was measured. Also, poisoning experiments on a commercial $CoMo/Al_2O_3$ catalyst were begun.

It has been reported that the amount of strongly adsorbed Mo on various supports is proportional to the active OH concentration which is replaceable

by fluoride ions.[1] This technique was employed to assess the active OH concentration on a series of SiO_2-Al_2O_3 supports previously employed in catalyst studies with CoMo and Mo added to the supports.[2,3] The results are given in Figure 1, where the relative HDS and HYD activities are plotted versus the OH concentration in mmoles/m^2 of support surface area. The OH concentration decreased with increase in SiO_2 content of the support. Both HDS and HYD activities decreased with decrease in OH concentration. For HDS activity for both CoMo and Mo catalysts a break in the curves is evident. It is significant that this break occurs at a point (between the 25% and 75% SiO_2 catalysts) corresponding to a change in the structural form of the Mo phase, i.e., from monolayer to three-dimensional crystallites (See Task 10, this report). The HYD correlation is not as clear in this regard, but a similar break can been seen. These results would seem to indicate that at an OH concentration somewhat below 1 x 10^{-3} mmol/m^2, the bonding between the Mo phase and the support becomes sufficiently weak that a monolayer distribution of Mo can no longer be maintained and crystallites form. Further work along this line for other supports will be performed under Task 10.

Deactivation of catalyst activity for HDS and HYD reactions is being undertaken using model heterocyclic nitrogen compounds as poisons. Due to strong adsorption on active sites, the N-compounds cause loss in catalyst activity.[4-7] Previous studies of HDS deactivation of benzothiophene with pyridine showed that at least two HDS sites exist, one easily poisoned and the other immune to poisoning.[8] The aim of these poisoning experiments is to determine the nature and strength distribution of active sites for HDS and HYD on CoMo catalysts.

The experimental data were obtained in a stirred-flow microbalance reactor[9] which allows simultaneous measurements of catalyst weight change and activity. About 300 mg of American Cyanamid 1442 CoMo/Al_2O_3 catalyst was contained in a gold mesh bucket surrounded by the reactor volume space and suspended from one arm of an electrobalance. Before the poisoning experiment, the catalyst was heated for 4 hours in helium at 400°C, sulfided for two hours in a 10% H_2S/H_2 gas mixture flow and followed by two hours in helium. Then the reactor temperature was lowered to 350°C and the catalyst treated for at least three days under standard reaction conditions, which consisted of the following reactant flow rates:

(1) 10% H_2S/H_2 mixture - 10 cc/min;

(2) H_2 (first stream) - 20 cc/min;

(3) H_2 (second stream) passing through a pair of temperature controlled bubblers (first room temperature, second - 0°C) containing thiophene - 20 cc/min.

Aniline, dissolved in benzene, was continuously injected into the reactor from a syringe pump. The catalyst was subjected to various levels of the poison by changing the concentration of amine in the benzene solution or the pump flow rate. Preliminary experiments showed that benzene in the reaction mixture did not effect weight or activity of the catalyst. HDS activity was determined from the conversion of thiophene and HYD activity from the conversion of butene to butane.

With each step change in the partial pressure of aniline, there was a relatively rapid increase in catalyst weight and concommitant decrease in catalyst activity for HDS and HYD. Subsequently, a slow gain in weight was observed over several hours without appreciable change in activities, signifying some adsorption of aniline on nonactive sites.

Figure 2 presents the poisoning results in terms of a relative activity for HDS and HYD. The activity function for a stirred reactor is given by $x/(1-x)$, where x is HDS or HYD conversion.[9] The relative activity, R, is given by the ratio of the activity functions of poisoned to unpoisoned catalyst. The results show a nonlinear deactivation with added aniline for both HDS and HYD. The tailing off of the curves may be due to some adsorption on nonactive sites as noted above. Of significance, thiophene HDS activity drops off faster than olefin HYD activity, indicating that different sites are involved in these two reactions, which has already been noted in the other studies.[2]

Future Work

Simulated poisoning experiments on the intrinsic activity functions of the CoMo catalyst will continue using other N-containing compounds having different basic strengths.

References

1. N. Yamagata, Y. Owada, S. Okazaki and K. Tanabe, J. Catal., 47, 358 (1977).
2. W.H. Wiser, F.E. Massoth, J. Shabtai and G. Muralidhar, DOE Contract No. DE-AC01-79ET14700, Quarterly Progress Report, Salt Lake City, Utah, April-June 1980.
3. ibid., July-Sept 1981.
4. C.N. Satterfield, M. Modell and J.F. Mayer, AIChE J., 21, 1100 (1975).
5. P. Desikan and C.A. Amberg, Can, J. Chem., 42, 843 (1964).
6. J.M.J.G. Lipsch and G.C.A. Schuit, J. Catal., 15, 179 (1969).
7. S.W. Cowley and F.E. Massoth, J. Catal., 15, 291 (1978).
8. R. Ramachandran, Ph.D. Thesis, University of Utah, Salt Lake City, Utah, 1980.
9. F.E. Massoth and S.W. Cowley, Ind. & Eng. Chem., Fundam., 15, 218 (1976).

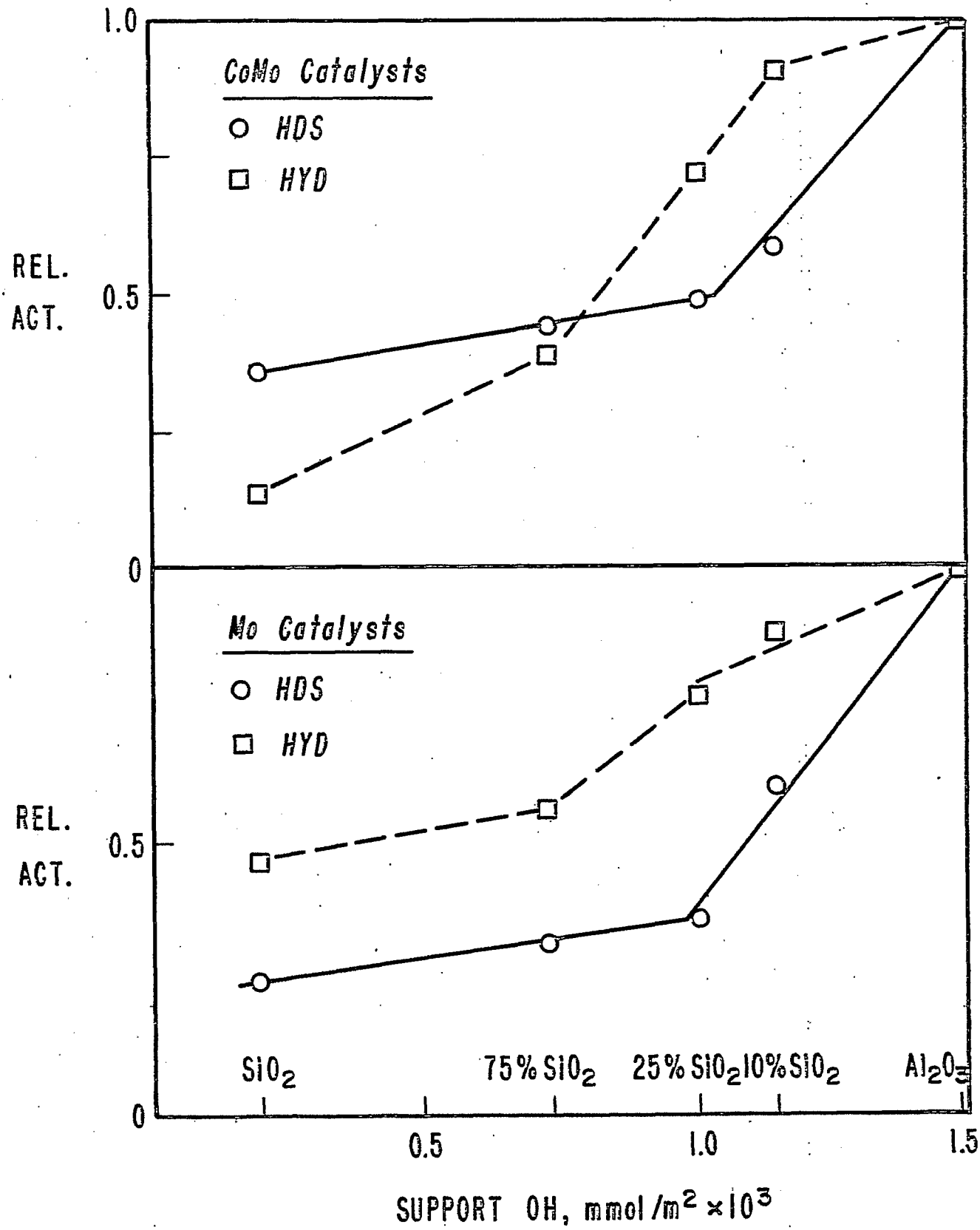

Figure 1. Relation between relative activities and OH concentration of support.

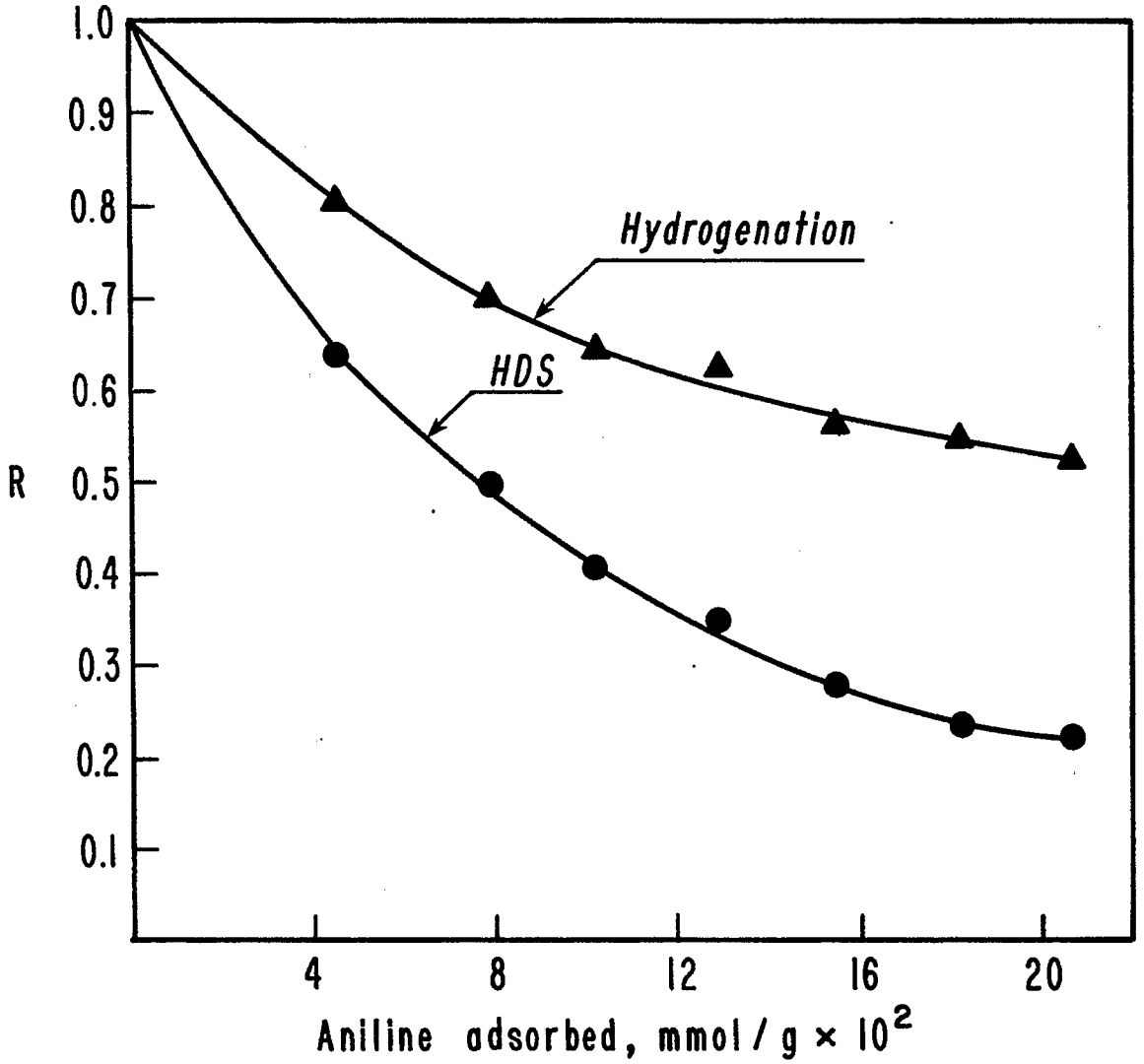

Figure 2. Effect of aniline poisoning on relative activities of $CoMo/Al_2O_3$ catalyst.

Task 13

Catalyst Research and Development

Faculty Advisor: F.V. Hanson
Graduate Student: C.S. Kim

Introduction

The objectives of this project are to develop a preparation technique for a Raney type catalyst (particularly Raney iron-manganese catalyst) and to determine the optimum process variables for the maximum production of gasoline boiling range hydrocarbons, low molecular weight olefins and BTX via the hydrogenation of carbon monoxide. A detailed discussion of the objectives were presented in a previous report.[1]

An electrical heating furnace was built to prepare Al-Fe and Al-Fe-Mn alloys. Several samples of alloys were prepared and the optimum preparation conditions were determined. A stirred tank reactor was fabricated to activate the alloys in an aqueous solution of sodium hydroxide at different activation conditions. A fixed-bed reactor system was built in which catalyst screening tests are being carried out to determine the catalyst composition and activation variables which will optimize the catalyst activity and selectivity. The same reactor system will be used for the process variable investigation. Two types of Raney iron catalysts were prepared at different activation conditions. These catalysts were tested in the fixed-bed reactor to determine the proper range of process variables (temp, pressure, space velocity) to carry out a standard catalyst screening test. The Raney iron catalysts were found to be more active, in terms of CO conversion even in an unreduced state, compared to a precipitated iron catalyst reduced at 500°C.

A series of tests have been carried out with a gas chromatograph to determine the response factors of each gas product from CO hydrogenation. A basic computer program was rewritten based on the new response factor. A carbon mass balance was achieved, especially at low levels of CO conversion, with the new computer program using the fixed-bed run of CO hydrogenation over a Raney iron catalyst. In the CO hydrogenation a reduced Raney iron catalyst showed stable catalytic activity and selectivity over a period of 24 hours at the following process variables: temp = 140-180°C, pressure = 500 psig, space velocity = 1-4 cm^3/g-sec.

Project Status

A series of Raney iron and Raney iron-manganese catalysts were prepared using different preparation conditions. An iron and an iron-manganese catalyst was also prepared by the precipitation technique presented in Tables 1 and 2.

Two methods have been used to prepare the Raney iron catalyst.

1) The addition of caustic solution to the water slurry of Al-Fe alloy particles (-25+50 mesh).

2) The stepwise addition of alloys into the caustic solution.

A detailed drawing of the activation reactor and washing bottle were shown in the previous report. The first method, which was advocated by Nishimura, involves stepwise addition of sodium hydroxide solution into the activation reactor which contained a stirred water slurry of alloy particles. Initially the reactor contained 50 g of alloys and 250 ml of deionized water. The initial temperature of this slurry was maintained at 10 to 20 degrees below the actual final leaching temperature, i.e., 70°C in the case of 90°C leaching. Another 250 ml of NaOH solution (37 wt % NaOH) was added as follows: Each 5 ml of solution was added at 3 min intervals for about 60 min. Then each 10 ml of caustic solution was added at 5 min intervals with the last 50 ml added all at once. The stepwise addition of the caustic solution into the reactor took 120 min. This stepwise addition technique enabled the reactor to control the temperature within ±5°C from the desired leaching temperature during the leaching reaction period. After the completion of the caustic addition, the leaching was continued for an additional 90 min at the leaching temperature. Total leaching time was 210 min.

The second method, which is a stepwise addition of ten equal amounts of the alloy into the solution has been widely used by previous workers[4-8] in the preparation of Raney nickel. Five grams of alloy particles were added to 500 ml of 21 wt % caustic solution at 3 min intervals. This technique maintained the reactor temperature constant during the leaching step. After all the alloy was added, an additional 90 min of digestion was needed. Total digestion time was 120 min.

In the preparation of the Raney iron-manganese catalysts, only the second method was used, since the first method (addition of caustic) was occasionally accompanied by the explosive evolution of H_2 gas and made it difficult to control the reactor's constant temperature.

The various preparation conditions for each catalyst are presented in Tables 1 and 2. The precent aluminum leaching was calculated with a dry testmeter by measuring the volume of H_2 gas evolved during the leaching reaction. This was based on the following equation.

$$2Al + 2NaOH + 2H_2O \longrightarrow 2NaAlO_2 + 3H_2 \qquad (1)$$

Although Equation (1) may be an oversimplification of more complicated reaction paths in the actual leaching step, it gives a reasonable value on the extent of aluminum leaching. Previous workers[8] reported that the wt % of the remaining aluminum calculated by Equation (1) agrees with the value obtained by actual elemental analysis. As will be explained later, Equation (1) is a predominant reaction occurring in a very basic solution (high pH values). The extent of aluminum leaching generally increased with an increase in leaching temperature.

When the alloy was added to a very dilute caustic solution, (4.4 wt %) a very small amount of aluminum was leached. This is quite different from the findings of previous workers when using Raney nickel alloys. Dirksen[9] and Anderson[8] found that extensive leaching of aluminum from the Ni-Al alloy could be achieved in a very dilute caustic solution. The different observations might be attributed to the different reactivities of the alloys

for the sodium hydroxide leaching reaction.

The volume of H_2 gas evolved at different stages of caustic addition when caustic solution was added to the water slurry of Al-Fe alloy is presented in Figure 1. From Figure 1 it is apparent that the reaction stops after the initial stage of reaction, then there is a sudden increase in the amount of H_2 gas evolved. This phenomenon was most apparent at the highest leaching temperatures, i.e., at 90°C.

B.A. Lure et al.[10] indicated that in the initial stage of the reaction of aluminum with water and alkalis, there is a gradual accumulation of a layer of solid products (boehmite, AlOOH and bayerite, $Al(OH)_3$) on the surface of the aluminum. The increase in the thickness of this layer prevents the penetration of water onto the surface of aluminum, which retards or halts the reaction.

Dirksen[9] reported that in a dilute basic solution the sodium aluminate formed (Equation 1) is hydrolyzed (Equation 2), resulting in a formation of water insoluble $Al_2O_3 \cdot 3H_2O$.

$$2NaAlO_2 + 4H_2O = Al_2O_3 \cdot 3H_2O + 2NaOH \qquad (2)$$

From the above discussions the sudden evolution of H_2 gas after no evolution can be explained as follows: At the very beginning of the reaction as caustic solution is added, there is a gradual formation of the solid products (aluminum oxide) on the surface of alloys. As the thickness of this layer grows, no reaction occurs due to the inaccessability of water to the aluminum surface. As more solution is added, i.e., high pH value, the insoluble solid products are dissolved forming a water-soluble $NaAlO_2$ as in Equation 2. As a consequence, the surface of aluminum is again exposed to the highly basic solution and the reaction (1) proceeds very fast.

The volume of H_2 gas evolved at various stages of digestion time is plotted in Figure 2. The volume of H_2 gas evolution increased continuously with reation time. Since the alloys were added to the very basic solutions (high pH value), the reaction (1) was the predominant reaction during leaching without any formation of solid products on the surface of alloys. The final extent of Al leaching increased with an increasing leaching temp.

The total BET surface aluminum surface area of each catalyst was measured at liquid N_2 temperature by a surface and pore analyzer (Micromeritics Model 2100 D). Mars et al.[11] reported that the total surface area of a Raney nickel catalyst stored under water showed a rapid decrease of surface area with increasing degassing temperature just prior to BET analysis. They ascribed the decrease to the highly exothermic reaction of aluminum with residual water, resulting in a sintering of catalyst.

The variation of the total BET surface area of a Raney iron catalyst (leached at 90°C) degassed at different temperatures is presented in Figure 3. One sample of the catalyst was first degassed at 80°C for 24 hours and the BET area was determined. Then the catalyst was degassed at successively higher temperatures for 24 hours and the BET area was determined just after each degassing. Another sample of the same catalyst was subjected to the same procedure but the first degassing was done at 250°C followed by higher temperatures.

From Figure 3 the BET area remained essentially constant except at the lowest temperature (80°C) and the highest temperature regions (>350°C). The low values of the BET surface area at low temperature degassing may be due to the incomplete removal of liquid (ethanol or water) remaining in the small pores of the catalyst. The low values of BET surface area with high temperature degassing indicates that reduction of the surface area may be related to catalyst sintering or pore structure change after degassing at high temperatures. All the Surface areas in Tables 1 and 2 were obtained after degassing each catalyst at 120°C for 24 hours.

The same tests (variation of surface area with different degassing temperature) have been carried out for precipitated Fe and coprecipitated Fe-Mn catalysts as shown in Figure 4. The trend was the same as observed for the Raney catalysts. The surface areas of the two precipitated catalysts in Tables 1 and 2 were also measured after degassing at 120°C for 24 hours. The Raney iron catalyst decreased in surface area less than the Raney nickel catalyst. The Raney iron catalysts were stored in absolute ethanol, thus reducing the possibility of an exothermic reaction between residual aluminum and water and thus avoiding sintering. However, sintering may still occur when the Raney nickel catalyst is stored under water.

From Table 1, no consistent trend could be found between the surface area of the catalyst and leaching temperature. However, there was a considerable decrease in the surface area of the Raney iron catalyst leached at 90°C. There may be considerable collapsing of pore structures when the alloy is leached at 90°C.

The catalyst prepared by the precipitation technique showed higher surface areas (about 5 times) than the Raney catalysts. However, the precipitated catalysts may undergo a marked decrease in surface area or change in pore structure during the reduction under flowing H_2 as was observed in the fixed-bed run of CO hydrogenation.[12] This is not yet understood.

X-Ray diffraction of each catalyst was obtained using the same technique and procedures as described in a previous report.[13] The samples of Raney catalysts were coated with 2% nitrocellulose in amylacetate to prevent exposure to air. Tables 1 and 2 list the phases found from the X-ray powder diffraction of each catalyst.

Alpha-Iron (α-Fe) was confirmed to be present in all Raney catalysts. The Raney catalysts prepared at relatively low temperatures (below or at 50°C) showed some remaining alloy phases. The Raney Fe prepared at 90°C by caustic addition included magnetite (Fe_3O_4) while the other catalyst prepared by alloy addition at 90°C showed only α-Fe. The presence of a magnetite phase in the one catalyst can be explained by the longer leaching time. This is quite consistent with the findings of Swartzendruber,[14] who found that magnetite was the major phase in the Raney iron which experienced a severe leaching condition when exposed twice to a high temperature. No manganese (metal or oxides) peaks were observed with Raney Fe-Mn catalysts. This indicates the Mn atoms are not forming a separate phase but are included in the Fe crystal lattice.

For precipitated iron catalysts, magnetite was the only phase while magnetite and hausmannite (Mn_3O_4) were identified from coprecipitated Fe-Mn catalysts.

A series of catalyst reduction studies has been carried out with a coprecipitated Fe-Mn catalyst (Mn/Fe = 5/100 atomic ratio). The flow diagram of the thermogravimetric analysis system is shown in Figure 5. A DuPont TGA Model 951 was used for analysis. The H_2 and He gas used were purified by a hydrogen purifier (Matheson, Model 8362) and a hydroxpurifier (Matheson, Model 8301), respectively. The flow rate of each gas used was 50 cc/min. The amount of sample used was about 20 to 40 mg. The isothermal or programmed temperature mode was used depending on the purpose of the experiment.

A weight loss curve for a coprecipitated Fe-Mn catalyst under He when the catalyst was heated from room temperature to 500°C at two different heating rates is presented in Figure 6. Heating the catalyst at the slower rate (0.5°C/min) resulted in a more complete removal of the volatile matter (water and NO_3^+ ion) that were left over after preparation. The catalyst sample did not lose any additional weight even after prolonged heating at 500°C.

The effect of different heating rates on the weight loss of the catalyst under H_2 is presented in Figure 7. All three heating rates showed the same final weight loss. After heating to 500°C under H_2, each sample was cooled to room temperature. The sample was flushed with purified He, then air was introduced into the TGA. The sample was again heated to 500°C under flowing air using the same heating rate, 0.5°C/min. The catalysts which have been heated under H_2 with heating rates of 0.5 and 2°C/min, gained weight up to the point, which corresponds to the final weight of catalyst obtained after heating under He, 9.4% (Figure 7). However, the sample heated under H_2 with a 5°C/min heating rate gained weight below that point, 13.2%. This experiment indicates there may be sintering or some changes in pore structure of the catalysts due to the vigorous reduction process carried out under H_2 with a high heating rate (5°C/min).

All the reduced iron should be transformed into iron oxide in the presence of flowing air. Thus, it is expected to gain the same weight if there is no change in the surface or pore structure of the catalyst. The lower curve (the first derivative of weight change during reduction under H_2) indicates that there are two regions of temperature at which the weight losses are appreciable. Most of the volatile matter was lost at about 260°C and most of the reduction of the iron oxides occurred at about 400°C. From Figure 7 it is concluded that the heating rate of 2°C/min during the reduction is a reasonable value to prevent any significant structural changes and to permit the completion of reduction. The optimum reduction temperature was determined in a series of experiments in which the catalyst underwent a series of successive isothermal heating conditions as shown in Figure 8. A programmed heating and an isothermal heating method using a DuPont TGA 951 could not be combined for a single TGA run. The catalyst was heated in a series of isothermal temperature steps to minimize the effect of a fast heating rate in each successive isothermal heating. First it was heated to 120°C and maintained until there was no weight change. The temperature was increased to the next higher temperature and so on. The total weight loss

at 500°C was 36.0% which is consistent with the value obtained from previous runs in Figure 7. After the catalyst weight stabilized at 500°C, the He gas was introduced to flush out all remaining H_2 gas from the TGA unit. Air was then introduced. The weight gain was 25.5% (cf. 26.0% in Figure 7). The final weight was 10.5% below the original weight of the catalyst, which is close to 9.4% (Figure 7). The optimum temperature for reduction was 400°C (Figure 8).

Figure 9 shows the effect of a very fast heating rate on reduction. The TGA was heated from room temperature to isothermal temperature (500°C) within 3 min. After the catalyst weight stabilized (35.4%), He and air were introduced as before. There was only a 2.5% weight gain. Figures 8 and 9 show that the use of a high heating rate may result in some structural changes of the catalyst during reduction. A minimum reduction time at 400°C for complete reduction of the catalyst could not be determined due to the limitations of the instrument, i.e., use of a programmed and an isothermal mode heating in a single run. This experiment will be pursued with another TGA unit, which can be used for the above purpose.

The same tests were attempted for a Raney iron catalyst (leached at 90°C). However, the catalyst gained weight as it was heated under purified He or H_2 up to about 450°C after which time the weight decreased. Possible explanations for this unexpected phenomena were:

1) Oxidation occurring on the catalyst surface. The source of O_2 may be the air left over in the balance jar which is connected to the furnace.

2) Occlusion of water formed from the reduction of iron oxides within the small pores of the catalyst.

3) Electromagnetic interaction between the ferromagnetic catalyst and metal parts in the balance.

The first possibility was excluded from further consideration, since the catalyst showed the same results even when the balance jar was flushed with purified H_2. The second possibility was also exluded when the catalyst gained weight even heated under the flow of purified He. The final possibility will be tested on a Perkin Elmer TGS-2 system. The TGS-2 system is known to be free of any such electromagnetic interactions within the balance system.

Future Work

More reduction studies with Raney catalysts will be made with a Perkin Elmer TGS-2 system. A series of catalyst activity and selectivity tests will be performed in the fixed-bed unit under a very narrow range of process variables as discussed previously. The promising catalysts found from the activity tests will be subjected to a selective chemisorption study using CO and H_2.

References

1. W.H. Wiser, F.V. Hanson and C.S. Kim, DOE Contract No. DE-AC01-79ET14700, Quarterly Progress Report, Salt Lake City, Utah, Oct-Dec 1979.

2. ibid., Jan-Mar 1981.

3. K. Shata, "Urushibara Catalysts," University of Tokyo Press, Tokyo, Japan, 1971.

4. R. Mozingo, Organic Synthesis, 21, 15 (1941).

5. A.A. Pavlic and H. Adkins, J. Amer. Chem. Soc., 68, 1471 (1946).

6. H. Adkins and H.R. Billicer, J. Amer. Chem. Soc., 70, 695 (1948).

7. N.A. Dominguez, I.C. Lopez and R. Franco, J. Org. Chem., 26, 1625 (1961).

8. J. Freel, W.J.M. Pieters and R.B. Anderson, J. Catal., 14, 247 (1969).

9. H.A. Dirksen and H.R. Linden, Research Bulletin No. 31, Institute of Gas Technology, Chicago, 1963.

10. B.A. Lure, A.N. Chernyshov, N.N. Perova and B.S. Svetlov, Kinetika: Kataliz, 17 (6), 1453 (1976).

11. P. Mars, J.J.F. Scholten and P. Zwietering, Proc. Internal. Congress Catalysis, Paris, France, 1961, Vol. 1, p 1245.

12. W.H. Wiser, F.V. Hanson and C.S. Kim, DOE Contract No. DE-AC01-79ET14700, Quarterly Progress Report, Salt Lake City, Utah, July-Sept 1981.

13. ibid., Jan-Mar, 1981.

14. L.J. Swartzendruber and B.J. Evans, J. Catal., 43, 207 (1976).

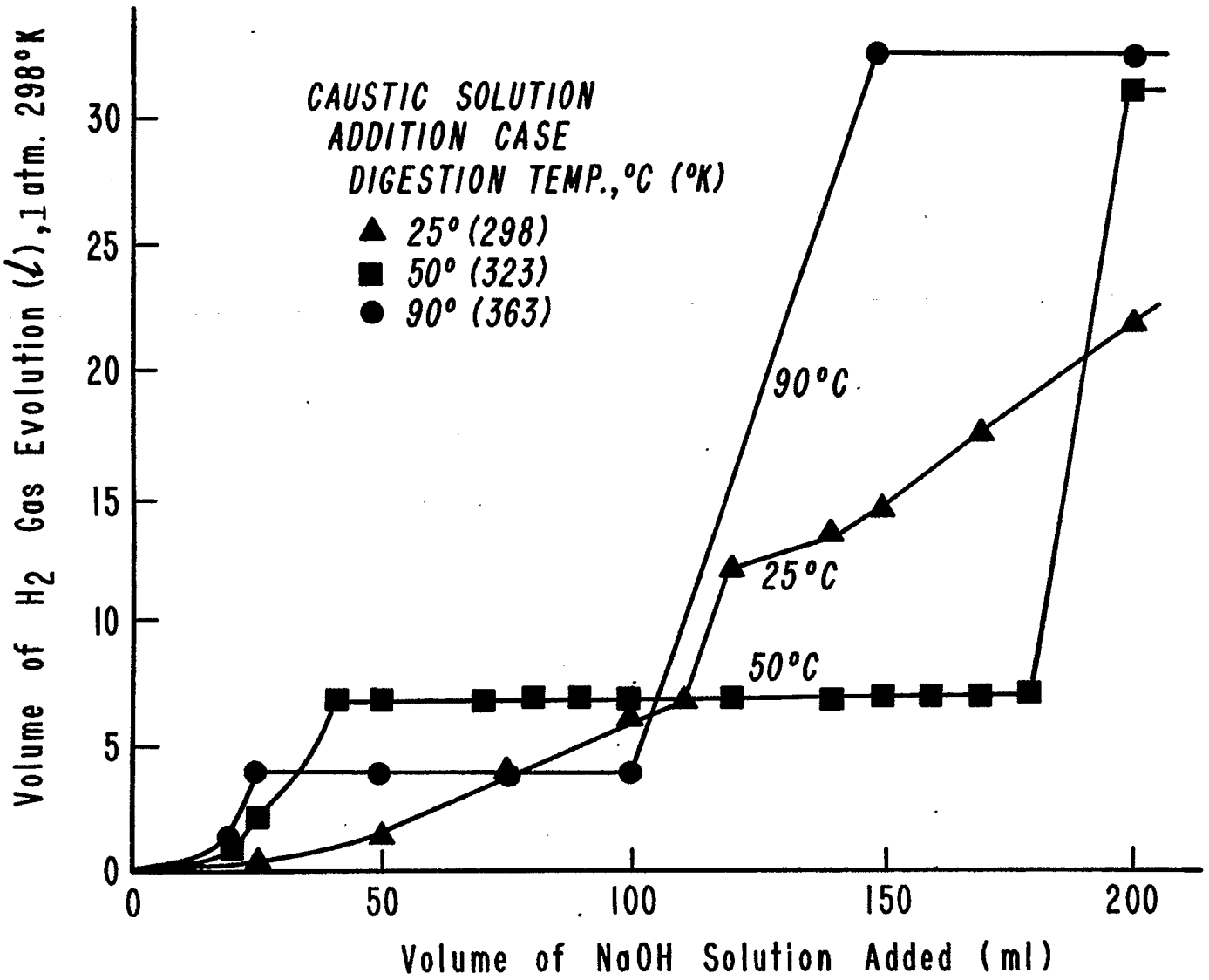

Figure 1. Hydrogen evolution vs. NaOH solution added.

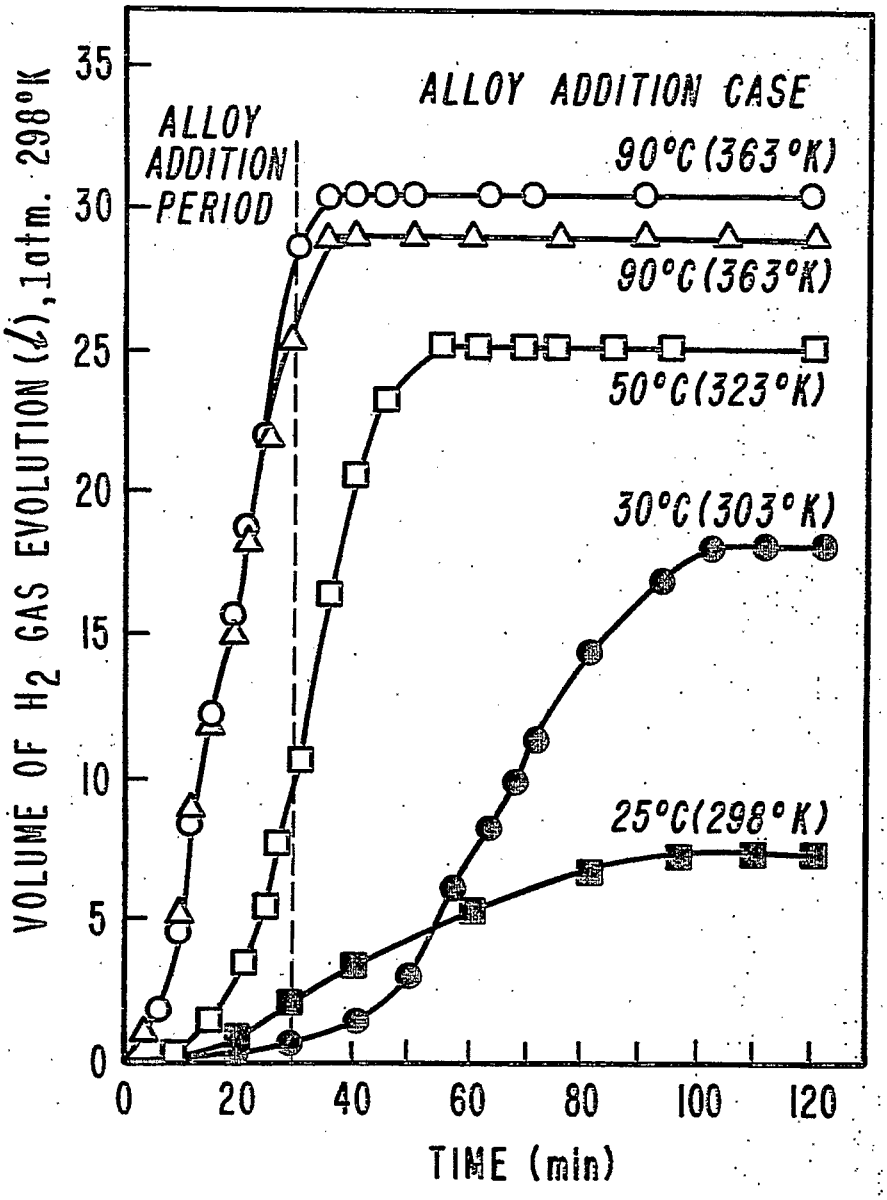

Figure 2. Hydrogen evolution vs. digestion time.
Δ: Sample made from a Al-Fe (50/50 wt %) alloy furnished by Alpha products.

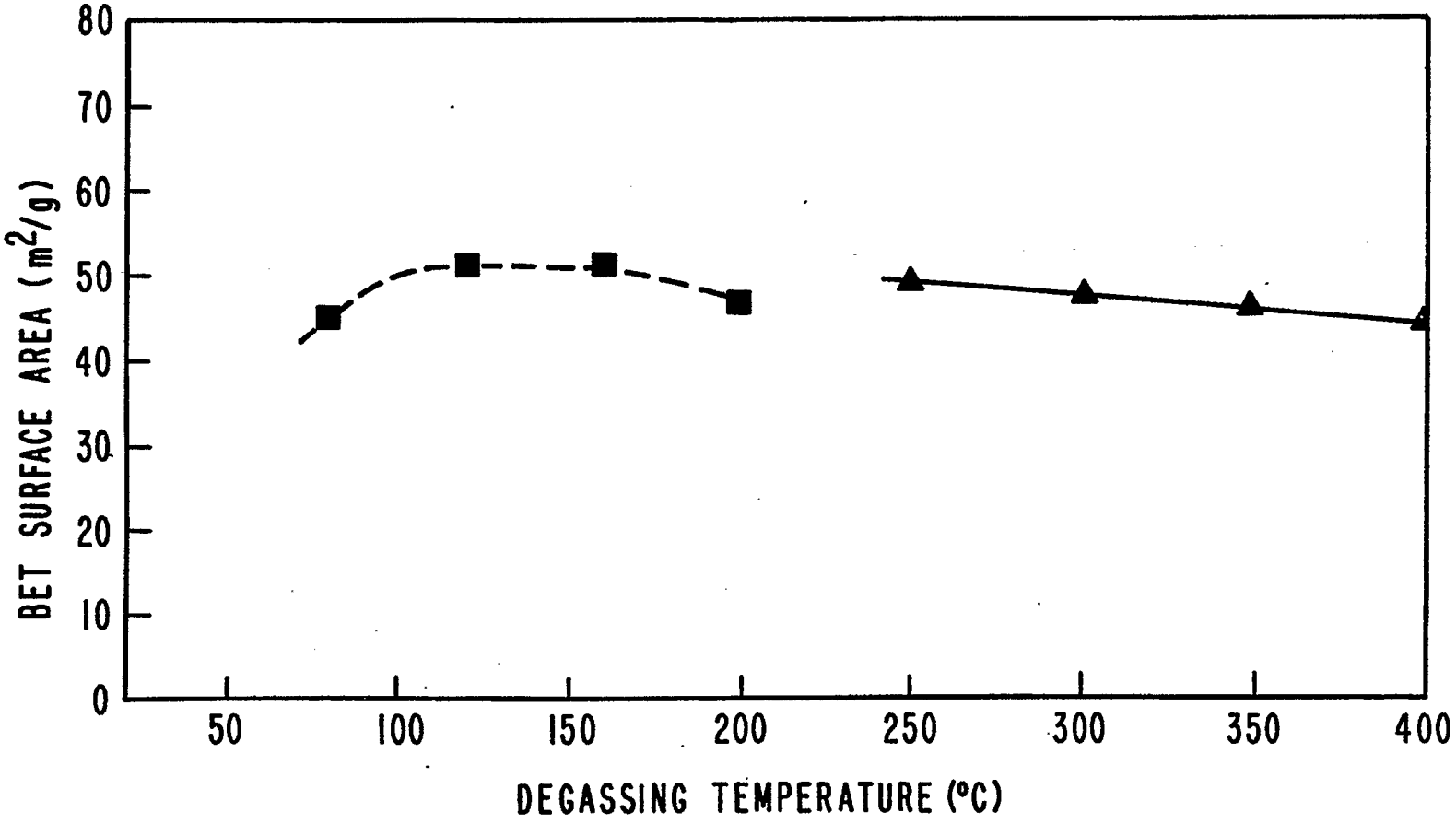

Figure 3. Effect of degassing temperature on BET surface area. Sample: Raney Fe leached at 90°C with caustic addition.

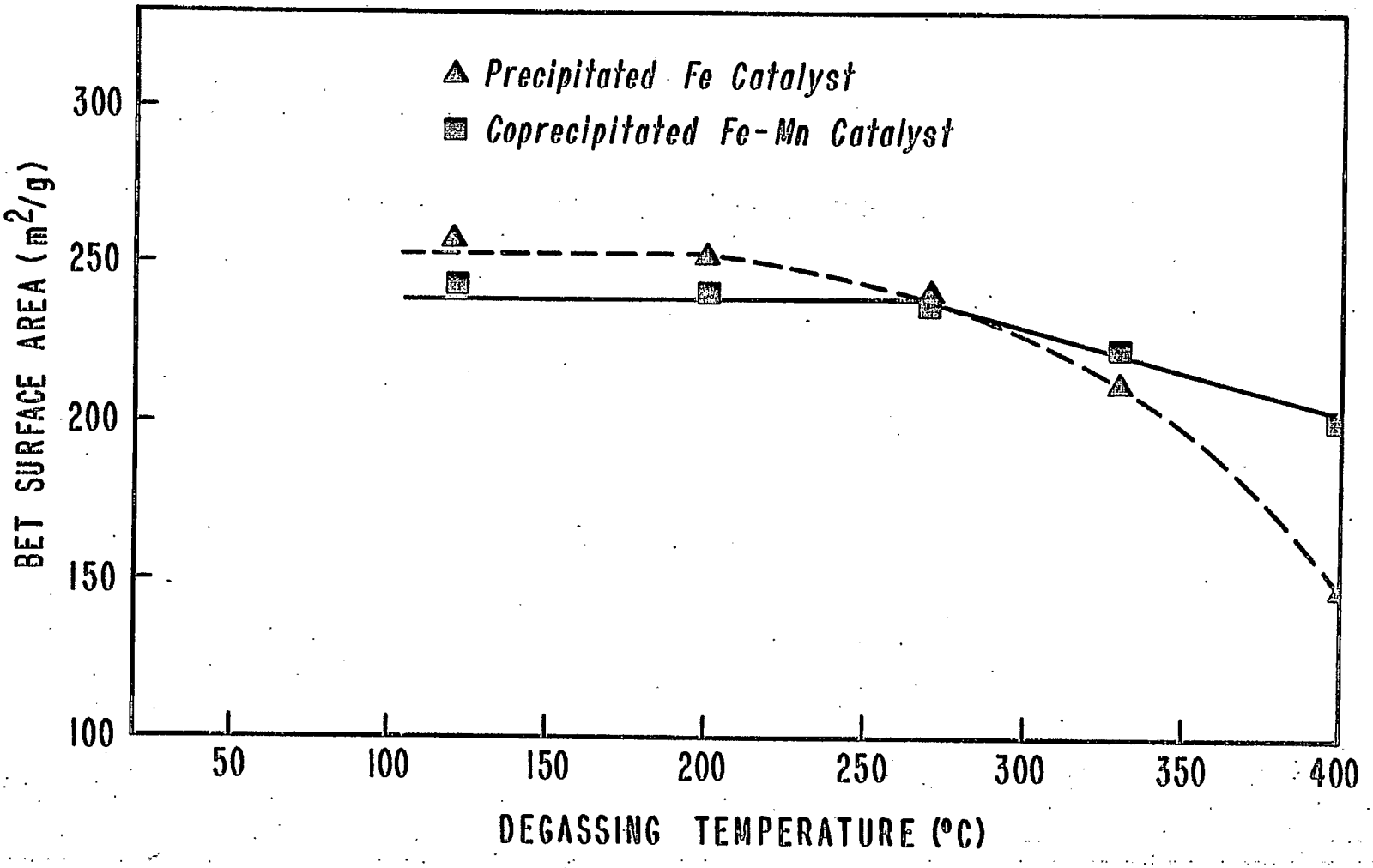

Figure 4. Effect of degassing temperature on BET surface area.

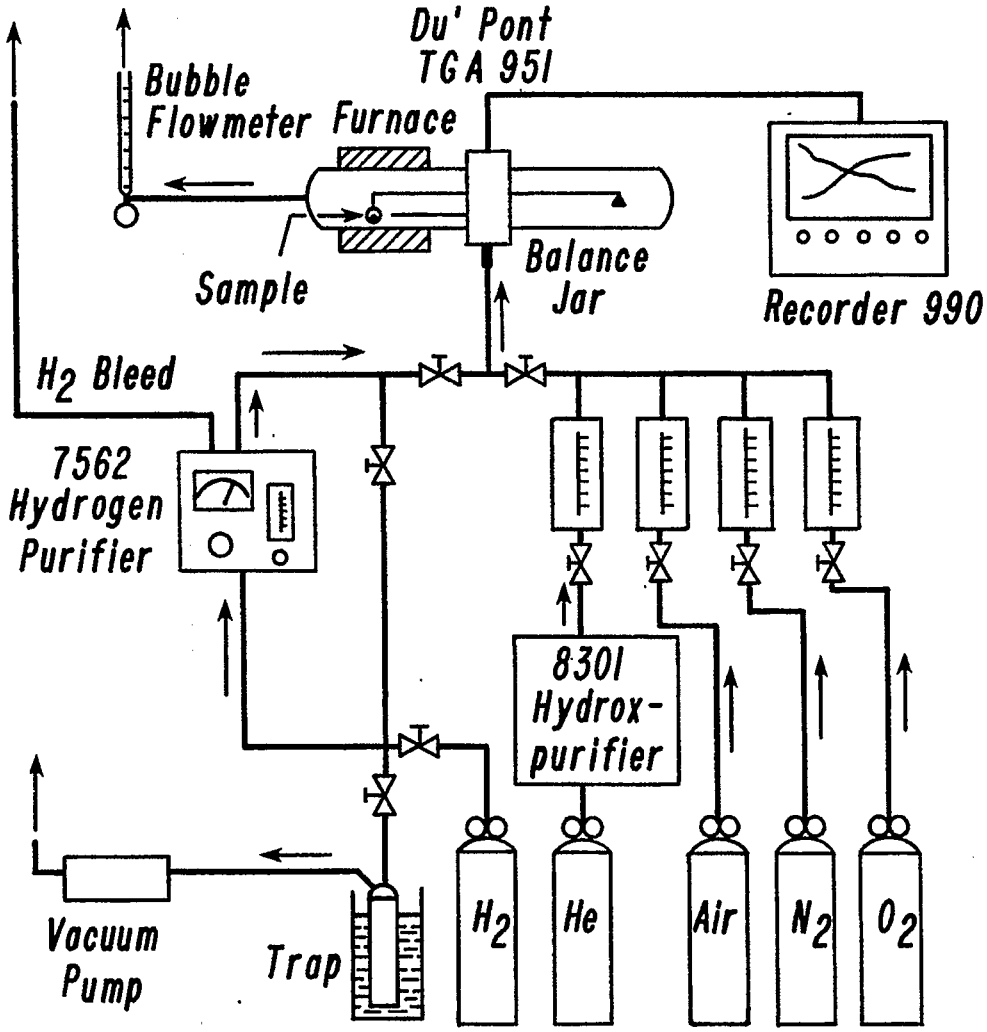

Figure 5. Flow diagram of TGA unit.

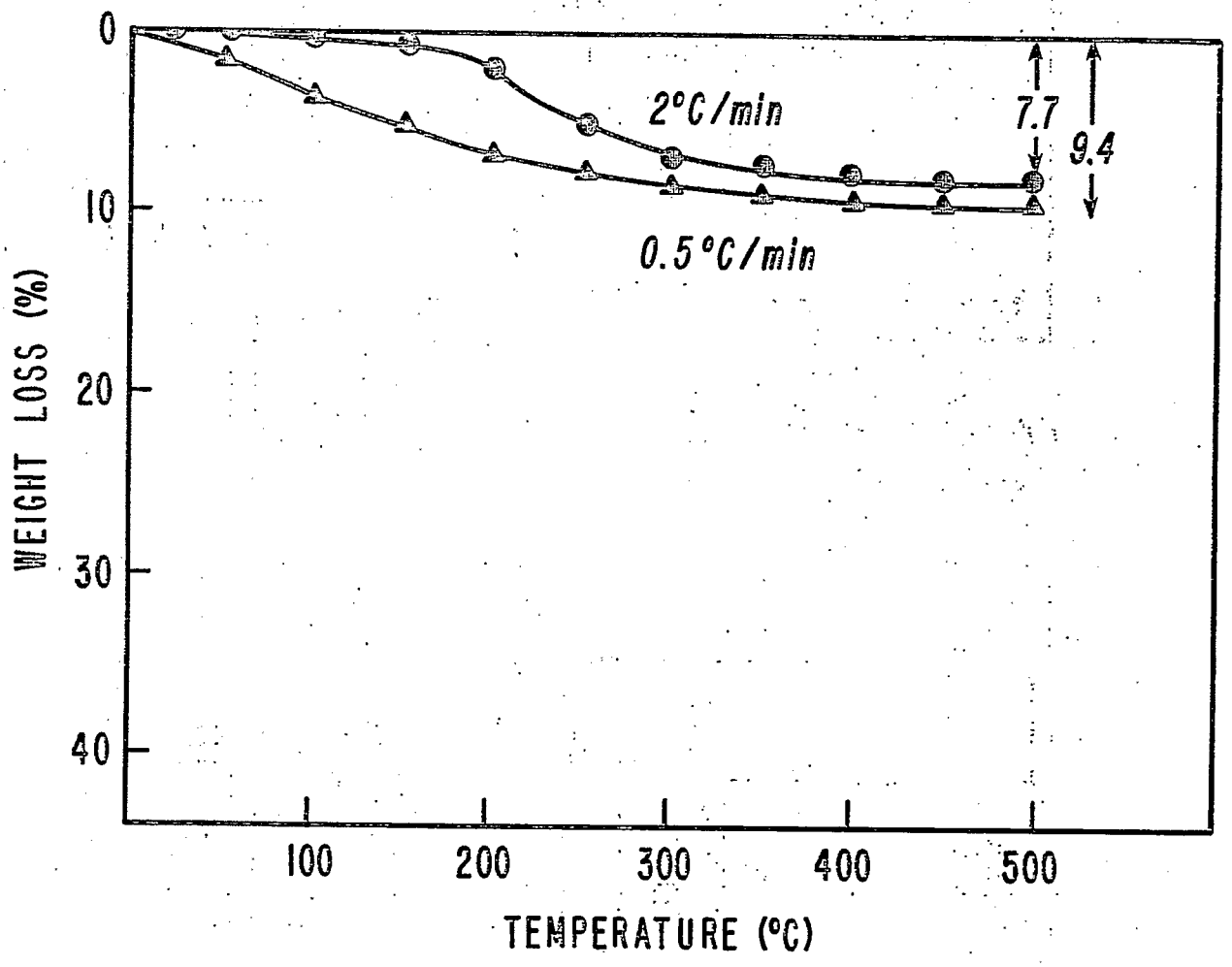

Figure 6. TGA run under helium. Sample: Fe-Mn (100:5 atomic ratio) coprecipitated catalyst.

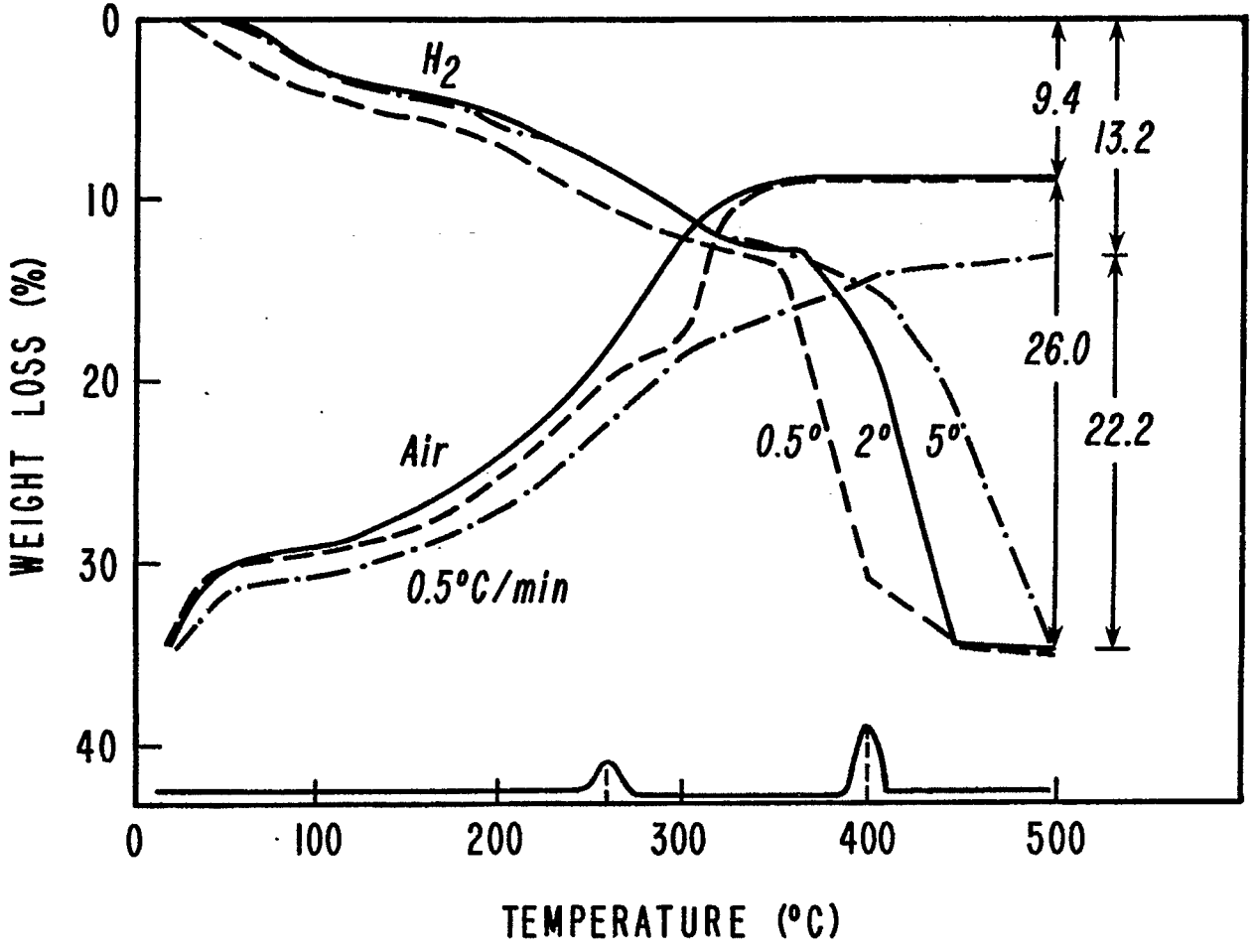

Figure 7. Effect of heating rate on reduction. Sample: Fe-Mn (100:5 atomic ratio) coprecipitated catalyst.

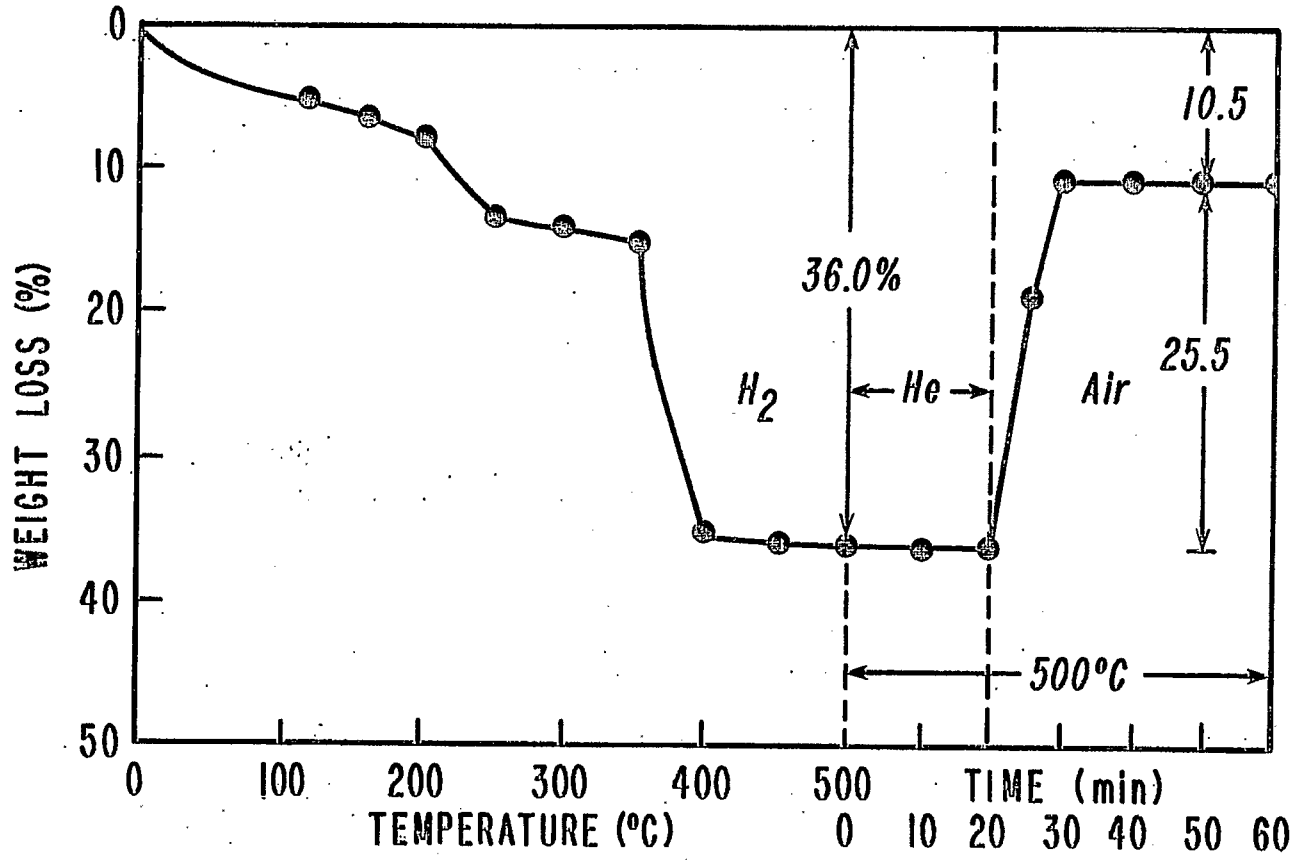

Figure 8. Series of isothermal heating. Sample: Fe-Mn (100:5) coprecipitated catalyst.

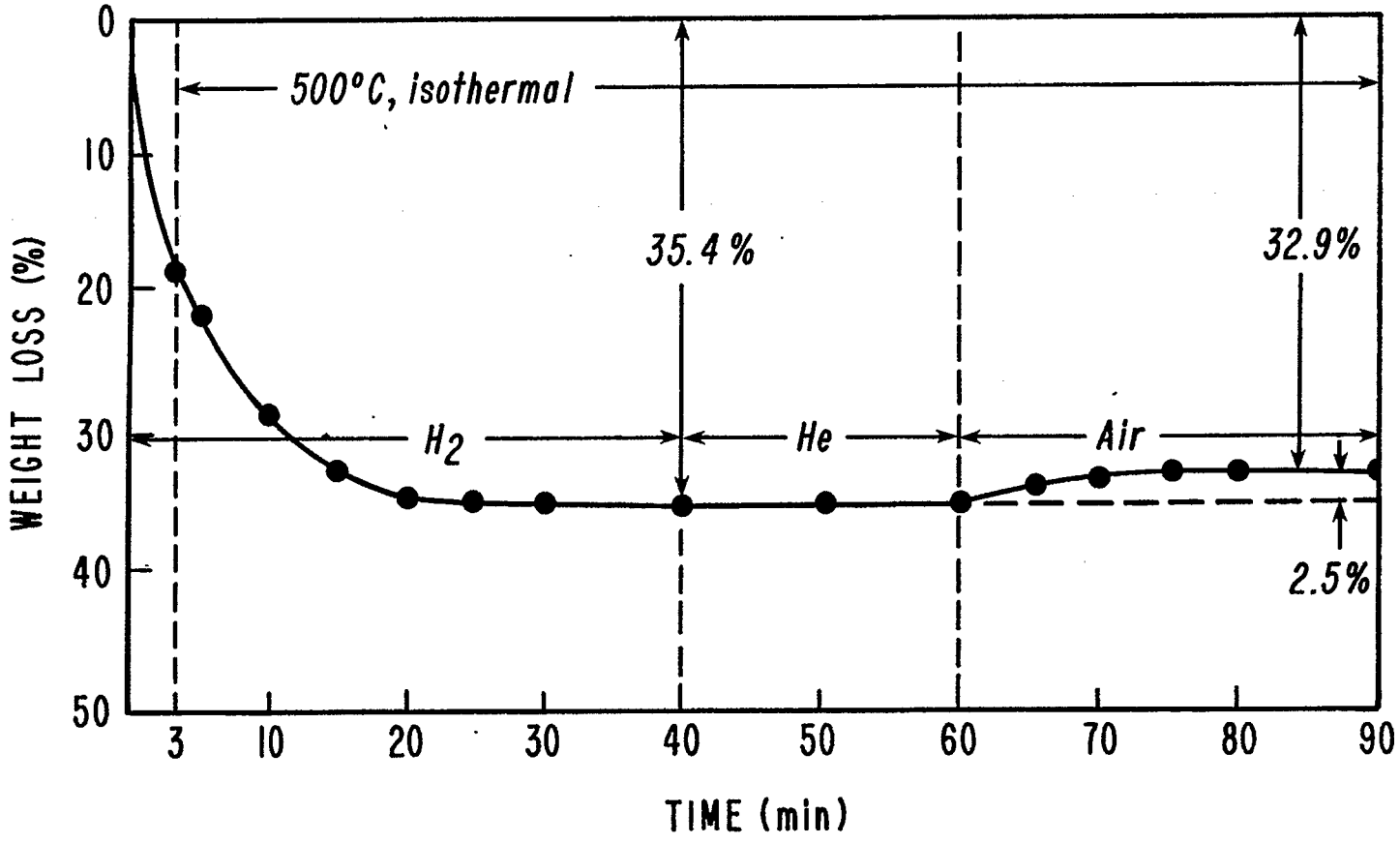

Figure 9. Effect of fast heating rate on reduction. Sample: Fe-Mn (100:5) coprecipitated catalyst.

Table 1. Preparation of Iron Catalysts.
Al-Fe Alloy (50/50 w/o)

Preparation Method	Digestion Temp, °C (°K)	Conc of NaOH Sol	Digestion* Time, min	% Al Leaching	Phases (XRD)	BET Surface Area, m^2/g
Raney Iron Addition of Caustic Solution	25(298) ± 5	21%	210(90)	79.7%	α-Fe Al-Fe alloy	53.5
	50(323)	21%	210(90)	79.1%	α-Fe	40.9
	90(363)	21%	210(90)	84.5%	α-Fe Fe_3O_4	49.4
	90(363)	21%	210(90)	83.7%	α-Fe Fe_3O_4	50.2
Precipitated Fe catalyst	-	-	-	-	Fe_3O_4	241.9
Raney Iron, Addition of Alloy	25(298)	21%	120(90)	21.6%	α-Fe Al-Fe alloy	45.8
	30(303)	21%	120(90)	55.3%	α-Fe Al-Fe alloy	51.3
	50(323)	21%	120(90)	73.6%	α-Fe	45.8
	90(363)	21%	120(90)	89.7%	α-Fe	26.0
	90**(363)	21%	120(90)	85.2%	α-Fe	29.1
	90(363)	4.4%	120(90)	9.2%	Al-Fe alloy	7.4

*The numbers in parenthesis indicate the additional digestion time after completion of the addition of caustic solution or alloys into the activation reactor. The other numer is the total digestion time.

**Al-Fe (50/50 wt %) alloy from Alpha Products.

Table 2. Preparation of Fe-Mn Catalysts.
Al-Fe-Mn Alloy (59/38/3 w/o)

Preparation Method	Digestion Time, °C. (°K)	Conc of NaOH Sol	Digestion Time, min	% Al Leaching	Phases (XRD)	BET Surface Area, m^2/g
Raney Fe-Mn, Addition of Alloy	35(308)	21%	120(90)	74.5	α-Fe $FeAl_3$	62.8
	50(323)	21%	120(90)	90.5	α-Fe $FeAl_3$	63.1
	50*** (323)	21%	120(90)	80.5	α-Fe	67.9
	90(363)	21%	120(90)	∿100	α-Fe	82.2
Coprecipitated Fe-Mn	-	-	-	-	Fe_3O_4 Mn_3O_4	241.5

***Al-Fe-Mn (59/38/3 wt %) alloy from Alpha Products.

Task 13

Catalyst Research and Development

Synthesis of Light Hydrocarbons from CO and H_2

Faculty Advisor: F.V. Hanson
Graduate Student: Y.S. Tsai

Introduction

The production of low molecular weight olefins (C_2-C_4) from the hydrogenation of carbon monoxide has been investigated over unsupported iron-manganese catalysts. The results from the preliminary tests which were performed in a bench-scale fixed-bed reactor system showed that the unsupported iron-manganese catalyst were very selective in the production of C_2-C_4 olefins. Data from the screening tests of the sixteen iron-manganese catalysts indicated that a catalyst composed of 2 parts of manganese per 100 parts of iron was the most selective. The effects of the process variables were also studied. The results mostly agreed with those found in the literature.

The experimental procedures are being developed to provide more comprehensive information on the iron-manganese catalysts. These procedures include the fabrication of a new fixed-bed reactor system for an accurate analysis of the products, an accurate mass balance analysis, the characterization of the catalyst, the catalyst preparation technique, the catalyst pretreatment and the calculations for the heat and mass transfer effects. These experiments should provide an understanding of the catalyst nature corresponding to the activity and selectivity of the iron-manganese catalyst for the synthesis of C_2-C_4 olefins.

Project Status

Four unsupported iron-manganese catalysts have been tested for approximately eight hours to provide information on the catalyst age and the effect of time on the activity and selectivity. Two of the four catalysts prepared in the previous work[1] were then tested approximately for 35 hours. The catalysts are composed of pure iron and 3.0 Mn/100 Fe. They were pretreated by flowing hydrogen at the flowrate of 2.50 cc sec^{-1}, ambient pressure and 400°C for 20 hours. The operating conditions for the long-term tests were based on a CO conversion of 5.0 ∿ 6.0% which would reduce the heat transfer problem to provide an isothermal condition for the catalyst bed. The YST-1 catalyst (pure Fe) was tested at $2H_2/1CO$, 500 psig, 1.093 cc $g^{-1}sec^{-1}$ and 170°C. The conditions for the YST-2 catalyst (3.0 Mn/100 Fe) were $2H_2/1CO$, 200 psig, 1.082 cc $g^{-1}sec^{-1}$ and 180°C.

The long-term effects on the CO conversion, the yield and the selectivity for YST-1 catalyst are shown in Figures 1 and 2. Figure 1 indicates that the CO conversion was increasing from 2.3% to about 5.0% in 15 hours. The conversion was then steady at 5.0% for 35 hours. The O/P ratio (olefin/paraffin) in C_2-C_4 hydrocarbons was constant at about 1.1. Figure 2 shows that C_2-C_4 hydrocarbon production increased slightly with time from 44% to 50%. The production of CH_4 and C_5^+ stablized after the catalyst was on stream for

about 12 hours. Both alcohols and CO_2 maintained constant selectivities throughout the test. A period of induction time is needed for the catalyst to reach the constant activity and selectivity. The age of the YST-1 catalyst has not been determined from the data obtained, however, it is safe to conclude that the catalyst is at least active up to 35 hours for the production of C_2-C_4 olefins.

Figures 3 and 4 show the long-term effects that the YST-2 catalyst has on the activity and selectivity. Figure 3 indicates that the CO conversion was constant at about 5.2%, however, the O/P ratio of the C_2-C_4 hydrocarbons did not increase to 2.6 until the catalyst had been on stream for about 12 hours. Figure 4 shows that the C_2-C_4 hydrocarbon production was constant at 54% and the alcohols maintained a low but constant level of yield throughout the test. The selectivities for C_5^+, CH_4 and CO_2 reached their respective constant levels after 12 hours. A period of induction time is also required for the YST-2 catalyst to maintain constant activity and selectivity. Similarly, the YST-2 catalyst is at least active up to 40 hours based on the data obtained. A period of induction time is therefore necessary for the test of the catalyst to acquire meaningful and reliable data concerning the catalyst performance in the production of C_2-C_4 hydrocarbons.

Future Work

The long-term effects for the other two catalysts (that is, YST-3 and YST-4)[1] will be investigated. The optimum catalyst preparation and pretreatment for the maximum production of C_2-C_4 olefins will be studied. Catalyst characterization procedures will be initiated. The literature survey on the CO hydrogenation as well as the heat and mass transfer for the fixed-bed reactor will be continued to update the information.

Reference

1. W.H. Wiser, F.V. Hanson and Y.S. Tsai, DOE Contract No. DE-AC22-79ET14700, Quarterly Progress Report, Salt Lake City, Utah, Oct-Dec 1981.

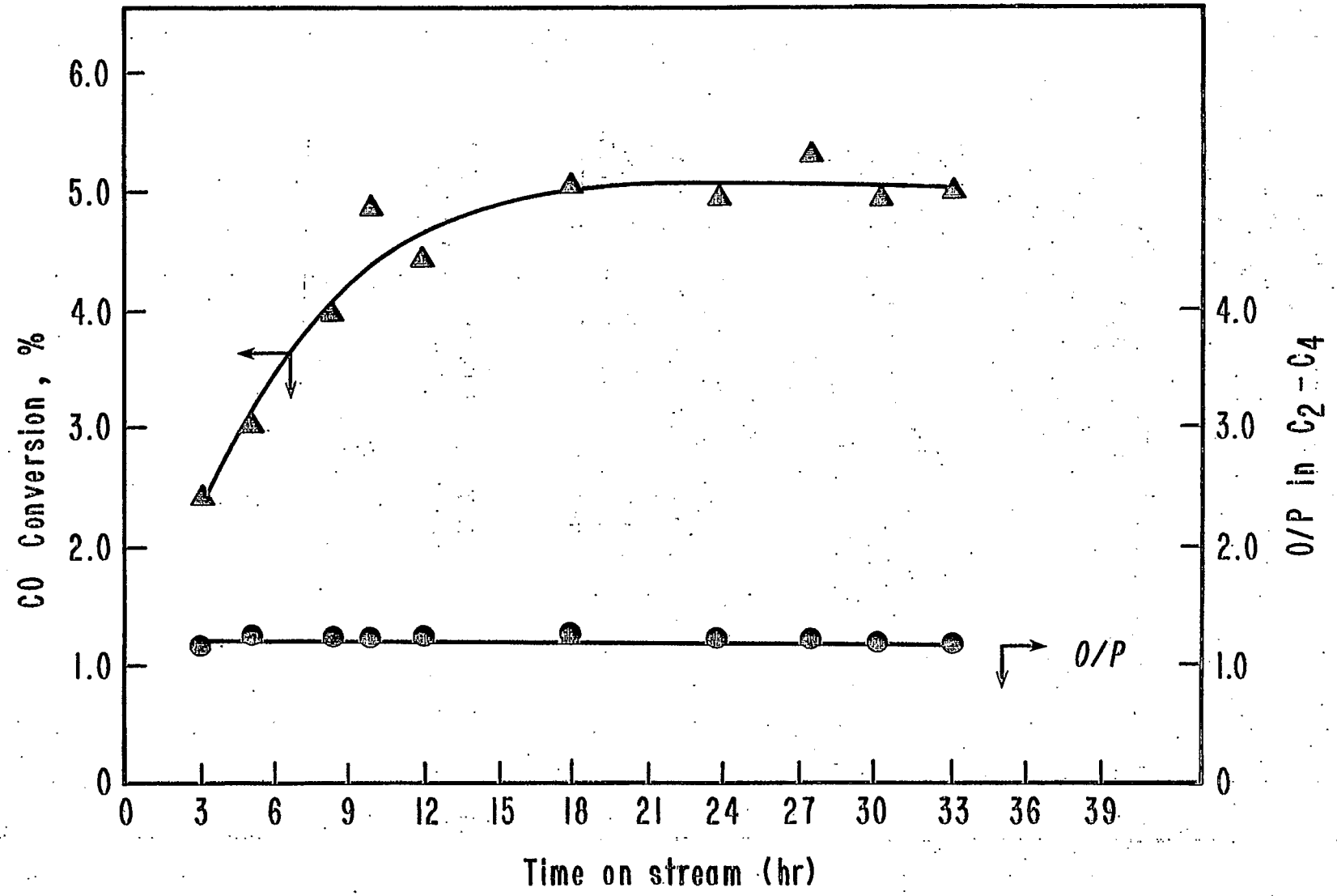

Figure 1. CO conversion vs. time for YST-1 catalyst (pure Fe); H_2/CO = 2/1; 500 psig; 1.093 cc g^{-1} sec^{-1}; 170°C.

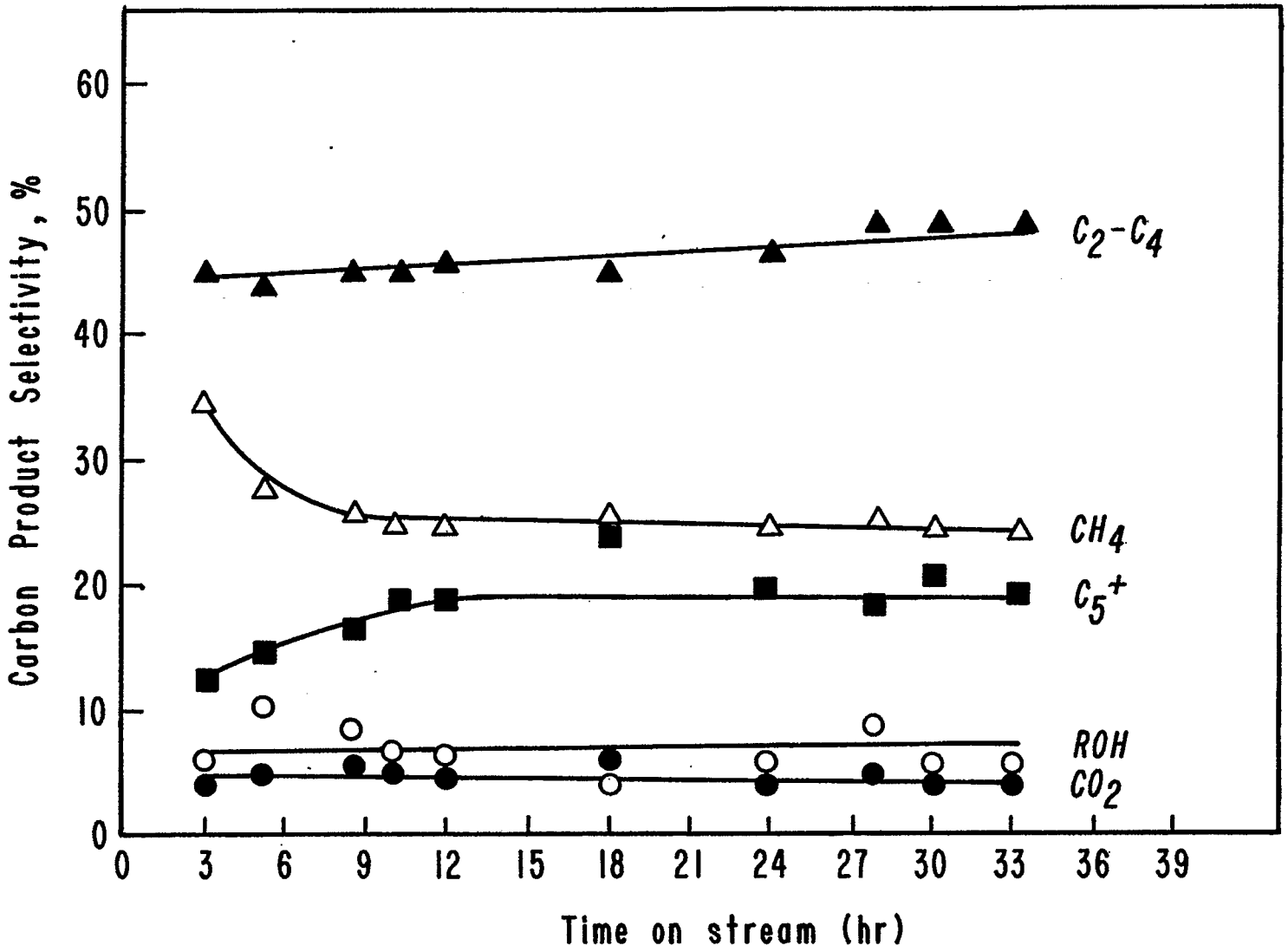

Figure 2. Hydrocarbon yield and selectivity for YST-1 catalyst (pure Fe); H_2/CO = 2/1; 500 psig; 1.093 cc g^{-1} sec^{-1}; 170°C.

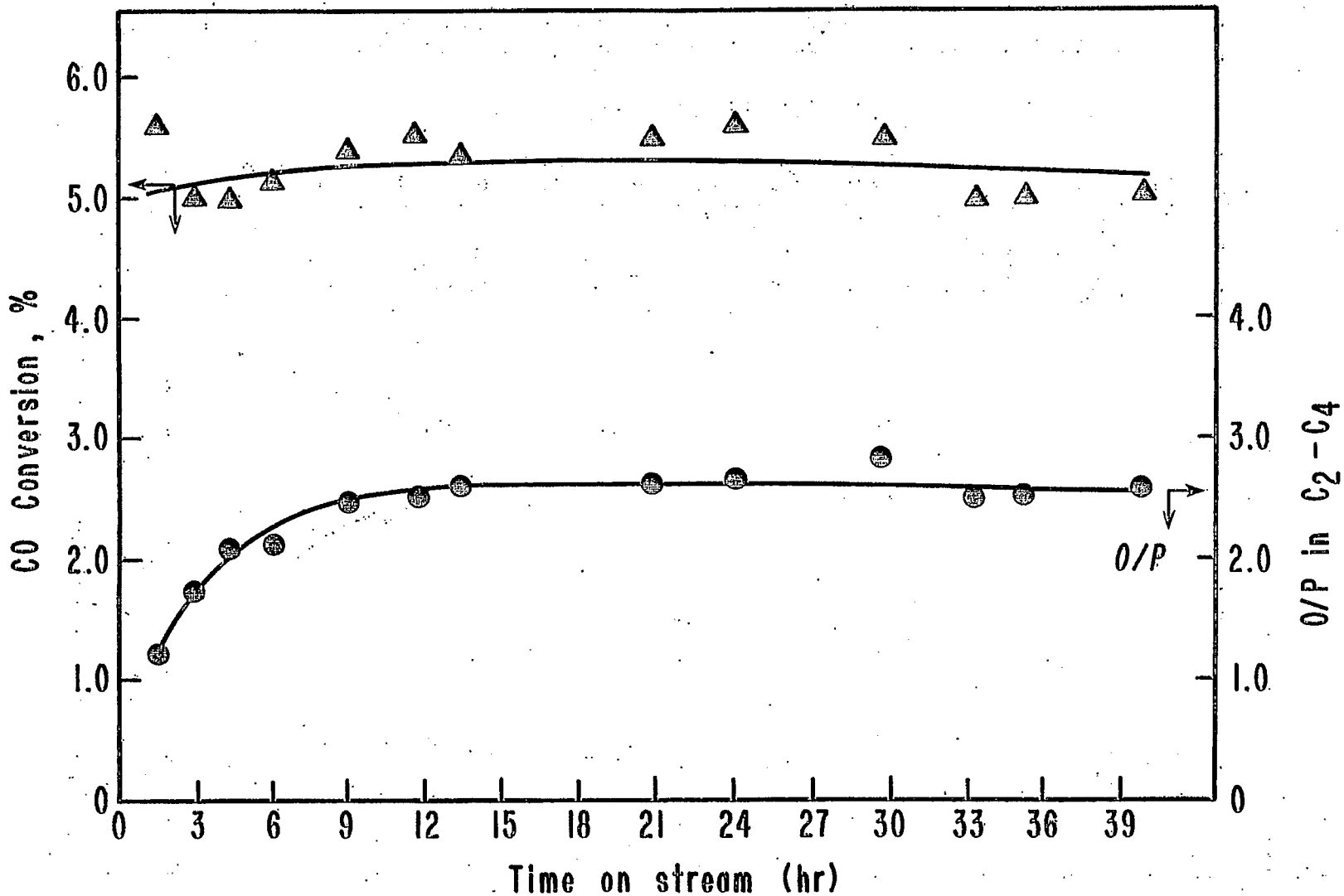

Figure 3. CO conversion vs. time for YST-2 catalyst (3.0 Mn/100 Fe); H_2/CO = 2/1; 200 psig; 1.082 cc g^{-1} sec^{-1}; 180°C.

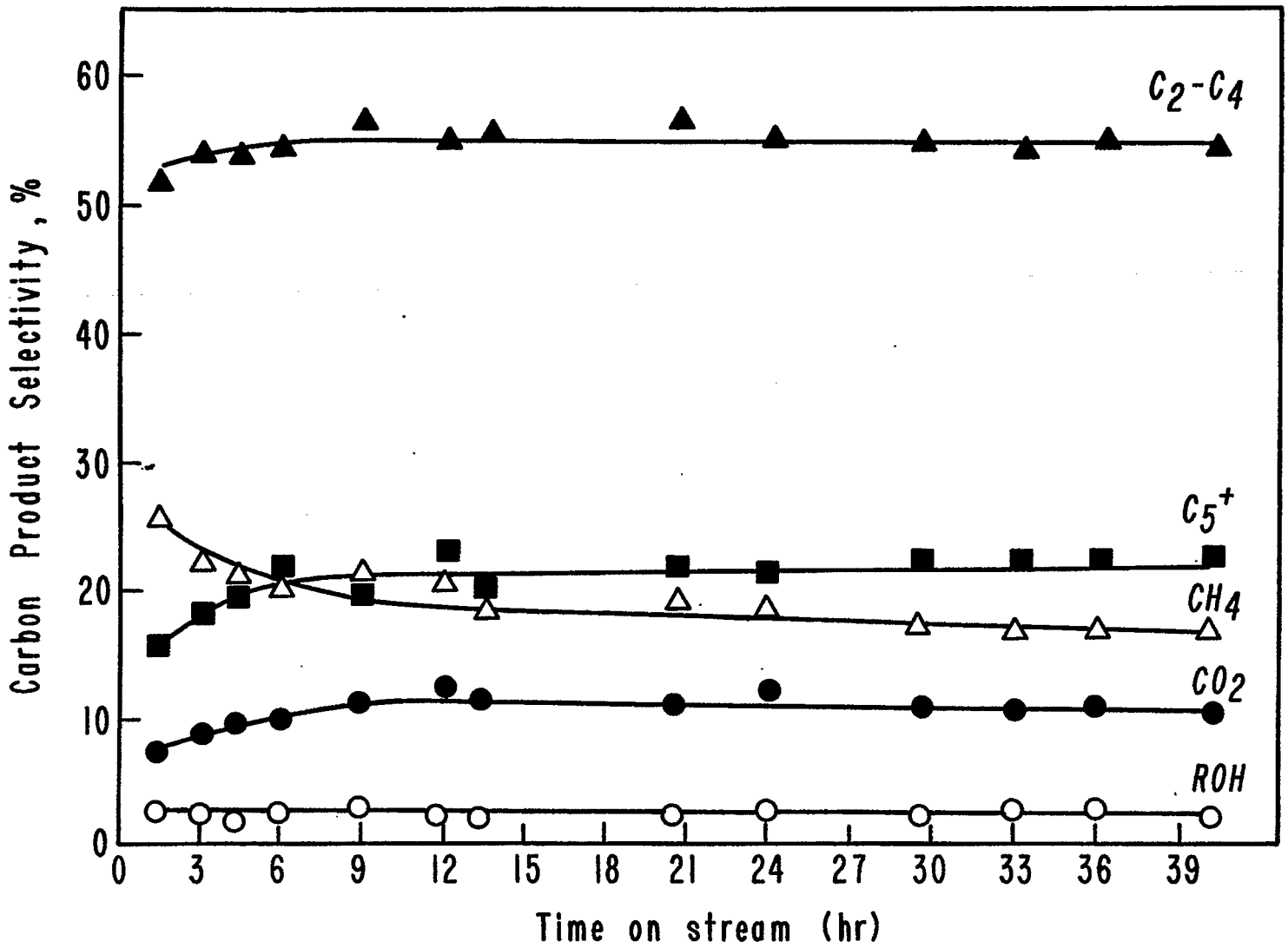

Figure 4. Hydrocarbon yield and selectivity for YST-2 catalyst (3.0 Mn/100 Fe); H_2/CO = 2/1; 200 psig; 1.082 cc g^{-1} sec^{-1}; 180°C.

V. Conclusions

Detailed conclusions are included in the reports for each task. Task 4 is no longer funded and has been discontinued. Tasks 12 and 14 are inactive. No work was done under Task 15.

* U.S. GOVERNMENT PRINTING OFFICE: 1982-646-069/289